Developing Geotechnical Applications for the Fiber Optic Pore Water Pressure Sensor

Final Report

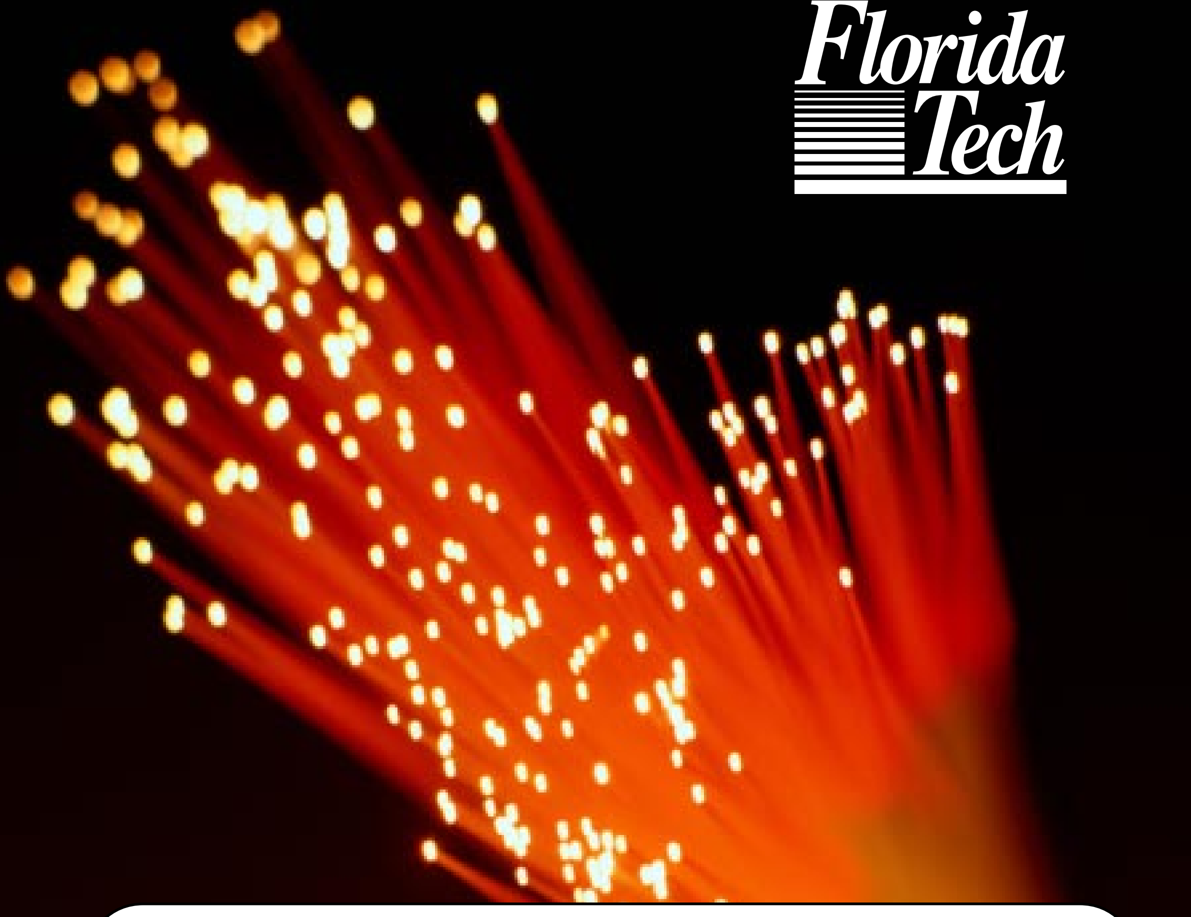

Florida Institute of Technology
150 W. University Blvd.
Melbourne, Florida 32901-6975
www.fit.edu • Phone (321) 674-7555 • Fax (321) 674-7565
April 17, 2002
Paul J. Cosentino, Ph.D., P.E., Principal Investigator
Barry G. Grossman, Ph.D. Co-Principal Investigator

Submitted to:
Peter W. Lai., P.E.
State Geotechnical Engineer,
Structures Design Office
Florida Department of Transportation
605 Suwannee St., MS -33, Tallahassee, Florida 32309-0540 (850) 414-4306
SunCom: 278-6351 •Fax: (850) 488-6352 Contract Number BC 796

Technical Report Documentation Page

1. Report No. FL/DOT/RMC/06650-7754	2. Government Accession No.	3. Recipient's Catalog No.
4. Title and Subtitle Developing Geotechnical Applications for the Fiber Optic Pore Water Pressure Sensor Phase I		5. Report Date April 15, 2002
		6. Performing Organization Code
7. Author's P. J. Cosentino, P. Bianca Lloyd, Franz Campero		8. Performing Organization Report No.
9. Performing Organization Name and Address Florida Institute of Technology (321) 674-7555 Civil Engineering Department 150 West University Blvd. Melbourne, FL 32901-6975		10. Work Unit No. (TRAIS)
		11. Contract or Grant No. Contract Number BC 796
12. Sponsoring Agency Name and Address Florida Department of Transportation 605 Suwannee Street Tallahassee, Florida 32399-0450		13. Type of Report and Period Covered Final Report September 2000 to April 2002
		14. Sponsoring Agency Code 99700-7601-119
15. Supplementary Notes		

A study was completed to determine feasible applications for fiber optic pore pressure sensors developed previously under the 1992 FDOT research project entitled *Development of a Fiber Optic Sensors to Measure Pore Pressures* Contract WPA-0510635. Based upon this and three other projects, two sizes of circular sensors were developed. Several combinations of materials were used resulting in eight types of sensors. Three working sensors of each type was constructed and tested using three compressive loading conditions, axial with stress concentrations, axial with no stress concentrations and hydrostatic pressurization.

Sensors were developed based on the relatively low cost single-sided microbend process using a multi-mode fiber. During loading of the sensing region, light, focused into the glass core of the fiber was refracted out using microbends from two mesh types with approximately 20 openings per inch. The stiffness of the meshes used varied by a factor of 2. Sensors were constructed in 1.25 and 2.25 inch diameters using 10 mil and 20 mil G-10 fiberglass protective outer plates. During compression light intensities decreased and were measured using opto-electronic equipment with photodiodes that convert light intensity to voltage.

The calibration process was evaluated by analyzing the sensor responses to 3 types of tests. The axial testing with stress concentrations was designed to simulate the signal if a sensor was placed against a retaining wall, while the axial testing with no stress concentrations was developed as a possible calibration process for comparison to the hydrostatic testing. The hydrostatic testing proved to be the most desirable, however, it is also the most costly.

All eight types of sensors functioned adequately up to 40 psi (280 kPa), producing repeatable pressure versus light loss curves. The sensors with the softest mesh ETFE yielded more reliable calibration curves than those constructed from polypropylene.

The data reduction using a third order polynomial properly fit the pressure versus light loss curves producing regression coefficients nearing one. Linear regression analysis was useful in defining a possible linear range for using the various sensors.

17. Key Words Pore Water Pressures, Fiber Optic Sensors	18. Distribution Statement Document is available to the U.S. public through the National Technical Information Service, Springfield, Virginia 22161

19. Security Classif. (of this report) Unclassified	20. Security Classif. (of this page) Unclassified	21. No of Pages 90	22. Price

Form DOT 1700.7 (8-72)

Reproduction of completed page authorized

Developing Geotechnical Applications for the Fiber Optic Pore Water Pressure Sensor

Phase I

By

Paul J. Cosentino Ph.D., P.E.

P. Bianca Lloyd,

Franz Campero

Abstract

A study was completed to determine feasible applications for fiber optic pore pressure sensors developed previously under the 1992 FDOT research project entitled *Development of a Fiber Optic Sensors to Measure Pore Pressures* Contract WPA-0510635. Based upon this and three other projects, two sizes of circular sensors were developed. Several combinations of materials were used resulting in eight types of sensors. Three working sensors of each type was constructed and tested using three compressive loading conditions, axial with stress concentrations, axial with no stress concentrations and hydrostatic pressurization.

Sensors were developed based on the relatively low cost single-sided microbend process using a multi-mode fiber. During loading of the sensing region, light, focused into the glass core of the fiber was refracted out using microbends from two mesh types with approximately 20 openings per inch. The stiffness of the meshes used varied by a factor of 2. Sensors were constructed in 1.25 and 2.25 inch diameters using 10 mil and 20 mil G-10 fiberglass protective outer plates. During compression light intensities decreased and were measured using opto-electronic equipment with photodiodes that convert light intensity to voltage.

The calibration process was evaluated by analyzing the sensor responses to 3 types of tests. The axial testing with stress concentrations was designed to simulate the signal if a sensor was placed against a retaining wall, while the axial testing with no stress concentrations was developed as a possible calibration process for comparison to the hydrostatic testing. The hydrostatic testing proved to be the most desirable, however, it is also the most costly.

All eight types of sensors functioned adequately up to 40 psi (280 kPa), producing repeatable pressure versus light loss curves. The sensors with the softest mesh ETFE yielded more reliable calibration curves than those constructed from polypropylene.

The data reduction using a third order polynomial properly fit the pressure versus light loss curves producing regression coefficients nearing one. Linear regression analysis was useful in defining a possible linear range for using the various sensors.

Acknowledgement

The authors would like to express their appreciation to Mr. Peter Lai, Project Manager Florida Department of Transportation for his guidance throughout this work. Also a special thanks goes to the graduate and undergraduate students who worked tirelessly to complete this work including: Mike Markanian, Tara van Orden, and Elizabeth Cleary.

Table of Contents

Developing Geotechnical Applications for the Fiber Optic Pore Water Pressure Sensor

Phase I

By
Paul J. Cosentino Ph.D., P.E.
P. Bianca Lloyd,
Franz Campero

Chapter 1 Background

1.1 Introduction

A 1992 laboratory study was conducted for the Florida Department of Transportation (FDOT) on the evaluation of fiber optic sensors for determining the variation of pore water pressure in soils. Results indicated that a prototype fiber optic sensor could be used under either lab or field conditions (Cosentino and Grossman, 1992). Beginning in 1994, a three-phase traffic-sensor study was completed for FDOT where fiberoptic sensors were developed and embedded in flexible and rigid pavements, (Cosentino and Grossman 1994, 1997, 2000). A complete sensor system was successfully deployed at 5 traffic sites in Central Florida. These sensors functioned under severe temperature and loading conditions, throughout the third phase of these studies. Data from these sensors was currently being taken and used by FDOT's Traffic Statistics Department.

Fiber optic pore pressure sensors may prove to be more accurate than the piezometers and more durable and economical than the pore pressure transducers currently used for field monitoring. In addition, they could be used in the laboratory to replace existing pore pressure transducers. These fiber optic sensors would be immune to electromagnetic interference and corrosion.

1.1.1 Fiber optic microbend sensors

The fiber optic pore pressure sensor was developed using a concept known as the fiber optic microbend theory. Although there are many types of fiber optic sensors used for measuring pressures or strains, the most economical ones are those based upon the microbend principals. If properly designed, these sensors can be constructed with relatively inexpensive components. The light source, for example can often be a light emitting diode (LED), while the fiber needs little or no preparation before placement in the sensing region. Other types of fiber optic sensors require costly lasers as the light source and very sophisticated electrical equipment for interpreting the signal (Udd, 1995).

Figure 1 shows a typical optical fiber, which contains two mediums through which light can pass; the core and cladding. A buffer, typically made of acrylic polymers, protects these materials. As shown in Figure 2, the light intensity in a microbend sensor decreases when an external force or pressure mechanically deforms the optical fiber as it is pressed against a relatively small screen or mesh. As the fiber bends over the small radii, light focused into the fiber's inner core is refracted out of the core into the fibers protective cladding layers causing the decrease in light intensity *[Cosentino and Grossman, 1994]*. The change in light intensity is monitored using data acquisition systems to yield percentage variations from the original intensity. Microbends can be applied to optical fibers from either both sides, termed double sided, or from one side of the fiber, termed single sided. The sensors developed for this study are single sided microbend sensors.

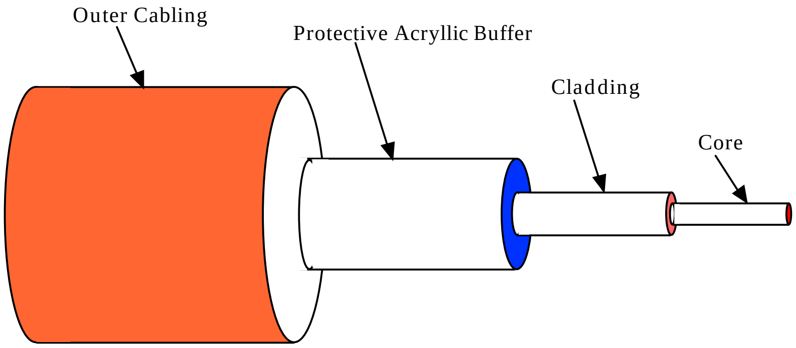

Figure 1.1 Typical optical fiber

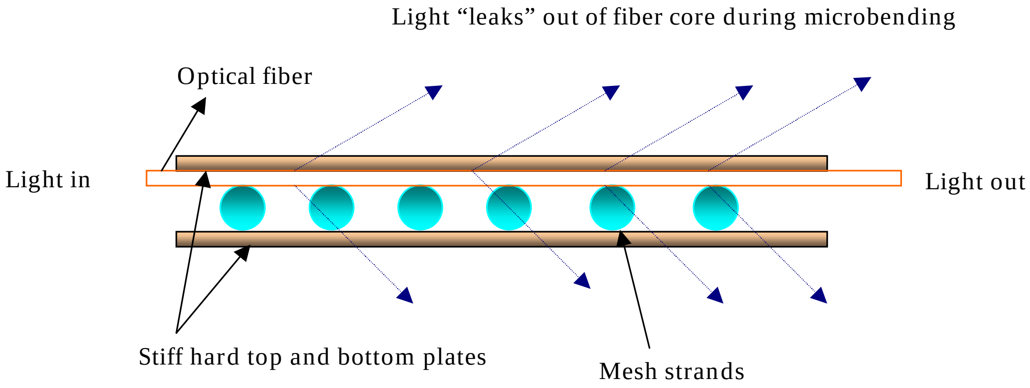

Figure 1.2 Light loss schematic during single sided microbending process

1.1.2 Complexities of Pore Pressure Measurements

Pore pressures control the shear strength of saturated soils. Accurate measurement of these pressures is complex requiring highly sophisticated equipment. Laboratory triaxial tests use pore pressure transducers that function based on small movements of thin metal diaphragms. Field pore pressure devices are exposed to many problems and require a great deal of expertise to use. These problems include, maintaining saturation of the device during installation and understanding the limitations of the various electrical and pneumatic transducers used. Advances in pore pressure technology are always a key issue for geotechnical engineers.

1.2 Objective

The objective of this research was to develop geotechnical applications for the fiber optic sensors developed during the 1992 study by Cosentino and Grossman. These applications can be to measure either pore pressures or total stresses.

1.3 Approach

A 12-month study was completed that enabled fabrication and laboratory testing of prototype fiberoptic pore pressure sensors. Forty circular sensors were fabricated using technology similar to that used on the traffic sensors. Various combinations of materials were used resulting in eight types of sensors. The size, stiffness and internal materials were varied to produce the eight types. Five working sensors of each type was constructed and tested using three compressive loading conditions; axial with stress concentrations, axial with no stress concentrations and hydrostatic pressurization.

Sensors were developed based on the relatively low cost single-sided microbend process using a commonly available optical fiber. During loading of the sensing region, light, focused into the glass core of the fiber was refracted out using microbends from two mesh types with approximately 20 openings per inch. The stiffness of the meshes used varied by a factor of 2. Sensors were constructed in 1.25 and 2.25 inch diameters using 10 mil and 20 mil G-10 fiberglass protective outer plates. During compression light intensities decreased and were measured using opto-electronic equipment with photodiodes that convert light intensity to voltage.

The following tasks were completed during this work and are summarized below.

TASK 1 FIBEROPTIC SENSOR OPTIMIZATION: The laboratory sensor was manufactured in a thin durable circular patch type configuration such that it can withstand both laboratory and field handling.

TASK 2 PURCHASE AND EVALUATE EXISTING PORE PRESSURE TRANSDUCERS: Existing pore pressure transducers were purchased and evaluated for comparison to the fiberoptic sensor.

TASK 3 TRIAXIAL TESTING: Triaxial tests were conducted on several soils. The results were analyzed and the fiber optic sensors underwent modifications until they produced pressures useful in soils.

TASK 4 INTERFACE ELECTRONICS: Interface electronics were developed to convert the light intensity signals to voltage.

TASK 5 SENSOR POTTING EVALUATION: Candidate materials were evaluated for potting or fixing the sensor into porous media. Sensors may be placed directly into a porous stone casting or any of the available porous plastics.

Chapter 2
Literature Review

2.1 Piezometers

Piezometers are normally used for the *in situ* monitoring of pore water pressure in soils. There are six types of piezometers commonly utilized. They are as follows:

- Pneumatic Piezometers
- Vibrating Wire Piezometers
- Electrical Resistance Piezometers
- Twin-tube Hydraulic Piezometers
- Standpipe Piezometers
- Fiber-Optic Piezometers

All six have a common element, the use of a filter for the separation of groundwater from the material in which the piezometer is installed. A description of each type of piezometer along with its advantages and disadvantages is presented below.

2.1.1 Pneumatic Piezometers

Pneumatic piezometers can be further classified according to the internal system used for monitoring pore water pressure, whether it involves a “normally closed” or “normally open” transducer (Dunnicliff, 1988). Both versions operate with the use of gas. Groundwater is allowed to enter, via a filter, on one side of a flexible diaphragm that is attached to the body of the transducer. Gas is passed through an inlet tube until the pressure barely exceeds the pore water pressure, resulting in the deflection of the diaphragm and thereby causing the gas to pass through the outlet tube. There are several advantages to this system including easy access for calibration and non-susceptibility to extreme cold. Furthermore, pneumatic piezometers have a low level of interference to construction.

There are also some cons to using the pneumatic piezometer. The mere task of selecting a particular pneumatic system requires experience and attention to many details (Dunnicliff, 1988). Secondly, there is potential for error because it is difficult to control the rate of gas flow through the system.

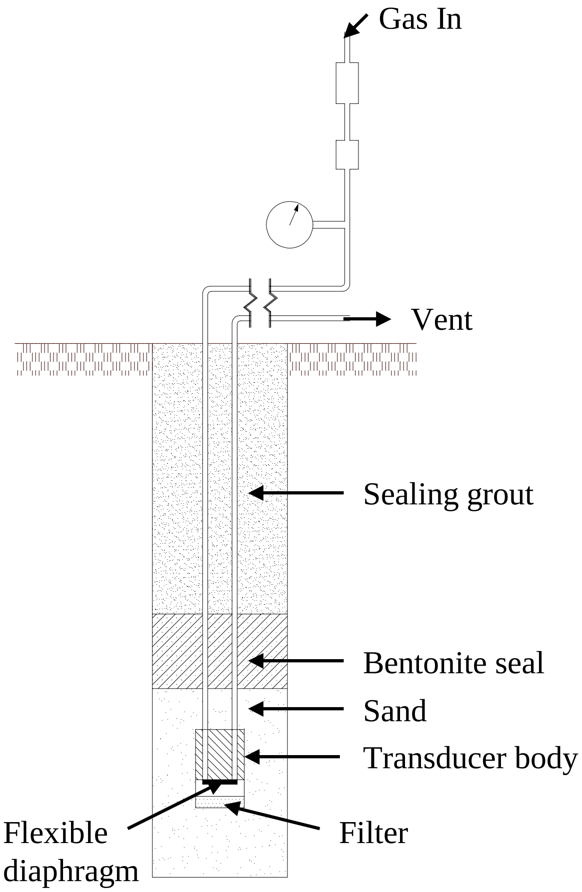

Figure 2.1a Pneumatic Piezometer (after Dunnicliff, 1988)

Figure 2.1b Pneumatic Piezometer (courtesy of Slope Indicator)

2.1.2 Vibrating Wire Piezometers

A metallic diaphragm is incorporated in the vibrating wire piezometer in order to separate the pore water from the measuring unit (Dunnicliff,1988). That diaphragm has a tensioned wire attached to its midpoint so that any deflection in the diaphragm results in wire vibrations. Subsequently, determining the difference between the natural and induced frequencies of the wire results in measurements. Some positive attributes of this system are the ease of recording data and the ease of installation thereby limiting its interference to construction. Vibrating wire piezometers also do not experience problems with freezing and can measure negative pore water pressures.

Unfortunately vibrating wire piezometers do not naturally have immunity against electromagnetic and radio frequency interferences therefore they are susceptible to lightning. Also, particular manufacturing actions are taken to minimize zero drift with no assurance that it can be eliminated.

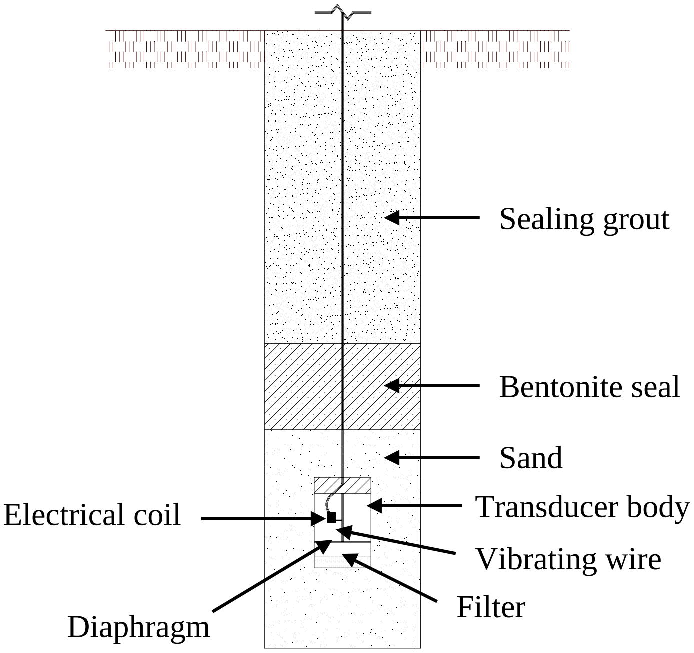

Figure 2.2a Vibrating Wire Piezometer (after Dunnicliff, 1988)

Figure 2.2b Vibrating Wire Piezometers (courtesy of Slope Indicator)

2.1.3 Electrical Resistance Piezometers

This type of piezometer is divided into two types, bonded and unbonded. In 1928 Roy Carlson invented the transducer used in the unbonded electrical resistance piezometers. On the other hand, the bonded type usually consist of semiconductor resistance strain gages. However, that type of strain gage is not exclusive to the bonded electrical resistance piezometers. Bonded resistance strain gage transducers are also available, however they are economically unattractive. The mode of operation of these piezometers is that any change in resistance is directly proportional to the length of the wires. Bonded electrical resistant piezometers are user-friendly, have a short time lag, experience slight interference with construction, are not susceptible to freezing and can measure negative pore water pressures. The unbonded type share the same positive attributes with the bonus of being able to measure temperature.

The electrical components, if subjected to moisture, can result in error. In addition, error can incur at points of electrical connections. Similar to the vibrating wire piezometers, electrical resistance piezometers are susceptible to lightening. In addition, the long-term stability of the bonded type is uncertain.

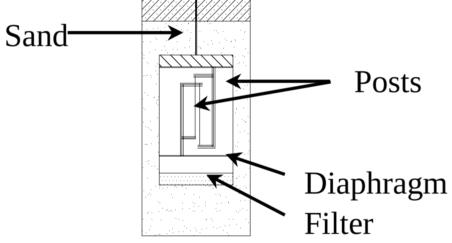

Figure 2.3a Unbonded Electrical Resistance Piezometer (after Dunnicliff, 1988)

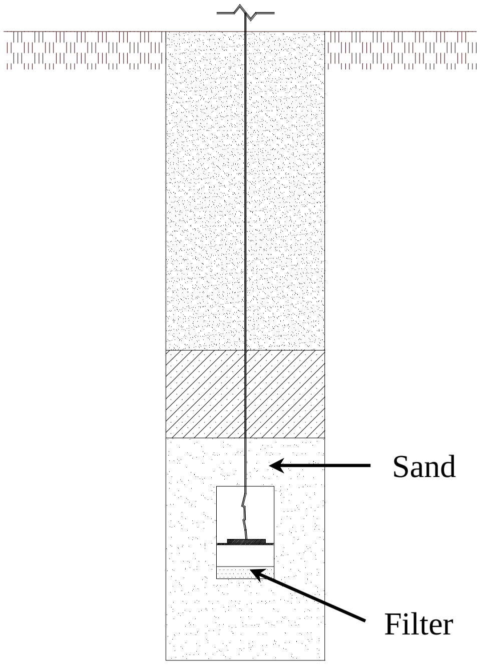

Figure 2.3b Bonded Electrical Resistance Piezometer (after Dunnicliff, 1988)

2.1.4 Twin-tube Hydraulic Piezometers

As its name suggests, twin-tube hydraulic piezometers have two flexible tubes attached to a porous filter element. A pressure gage, whether it is in the form of a Bourdon tube pressure gage, U-tube manometer or electrical pressure transducer, is positioned on the end of each tube. The specific design application is for long-term monitoring of pore water pressures in embankment dams. One of the earliest uses of this type of piezometer was in 1939 when the U.S. Bureau of Reclamation (U.S.B.R) installed them at the Fresno Dam (Sherard, 1981). Hydraulic piezometers have a history of reliability. Furthermore, the reliability of the system can be checked even after installation. This type of piezometer also has the ability to measure permeability. An additional advantageous aspect of this system, when compared to other piezometers, is its capability of flushing the piezometer cavity.

The high cost of automation and the difficulty of installation diminished the popularity of hydraulic piezometers. In fact, in 1978 the U.S.B.R discontinued the use of hydraulic piezometers and opted for pneumatic piezometers because they were easier to operate (Sherard, 1981).

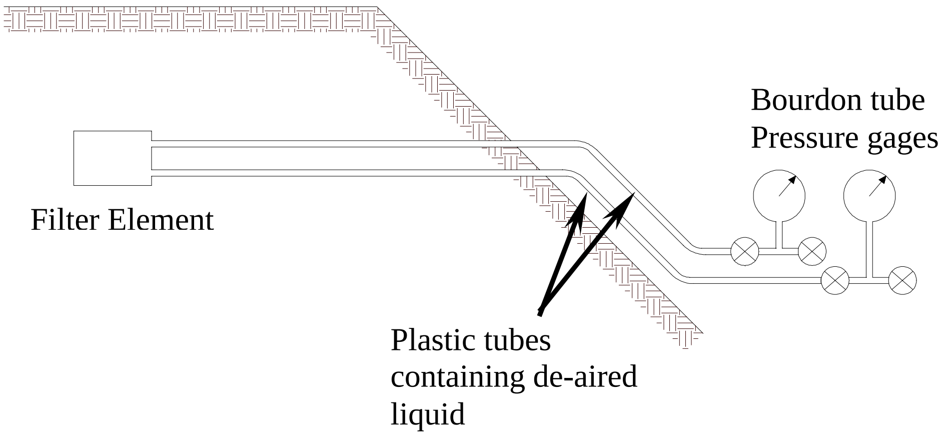

Figure 2.4 Schematic of Twin-tube hydraulic piezometer installed in embankment fill (after Dunnicliff, 1988)

2.1.5 Standpipe Piezometers

Standpipe piezometers, also known as Casagrande piezometers, perform by measuring pore water pressure only at the location of its sealed porous filter component. Water enters the standpipe until it equalizes the pore-water pressure that at the piezometer elevation. The pore pressure is then determined by subtracting the water level from the piezometer subsurface elevation (Holtz & Kovacs, 1981). Standpipe piezometer, are reliable and therefore are sometimes used to substantiate data from other piezometers. Added features include the ability to use the system for sampling of groundwater and measuring permeability.

A major disadvantage of the standpipe piezometer is its presence. It may experience damage from construction equipment and surrounding compaction tends to be substandard. There is a long time lag because a large volume of water is required to register a change in head. Another limitation to the system is that the porous filter is susceptible to clogging.

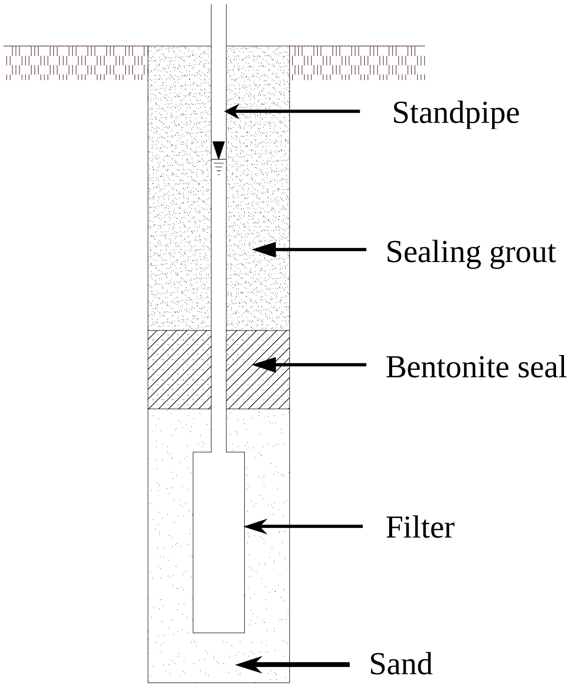

Figure 2.5a Open Standpipe Piezometer (after Dunnicliff, 1988)

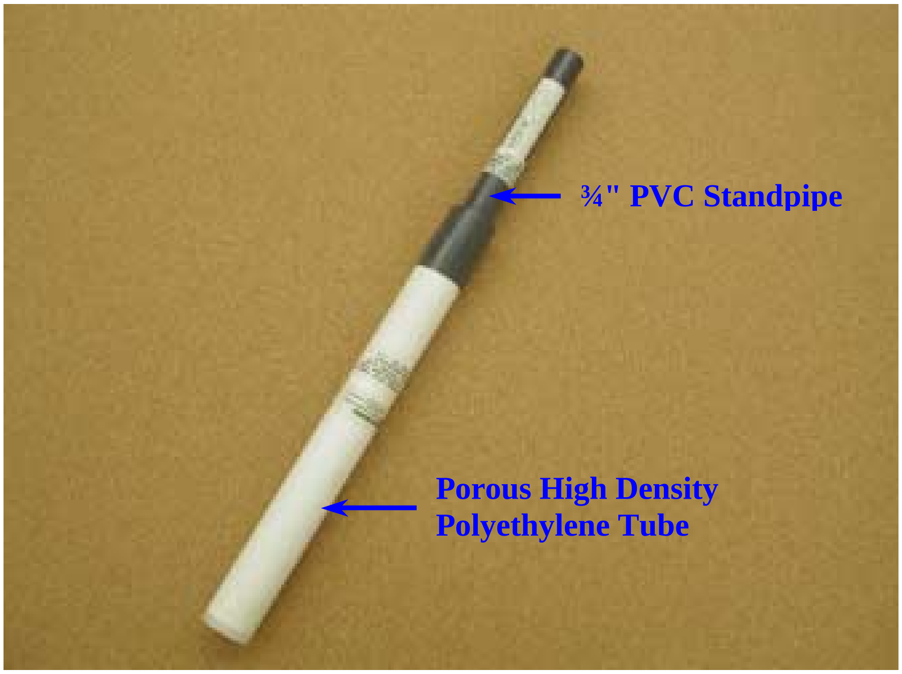

Figure 2.5b Standpipe Piezometer

2.1.6 Fiber-Optic Piezometers

There have been developments of piezometers with fiber-optic technology. One company that has marketed such equipment is ROCTEST. The design of the pressure transducer used in their FOP Series fiber-optic piezometers is based upon the theory of Fabry-Perot interferometry.

The fiber-optic pressure sensors, integrated in the ROCTEST FOP Series, have an unconventional design based on a non-contact measurement of the deflection of a stainless steel diaphragm [Choquet, 2000]. When pressure is applied to the sensor the diaphragm inner surface deflects resulting in changes in the gap between that surface and the end of a stationary optical fiber. The technical term for that gap is the Fabry-Perot cavity. Figure 2.6a highlights the

Fabry-Perot cavity of a typical ROCTEST fiber-optic piezometer with its length ranging from 0 to 9,000 nm. Figure 2.6b is a photo of these sensors.

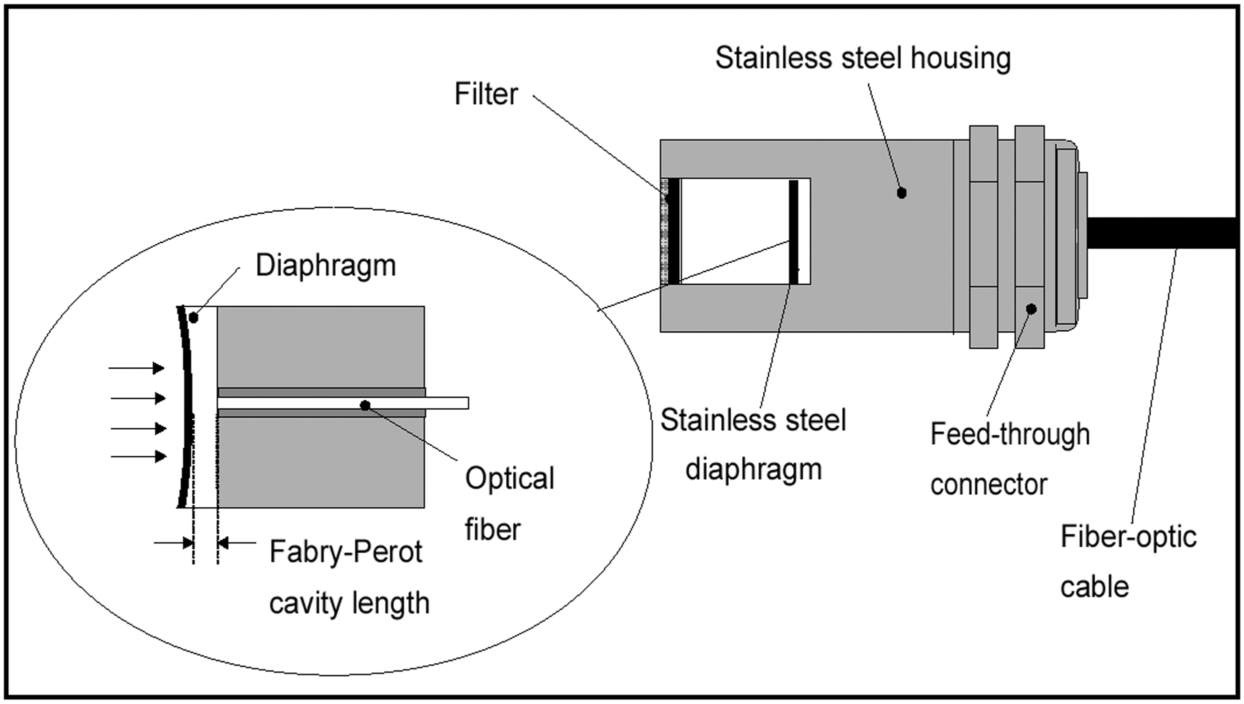

Figure 2.6a Fiber Optic Piezometer depicting the Fabry-Perot cavity length (Courtesy of Roctest)

Figure 2.6b FOP Series Piezometers (courtesy of ROCTEST)

2.2 Fiber-Optic Microbend Loss Theory

The most economical type of fiber optic sensors is the microbend sensor. The costs of these sensors remain low because the light source can be a low cost light emitting diode (LED). Microbend losses occur when small bends in the core-cladding interface of the optical fiber, causes the propagating light intensity to be coupled out of the core (John Powers, 1997). For the purpose of a microbend sensor, microbend losses are incurred mechanically when an external force causes the optical fiber to be squeezed between corrugated plates. Figure 1.2 displays the concept of the microbend sensor.

Microbend sensors have several advantages that set them apart from other types of fiber-optic sensors.

- Simple mechanical assembly
- Low cost and parts count - result of optical and mechanical efficiency
- Fail-safe – either produces a calibrated output signal or fails and produces no light output.

Fiber-optic sensors based on microbend loss theory can also be used to measure parameters such as pressure, temperature, acceleration, speed, flow, magnetic or electric field, and local strain.

Equation (2-1) is the general equation used in modeling and designing microbend sensors. The change in light transmission, ΔT, propagating through a microbend sensor is a function of a constant (*D*) and the environmental change ΔE. In addition, ΔE results in the deformer plates applying a force ΔF to the bent fiber, thereby causing a deformation of the fiber by an amount ΔX (Lagakos, 1987). The deformation is often expressed as the product of the environmental change times the constant or $\Delta X = D\Delta E$.

$$\Delta T = \left(\frac{\Delta T}{\Delta X}\right) D\Delta E \qquad (2\text{-}1)$$

Equation (2-1) written in terms of the force ΔF applied to the bent fiber becomes

$$\Delta T = \left(\frac{\Delta T}{\Delta X} \right) \Delta F \left(K_f + \frac{A_s Y_s}{l_s} \right)^{-1} \qquad (2\text{-}2)$$

Here the terms K_f and $A_s Y_s / l_s$ represent the bent fiber force constant and the force constant involved with changing the length of the deformer spacers. Furthermore, the parameters A_s, Y_s, and l_s are representative of the cross-sectional area, Young's modulus, and length or thickness of the spacer material. In relevance to this research, where pressure is the detected environmental change, equation (2-2) becomes

$$\Delta T = \frac{\Delta T}{\Delta X} \bullet A_p \left(K_f + \frac{A_s Y_s}{l_s} \right)^{-1} \Delta P \qquad (2\text{-}3)$$

where the change in pressure is denoted by ΔP. Therefore if $A_s Y_s / l_s$ is so small such that the effective conformity of the pressure sensor is determined by that of the bent fiber, then equation (2-3) results in equation (2-4)

$$\Delta T = \frac{\Delta T}{\Delta X} \bullet A_p k_f^{-1} \Delta P \qquad (2\text{-}4)$$

where $$k_f^{-1} = \frac{\Lambda^3}{3\pi Y d^4 \eta} \qquad (2\text{-}5)$$

When designing a microbend fiber optic sensor, equation (2-5) is an important parameter. The term k_f^{-1} is recognized as the effective spring constant for the assembled microbend sensor. The effective spring constant is a function of the deformer tooth spacing Λ, the Young's modulus or modulus of elasticity of the glass, Y, the fiber diameter, d, and the number of bends, η (Lagakos, 1987). However, the validity of equation (2-5) remains in effect only for optical fibers with hard coatings.

Chapter 3

Testing Program

The testing program consisted of two main steps. First, a basic sensor had to be designed that was inexpensive and able to detect pore water pressures for several applications. Second, this basic design had to be thoroughly evaluated in the lab under several loading conditions.

3.1 Sensor Design

Fiber optic sensors (FOS) based on the microbend theory have been designed and constructed for various FDOT needs since 1992 (Cosentino et al, 1994, Cosentino and Grossman, 1996, 1997, 2000). The basic process of building FOSs involved placing the microbenders and optical fiber between two thin fiberglass plates [Eckroth, 1999]. For the previous work those plates were long rectangular shapes, for this research sensors were constructed using a circular geometry, to enable their placement in soils.

A basic sensor consisted of two circular plates, with microbending mesh and optical fiber sandwiched between them (Figure 3.1). The mesh was glued to one of the plates and optical fiber placed on two "highlighted" mesh tracks with a 180° loop allowing for the fiber return. The second fiberglass plate was placed on top and the outer edges sealed with a waterproof sealant. The optical fiber lead ends were fitted with ST type connectors for protection and to allow light to pass from a light source. Figure 3.2 shows 1.25 and 2.25 inch diameter completed sensors. A detailed construction procedure is provided in the Appendix A.

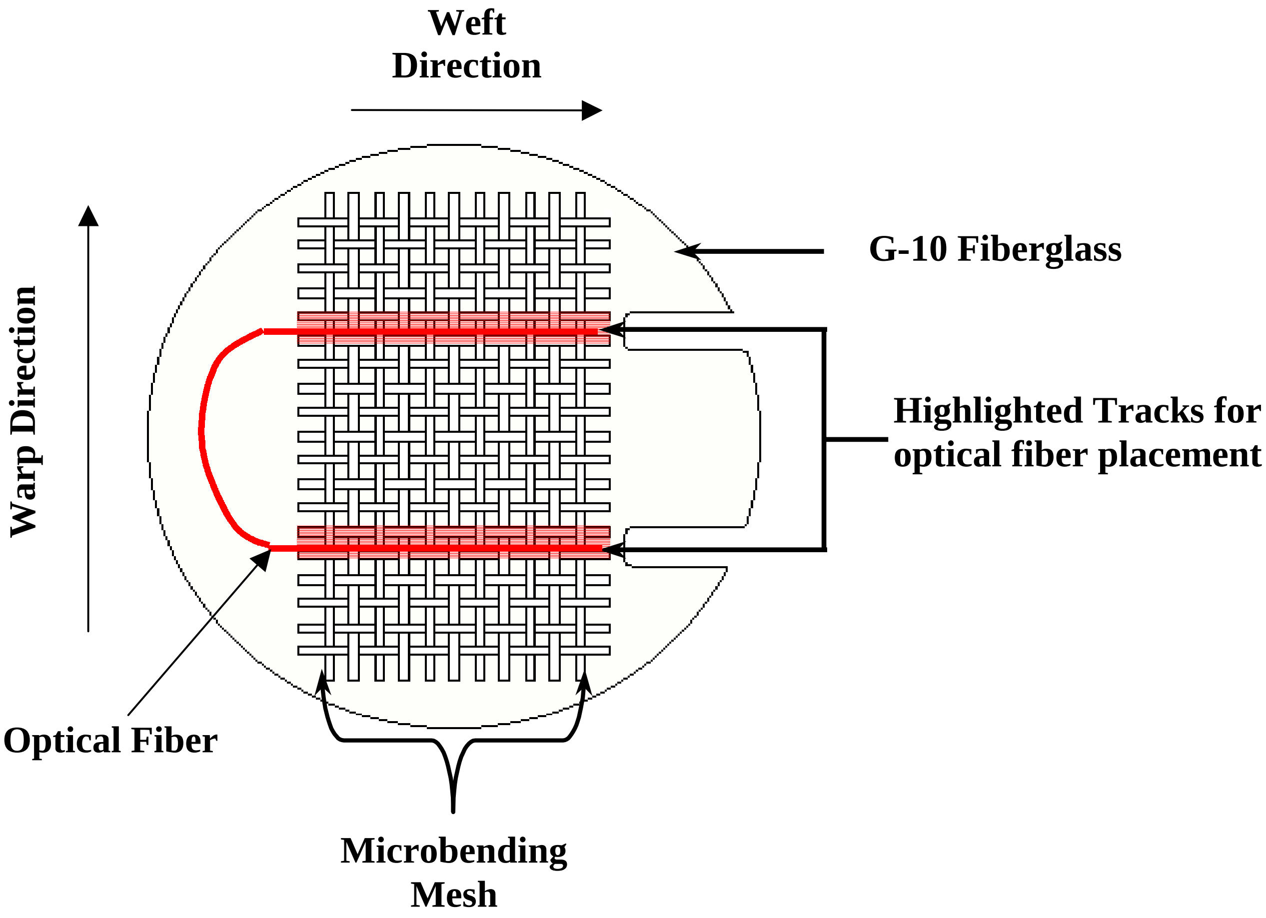

Figure 3.1 Sketch of Mesh on G-10 Prior to Optical Fiber Placement

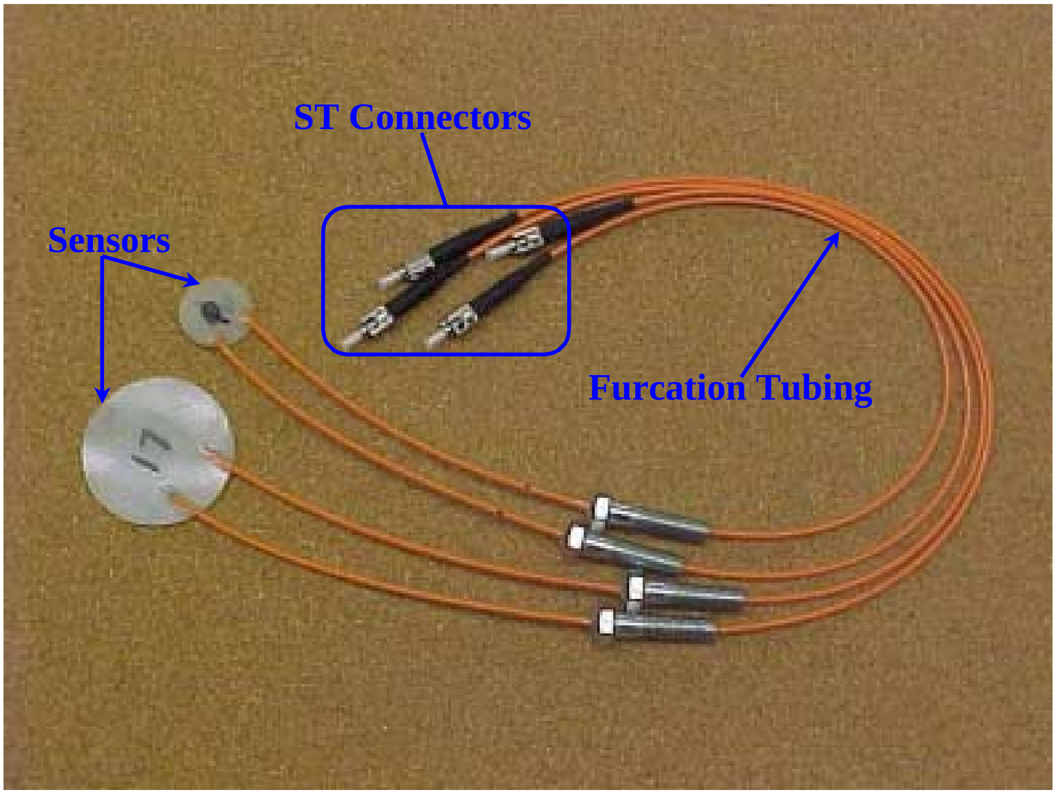

Figure 3.2 Completed 2.25 and 1.25 inch diameter sensors (Note: the bolts shown were used to test the sensors in the hydrostatic testing chamber)

Corning® 50/125/250 multimode optical fiber was chosen for FOS construction since it has been used in the past research by Cosentino and Grossman (1996, 1997, 2000). The numbers identifying the fiber denote a 50-µm inner diameter glass fiber core, glass cladding diameter of 125-µm and a 250-µm outer diameter of acrylate coating. Figure 3.3 is a scanning electron microscope photo that displays two of the annuli that make up Corning® 50/125/250, the cladding and the acrylate. The glass core is within the cladding and is not visible, however, the acrylate coatings, which consists an inner soft layer that absorbs energy dunring bending and a hard cover to protect the fiber, are depicted. Taylor (1995) showed that Corning® 50/125/250 subjected to a microbending period of 1.06 mm would produce the most sensitivity. Therefore, the microbending materials selected had periods close to the optimum period.

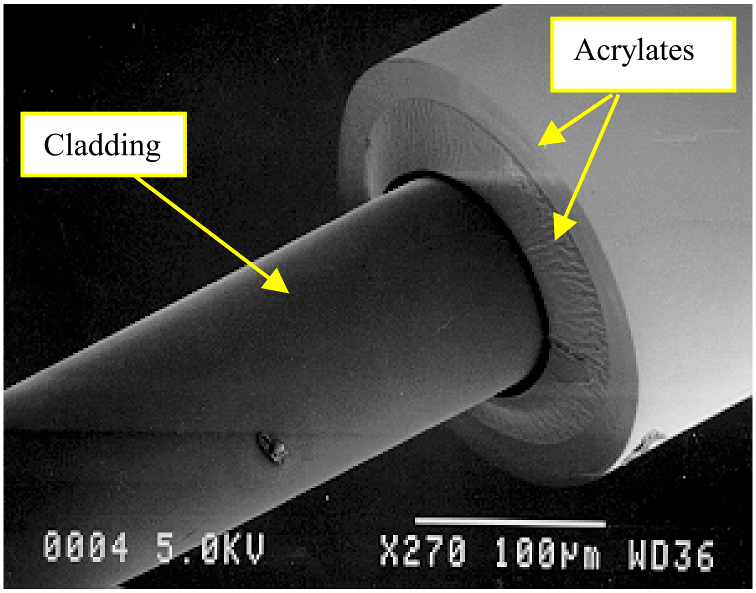

Figure 3.3 Scanning Electron Microscope Photo of Corning's Optical Fiber Glass Cladding Protruding from the two different Acrylate Coatings

3.2 Sensor Characterization

A total of 40 sensors were built for the testing program. An opto-electronics box was designed and constructed to allow for the characterization of the sensors. This device, approximately 4 x 6 x 2 inches, housed a light emitting diode (LED), a photo diode and other circuitry. The LED transmits a light signal through the fiber and the photo diode converts the returned light signal to voltage. Therefore, when pressure was applied to the sensor, the microbenders produce a deformation in the optical fiber creating a loss of light and a corresponding voltage decrease. The light loss was correlated to the applied pressure thereby resulting in sensor calibration.

3.2.1 Sensor Components used as Variables in Testing Program

Four sensor components were varied during the course of FOS testing program to note their effects, on the sensitivity and the calibration curves of the sensors. Those parameters included the G-10's thickness and diameter, the mesh type and the sealant type.

The two outer plates of the sensor configuration were cut from a sheet of G-10. This material produced, in a variety of thicknesses, is a glass epoxy laminate, having 10 ounces of glass per square yard. The G-10 used in this research was 10 and 20 mils thick. Varying the diameter of the G-10 essentially changed the number of microbenders. There were 24 microbenders in the 2.25-inch diameter sensors and 11 in the 1.25-inch diameter sensors.

Polypropylene and Fluortex®ETFE were the meshes used to act as microbenders in the sensors. Both meshes have a plain weave consisting of an over-and-under pattern. However they differ in stiffness and in the mesh count (number of threads per linear inch). The polyproylene has a mesh count of 24 x 20 with the former of the two numbers being in the weft direction and the latter in the warp direction (Castro, 1997). Conversely, the Fluortex® has a mesh count of 22.6 per inch in both weft and warp directions.

Two sealants, five minute epoxy and 3M™ Marine Adhesive Sealant Fast Cure 5200 (3M™ 5200), were evaluated. Preliminary testing on sensors indicated that the 3M™ 5200 provided a better seal than the epoxy especially around the leads. This testing also revealed that there were no major differences on the sensor's sensitivity between the two sealants. Therefore, the 3M™ 5200 was used in all subsequent sensor construction.

Once the 3M™ 5200 was chosen as the sealant, two thicknesses, diameters and mesh types were used in the evaluation, yielding twenty sensors of each diameter. Five sensors for each mesh, thickness and diameter were constructed. Table 3.1 shows the matrix of sensor variables that resulted. For each of the 8 groups, five sensors were constructed to produce the 40 sensors.

Table 3.1 Sensor Testing Variable Combinations

G-10 Diameter (inches)	G-10 Thickness (mils)	Mesh	No. of Microbenders	Average Thickness (inches)
2.25	20	Polypropylene	24	0.073
2.25	10	Polypropylene	24	0.052
2.25	20	FluortexETFE	24	0.064
2.25	10	FluortexETFE	24	0.043
1.25	20	Polypropylene	11	0.073
1.25	10	Polypropylene	11	0.052
1.25	20	FluortexETFE	11	0.064
1.25	10	FluortexETFE	11	0.041

3.2.2 Compression Testing

Initial testing of the FOSs was conducted using an unconfined compression machine (UCC) with a load cell signal conditioner, an opto-electronics box and a voltmeter as seen in Figure 3.4. To allow for direct compression of the sensor, two-inch diameter loading platens with a ball bearing and rubber bands configuration was incorporated in the machine setup. A stiff piece of rubber was adhered to the bottom platen with spray adhesive to provide a known contact area for the sensors. During the testing procedure sensors were placed on a ⅛″ thick aluminum plate for levelness, and hand loaded at a rate of 2.8 mil/rev (71.12 μm/rev).

Each sensor was statically loaded until 30 percent light loss was observed, unloaded, allowed to "recover" for five minutes and then reloaded. That procedure was carried out for a total of five cycles. Measurements were also taken during the rebound phase of the first two cycles. The load, at ten percent increments of light loss, was recorded from the digital display and converted to an average pressure. Subsequently, the results yielded a curve of light loss versus pressure.

3.2.3 Pressure Vessel Testing

A six-inch diameter by 29-inch long acrylic pressure vessel was used for the second phase of the sensor characterization process. The vessel, designed by Eckroth (1999), had two aluminum end caps with bore through holes to accommodate the sensors for testing. Eckroth (1999) connected the sensor leads to the opto-electronics equipment using bulkhead connectors, however, with the use of ST connectors for this research, the existing holes in the end caps required enlargement in order to fit the necessary bolts. This test was conducted to simulate a hydrostatic loading condition on the sensor. There were two sets of data desired of the sensor characterization process that included transmitted light loss and applied pressure.

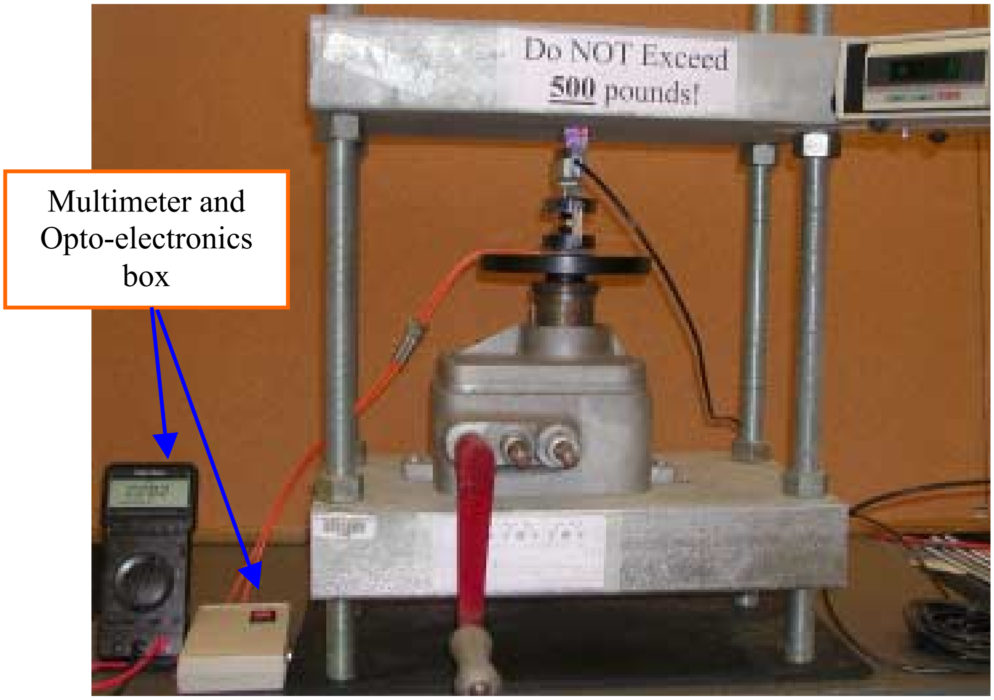

Figure 3.4 Static Compression Testing of Sensor with mulitmeter displaying voltage from opto-electronics box

3.2.3.1 Pressure Gauge

A Bourdon tube Heise® gage (0 to 250 psi) in conjunction with a Validyne DP15TL diaphragm pressure transducer was used to directly measure the internal pressure in the pressure chamber. Validyne's Model CD12 transducer indicator acted as the signal conditioner interface with the data acquisition system for the DP15TL. Prior to testing, the pressure gauge was calibrated with the CD12 in order to correlate the pressure readings with the voltage output received by the data acquisition software from the signal conditioner. This particular system was calibrated for 1 volt equal to twenty psi.

3.2.3.2 Data Acquisition Software

National Instruments™ LabVIEW® the data acquisition software was programmed to record the data from the pressure vessel testing of the FOSs. With National Instruments™ BNC-2120 shielded connector block, analog inputs from the opto-electronic boxes and the CD12 were directly interfaced with LabVIEW®. Three channels were set up in LabVIEW® to collect the applied air pressure, and voltage outputs simultaneously from two sensors. Figure. 3.5 displays the LabVIEW® screen shown during testing. These measurements were taken at a rate of 50 scans over five seconds with each scan taken at 0.10 seconds. The pressure increments at which the measurements were recorded were 2.5 and 10 psi, depending upon the degree of sensitivity of the sensor.

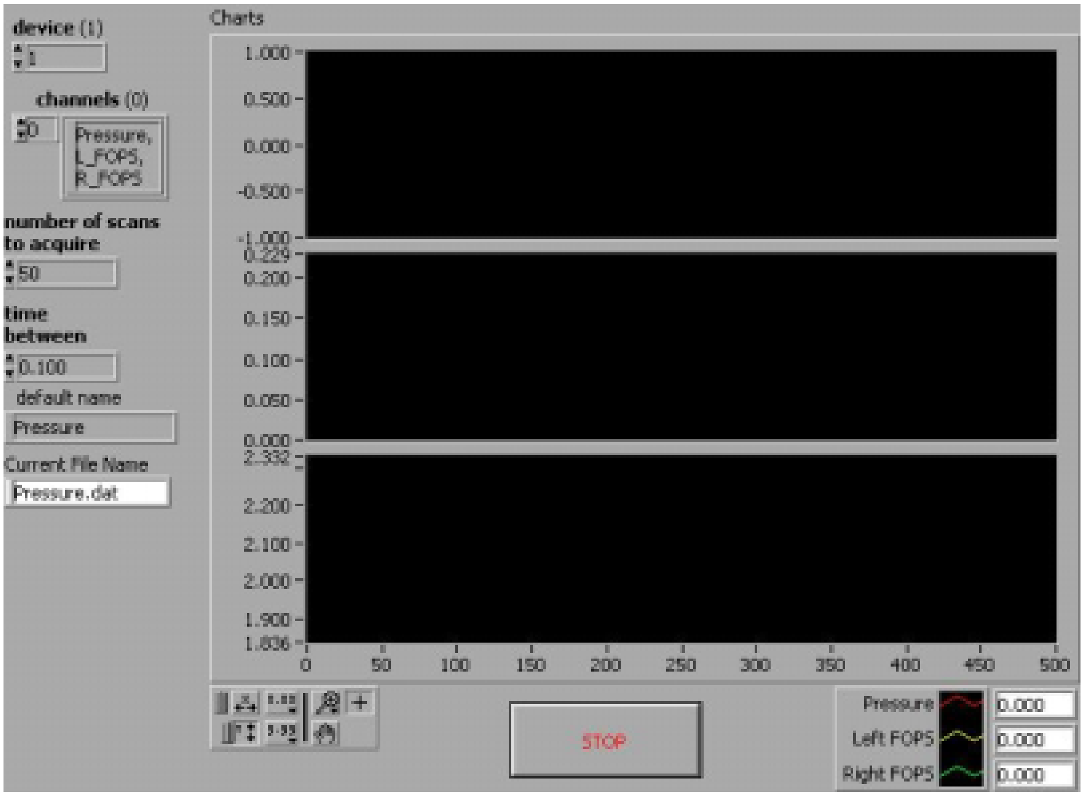

device (1): 1

channels (0): 0

Pressure,
L_FOPS,
R_FOPS

number of scans to acquire: 50

time between: 0.100

default name: Pressure

Current File Name: Pressure.dat

Pressure: 0.000

Left FOPS: 0.000

Right FOPS: 0.000

Figure 3.5. LabVIEW® Display Screen for Data Acquisition during Hydrostatic Testing of Sensors

Chapter 4

Presentation and Discussion of Results

4.1 Introduction

To properly present the results obtained during this research, there are several technical terms that require clarification. ***Sensitivity*** was defined as the average slope of the linear potion of the Light Loss versus Pressure curve. A sensor producing a steep slope was identified as having a high sensitivity because it took very little pressure to produce a large light loss. A sensor that produced a flatter slope was construed as having a low sensitivity because it required higher pressures to produce a smaller light loss. The maximum distance between the calibration curve and a line drawn to intersect that curve at a specified point is typically defined as ***Linearity*** and presented as a percentage of the ***full-scale*** (% FS). The location for the full scale is based on the designers' choice for the useful range of the sensor. This process is shown pictorially in Figure 4.1.

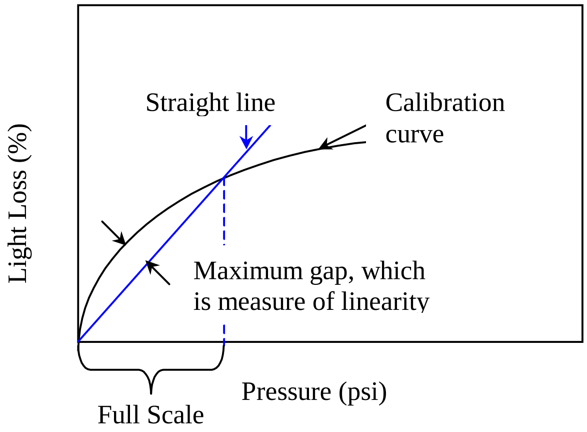

Figure 4.1 Determination of Linearity as a percent of full-scale.

4.2 Sensor Calibration

4.2.1 Axial Tests with a Rubber Cushion on top and Aluminum on the bottom

From the batch of 40 sensors constructed for the testing program 16 sensors were tested in the hand operated static compression mode with one piece of rubber over the sensors as it base rested on a rigid aluminum pedestal. This testing was conducted to simulate possible stress concentrations from using the sensor in field applications. One piece of rubber was used to allow the optical leads sit properly under the loading platens. If no cushioning had been provided, the leads, which are thicker than the circular portion of the sensor, would have been subjected to high shear stresses, consequently failing the fiber. The resulting data from these tests are presented Appendix B.

4.2.2 Axial Tests with Rubber Cushions on top and bottom

From the batch of 40 sensors constructed for the testing program the same 16 sensors were tested in the hand operated static compression mode with rubber pads on both sides of the sensors. This testing was performed to determine if it could be used as a possible calibration process for the sensors. The rubber cushions would prevent stress concentrations from occurring during loading. Results from this testing are to be compared to the hydrostatic testing results. The data from these tests are presented Appendix C.

4.2.3 Hydrostatic Tests

From the batch of 40 sensors constructed for the testing program the same 16 sensors were tested in the pneumatically in compression using the testing chamber detailed in Section 3.3.2. This testing was performed to determine if it could be used as a possible calibration process for the sensors. It is more complex than the axial tests with two rubber cushions, however, it will eliminate stress concentrations from occurring on the sensor during loading. The data from these tests are presented Appendix D.

4.3 Analysis

4.3.1 General Discussion

Upon evaluation of the curves shown in Appendices B, C and D, it can be seen that they have a nonlinear shape, similar to the stress-strain behavior of many soils. The initial portion of the curve is relatively linear, followed by a curve that becomes asymptotic to a line at about 80 percent light loss.

These curves were analyzed using numerous linear and nonlinear curve-fitting techniques. The linear analyses produced a larger than the nonlinear analyses. A general discussion of both follows.

4.3.2 Sensor Reliability

Six “best-fit” or calibration curves were developed for each sensor’s data producing, calibrations ranging from a linear to a sixth order polynomial. The reliability of each curve was documented using the coefficient of determination (R^2) in order to assist with the selection process of a calibration curve for each of the sensors (Ott, 1984). A summary of the R^2 values is shown in Tables 4.1, 2 and 3, where the results represent the data from the axial test with one rubber cushion, two rubber cushions and hydrostatic testing, respectively. The R^2 values were also plotted versus the degree of the best-fit curves and are presented in Figures 4.2, 4.3 and 4.4. An evaluation of the data from all 16 sensors showed that a 2nd or 3rd order polynomial curve produced realistic fits of the data.

From the average values summarized in Tables 4.1, 4.2 and 4.3, it was observed that the ETFE microbending mesh produces a more reliable sensor than the polypropylene mesh. This finding is most obvious from the linear analysis, but is evident for all levels of the analysis.

Minor differences were noted as the sensor diameter varied. The R^2 values for the linear analysis of the 2.25-inch diameter sensors were slightly lower than those for the 1.25-inch diameter sensors. However, the R^2 values from the 3^{rd} order polynomial fit based on the most accurate test, (i.e. the hydrostatic tests) showed no difference between the two diameters.

Table 4.1 Summary of Regression Analysis for Axial Testing with 1 Piece of Rubber on Top of Sensors

Sensor No.	Diameter (inches)	Cover Plate (mils)	Mesh Type	Coefficient of Determinination R^2					
				1st Deg	2nd Deg	3rd Deg	4th Deg	5th Deg	6th Deg
1	2.25	20	PP	0.77	0.94	0.98	0.99	0.99	0.99
2	2.25	20	PP	0.74	0.88	0.92	0.94	0.95	0.95
7	2.25	10	PP	0.92	0.99	0.99	0.99	0.99	0.99
8	2.25	10	PP	0.9	0.99	0.99	0.99	0.99	0.99
12	2.25	20	ETFE	0.94	0.99	0.99	0.99	0.99	0.99
13	2.25	20	ETFE	0.96	0.97	0.98	0.98	0.98	0.98
17	2.25	10	ETFE	0.95	0.98	0.98	0.98	0.98	0.98
18	2.25	10	ETFE	0.94	0.96	0.97	0.97	0.97	0.97
21	1.25	20	PP	0.84	0.91	0.91	0.91	0.91	0.91
23	1.25	20	PP	0.91	0.95	0.95	0.95	0.95	0.95
26	1.25	10	PP	0.82	0.94	0.96	0.96	0.96	0.96
27	1.25	10	PP	0.92	0.99	0.99	1.00	1.00	1.00
33	1.25	20	ETFE	0.95	0.99	0.99	0.99	0.99	0.99
34	1.25	20	ETFE	0.96	0.96	0.98	0.99	0.99	1.00
36	1.25	10	ETFE	0.91	0.96	0.96	0.96	0.96	0.96
37	1.25	10	ETFE	0.96	0.97	0.99	1.00	1.00	1.00

Average PP	0.85	0.95	0.96	0.97	0.97	0.97
Average ETFE	0.95	0.97	0.98	0.98	0.98	0.98
Percent Differen	90%	98%	98%	98%	98%	98%

Table 4.2 Summary of Regression Analysis for Axial Testing with 2 Pieces of Rubber on Top of Sensors

Sensor No.	Diameter (inches)	Cover Plate (mils)	Mesh Type	Coefficient of Determinination R^2					
				1st Deg	2nd Deg	3rd Deg	4th Deg	5th Deg	6th Deg
1	2.25	20	PP	0.85	0.98	0.99	0.98	0.99	0.99
2	2.25	20	PP	0.76	0.91	0.96	0.97	0.98	0.98
7	2.25	10	PP	0.83	0.91	0.94	0.96	0.97	0.99
8	2.25	10	PP	0.81	0.87	0.93	0.98	0.99	0.99
12	2.25	20	ETFE	0.98	0.98	1.00	1.00	1.00	1.00
13	2.25	20	ETFE	0.96	0.99	0.99	0.99	0.99	0.99
17	2.25	10	ETFE	0.93	0.99	0.99	0.99	0.99	0.99
18	2.25	10	ETFE	0.99	0.99	1.00	1.00	1.00	1.00
21	1.25	20	PP	0.76	0.94	0.98	0.98	0.98	0.98
23	1.25	20	PP	0.89	0.97	0.98	0.98	0.98	0.98
26	1.25	10	PP	0.74	0.91	0.94	0.94	0.95	0.95
27	1.25	10	PP	0.95	1.00	1.00	1.00	1.00	1.00
33	1.25	20	ETFE	0.95	0.98	0.98	0.98	0.98	0.98
34	1.25	20	ETFE	0.96	0.96	0.99	0.99	0.99	1.00
36	1.25	10	ETFE	0.93	0.97	0.98	0.98	0.98	0.98
37	1.25	10	ETFE	0.98	0.98	0.99	1.00	1.00	1.00

Average PP	0.82	0.94	0.97	0.97	0.98	0.98
Average ETFE	0.96	0.98	0.99	0.99	0.99	0.99
Percent Differen	86%	96%	97%	98%	99%	99%

Table 4.3 Summary of Regression Analysis for Hydrostatic Testing of Sensors

Sensor No.	Diameter (inches)	Cover Plate (mils)	Mesh Type	Coefficient of Determinination R^2					
				1st Deg	2nd Deg	3rd Deg	4th Deg	5th Deg	6th Deg
1	2.25	20	PP	0.87	0.97	0.97	0.98	0.99	0.99
2	2.25	20	PP	0.75	0.92	0.96	0.97	0.97	0.97
7	2.25	10	PP	0.98	0.98	0.98	0.98	0.99	0.99
8	2.25	10	PP	0.92	0.94	0.99	1.00	1.00	1.00
12	2.25	20	ETFE	0.96	1.00	1.00	1.00	1.00	1.00
13	2.25	20	ETFE	0.97	0.97	0.99	0.99	0.99	0.99
17	2.25	10	ETFE	0.98	0.99	1.00	1.00	1.00	1.00
18	2.25	10	ETFE	0.99	0.99	1.00	1.00	1.00	1.00
21	1.25	20	PP	0.96	0.99	0.99	0.99	0.99	0.99
23	1.25	20	PP	0.92	0.98	0.99	0.99	0.99	0.99
26	1.25	10	PP	0.96	0.98	0.98	0.99	0.99	0.99
27	1.25	10	PP	0.99	0.99	1.00	1.00	1.00	1.00
33	1.25	20	ETFE	0.99	0.99	0.99	1.00	1.00	1.00
34	1.25	20	ETFE	0.98	0.99	0.99	1.00	1.00	1.00
36	1.25	10	ETFE	0.98	0.98	0.99	0.99	0.99	0.99
37	1.25	10	ETFE	0.98	0.98	1.00	1.00	1.00	1.00

Average PP	0.92	0.97	0.98	0.99	0.99	0.99
Average ETFE	0.98	0.99	1.00	1.00	1.00	1.00
Percent Differen	94%	98%	99%	99%	99%	99%

The data shown in Figure 4.2 contains the largest scatter of the three, indicating that using one piece of rubber during the loading process may induce stress concentrations that adversely affect the calibration curves. Figure 4.3 shows less scatter than Figure 4.2, but more scatter than the hydrostatic results. Therefore, cushioning the sensor on both sides improves the reliability, however, field conditions with stress concentrations may yield data similar to that shown in Figure 4.2. The notable improvement of the data in Figure 4.3 indicates that hydrostatic testing would be preferred for calibrating sensors. Noting that the results from Sensor 1 are less reliable than those from the remaining sensors, it may also be used to determine the quality of the sensors.

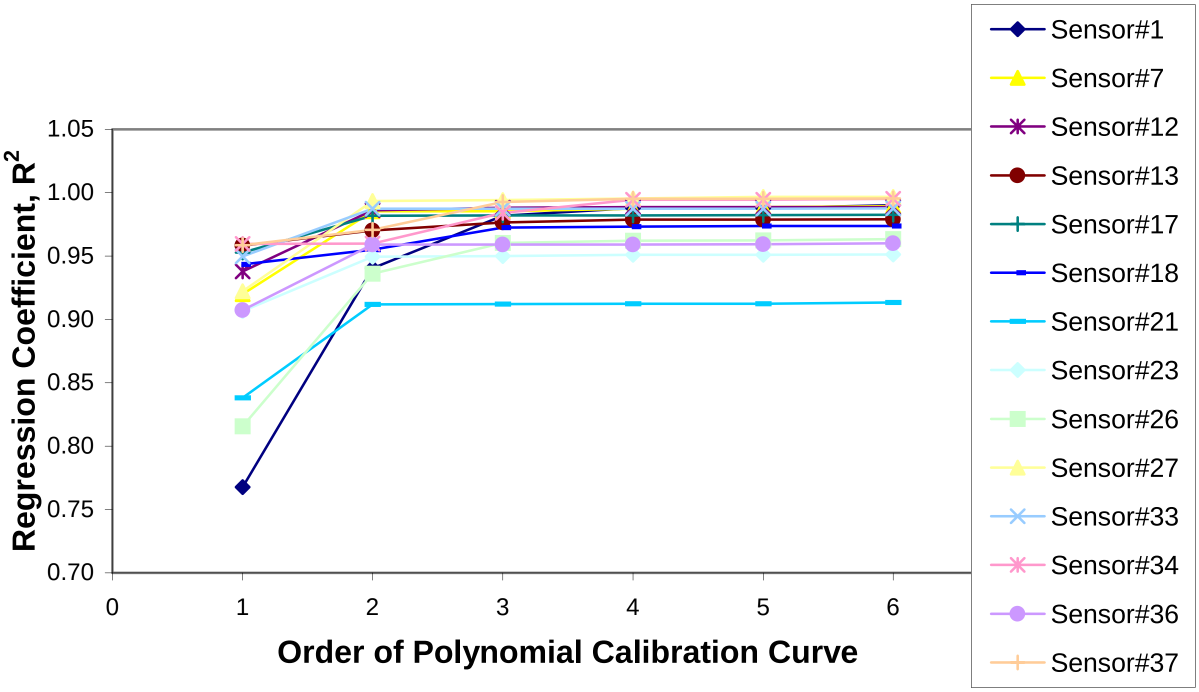

Figure 4.2. Regression coefficient R^2 vs. order of polynomial, axial testing with one contact side covered with rubber

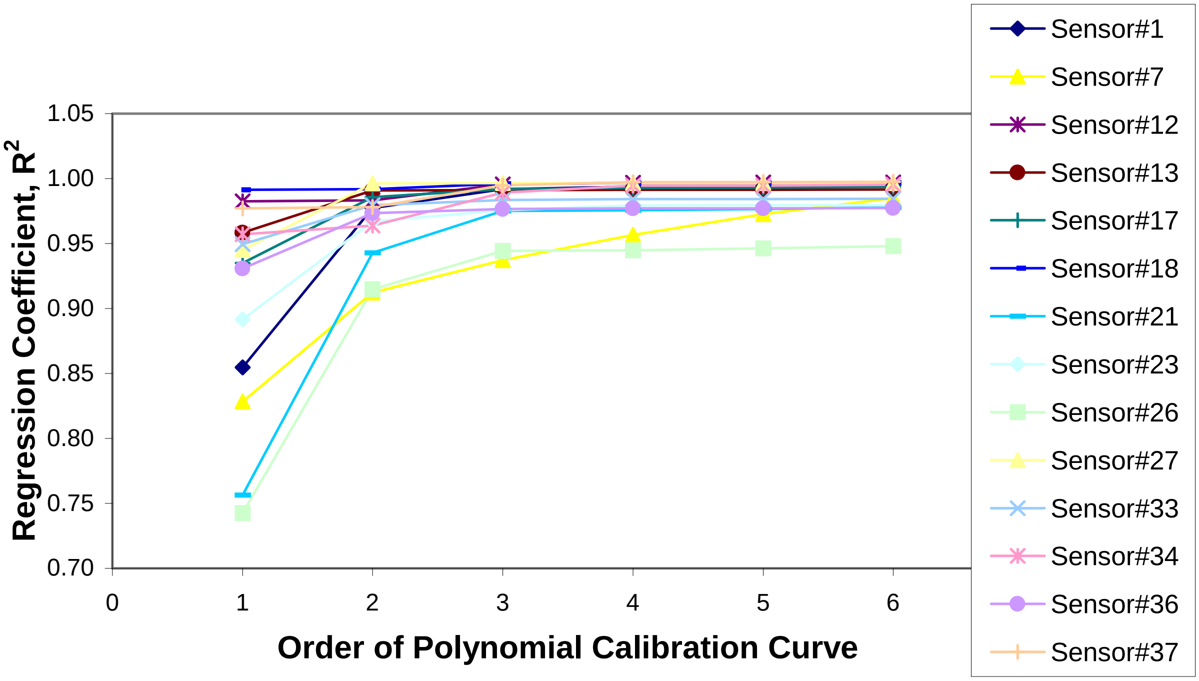

Figure 4.3. Regression coefficient R^2 vs. order of polynomial, axial testing with both contact sides covered with rubber

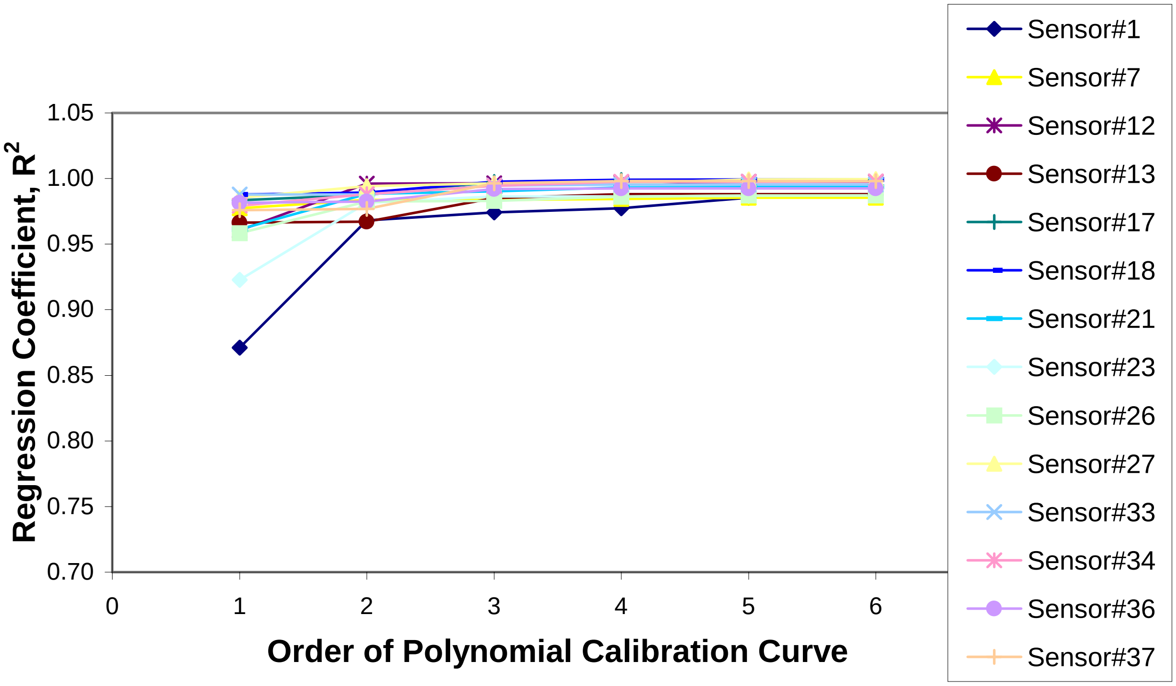

Figure 4.4. Regression coefficient R^2 vs. order of polynomial, hydrostatic testing

4.3.3 Effects of Variables on Sensor Performance

To make conclusions concerning the effects of the variable of diameter, cover plate thickness and mesh type the hydrostatic testing was results were used, since they produced the most reliable data of the three testing techniques.

4.3.3.1 Effects of Sensor Diameter

The 2.25-inch diameter sensors, or the sensors having 24 microbenders, displayed a smaller usable pressure range than the 1.25-inch diameter sensors (11 microbenders). The smaller sensors had a better working range than the larger sensors when evaluating the results at 40% light loss. This range was nearly double that of the larger sensors.

4.3.3.2 Effects of Cover Thickness

Based on linear regression analyses, the 20-mil thick fiberglass cover plates had a greater effect on the polypropylene sensors than the ETFE sensors. For these sensors the thicker 20-mil covers produced lower R^2 values than the 10-mil covers. There was no discernable difference between the 10 and 20 mil covers for the ETFE sensors. .

4.3.3.3 Effects of Mesh Material Type

The sensors constructed with the Fluortex® ETFE microbending mesh produced more reliable calibration curves than those constructed with polypropylene mesh. This was observed with the R^2 values for the first, second and third order calibration curves from the hydrostatic testing. Based on the linear calibrations, the lowest R^2 value for sensors having polypropylene mesh was 0.75 for the hydrostatic testing. Whereas the lowest R^2 value from the linear calibrations, for sensors having ETFE mesh was 0.96. There was, on average for the linear model, a 6 percent improvement in R^2 for the sensors having ETFE mesh. For the second and third order curve this improvement decreased to about 2 percent.

The polypropylene mesh was also observed to have an effect on the mechanics of the sensor. During hydrostatic testing several of the FOPS having polypropylene mesh, in conjunction with the 10-mil outer plates, could only be tested for one or two cycles. A strange phenomenon occurred where the plates became somewhat concave during the application of pressure and convex during pressure release. In fact only one sensor with that combination was able to provide enough data for statistical analysis for the hydrostatic testing.

4.3.3.4 Effects of Loading Condition

With hydrostatic testing pressure is normally applied uniformly to the test subject unlike axial testing where there is a possibility for stress concentrations to incur. Therefore it was expected to witness better results from the sensors that underwent hydrostatic loading conditions. The statistical analysis clearly substantiated that perception with a 48 percent difference between the highest error values for the axial and hydrostatic testing. In addition, the R^2 values of the FOPS that underwent hydrostatic loading were better than those from the FOPS that underwent axial loading. In fact the majority of the values were over 0.9 for the hydrostatic loading condition, even with a first-degree polynomial calibration curve.

4.3.4 Pore Pressure Validation

Upon completion of the sensor characterization, a testing program was developed to determine how the microbend sensors would perform if they were used as pore pressure sensors. The approach used was to test the sensors after they were encased in a porous shell using pneumatic pressures to simulate the pore water pressures. It was assumed that air pressures would more readily detect leaks in the seals at the sensor edges than water.

To accomplish this task, three sensors from the 16 used for the calibration testing were selected for testing. Two sensors were 2.25 inches in diameter and the third 1.25 inches in diameter. All yielded reliable test data, with the most consistent sensors containing the ETFE microbending mesh. To expedite the testing process the smaller diameter sensor was eliminated from the testing. This allowed a single device to be deigned to encase the sensor in further testing. Sensor #1 has a 2.25-inch diameter, with 20-mil thick G-10 fiberglass covers and polypropylene mesh and Sensor # 17, has a 2.25-inch diameter, with 10-mil thick G-10 fiberglass covers and ETFE mesh were selected for testing.

To protect the sensors the encasement, shown in Figure 4.4, was designed, it included a set of aluminum rings covered with a porous plastic. This plastic is a porous polyethylene 1/8” fluid grade produced by Atlas Minerals & Chemicals Inc. A photograph of a sensor, along with the encasing components is shown in Figure 4.5.

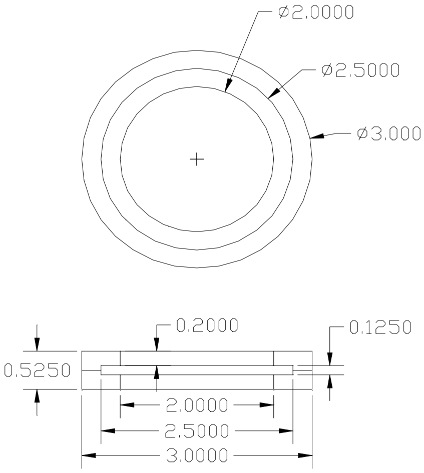

Figure 4.4. Schematic of aluminum rings (all measurements are in inches).

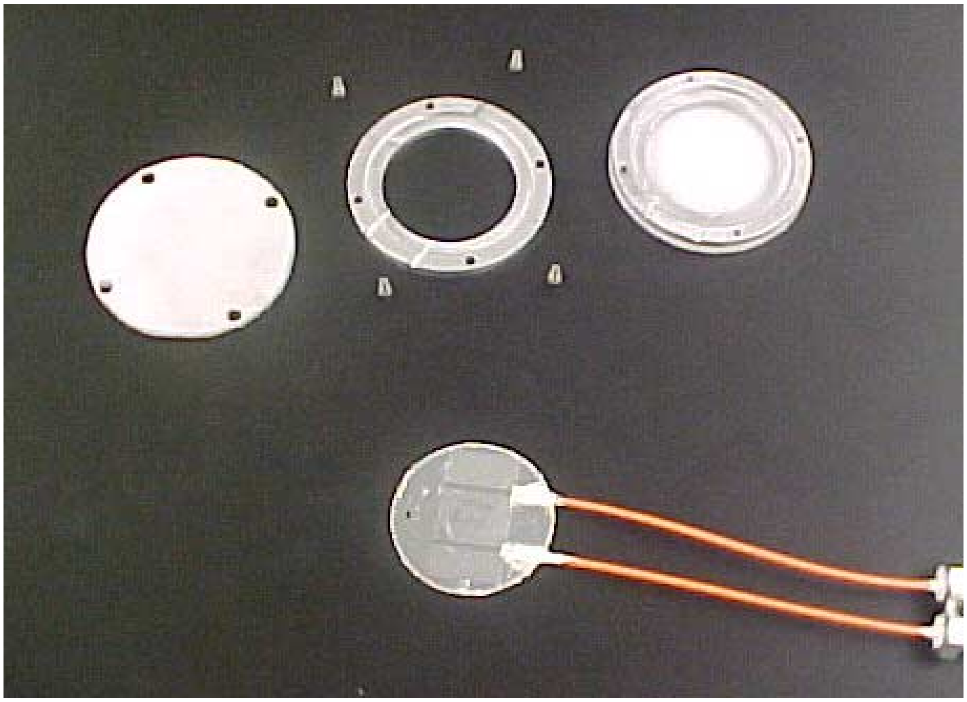

Figure 4.5. Photograph of rings, porous plastic and fiber optic microbend sensor.

The encased sensors were evaluated following the hydrostatic testing procedures outlined in Section 3.2 of this report. Pressures were applied to the chamber and held constant for approximately 1 minute while data was acquired through the Labview® data acquisition system. Figure 4.6 is a photograph of this testing equipment with the encased sensor. Figures 4.7 and 4.8 show data from sensors 1 and 17 respectively. Sensor 1 has a polypropylene microbending mesh and the data have a larger variation than Sensor 17 that has the ETFE mesh. The results when the sensors were subjected to hydrostatic pressure up to 35 psi show no variation between bare and encased sensors. This implies that the protecting/isolating encasing has no negative influence on the performance of the sensor.

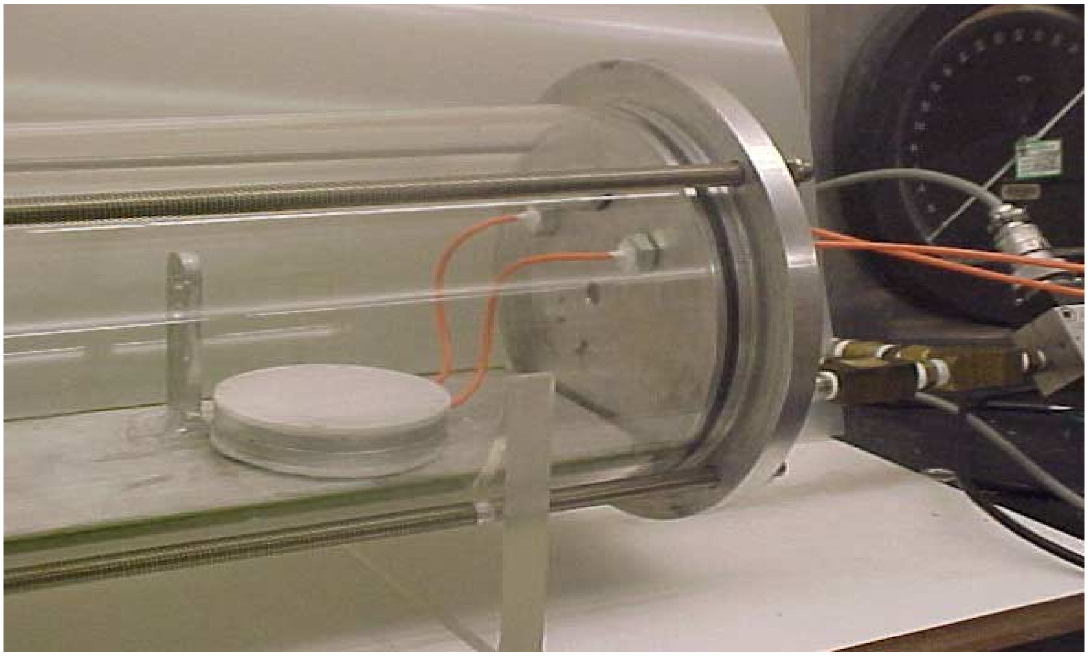

Figure 4.6. Photograph of the encased sensor in the pressure chamber.

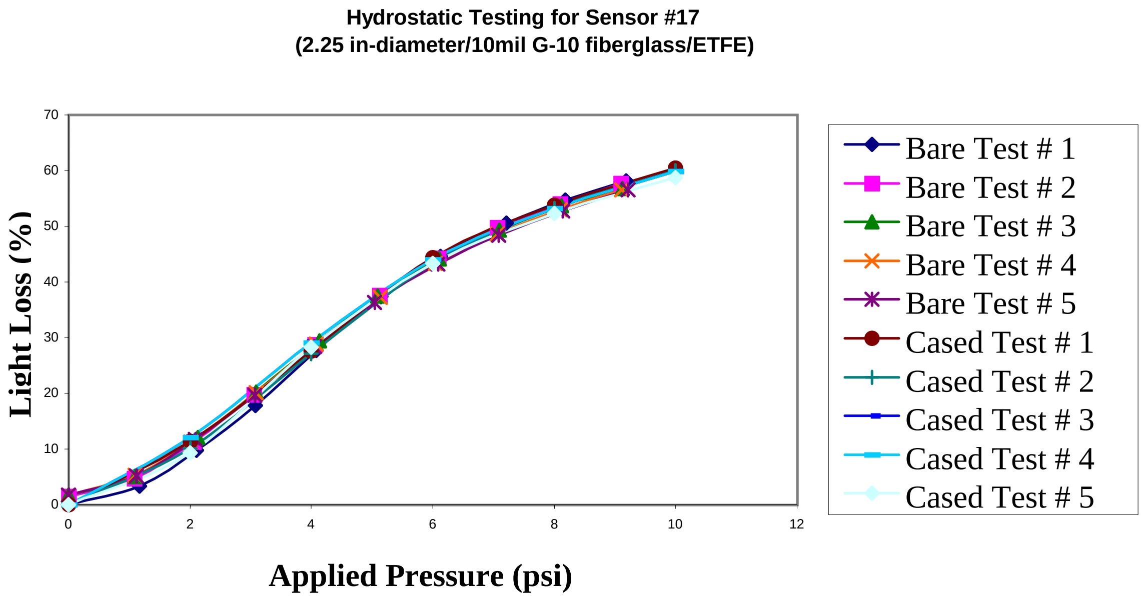

Figure 4.7. Output from hydrostatic testing with and without porous casing on Sensor 17.

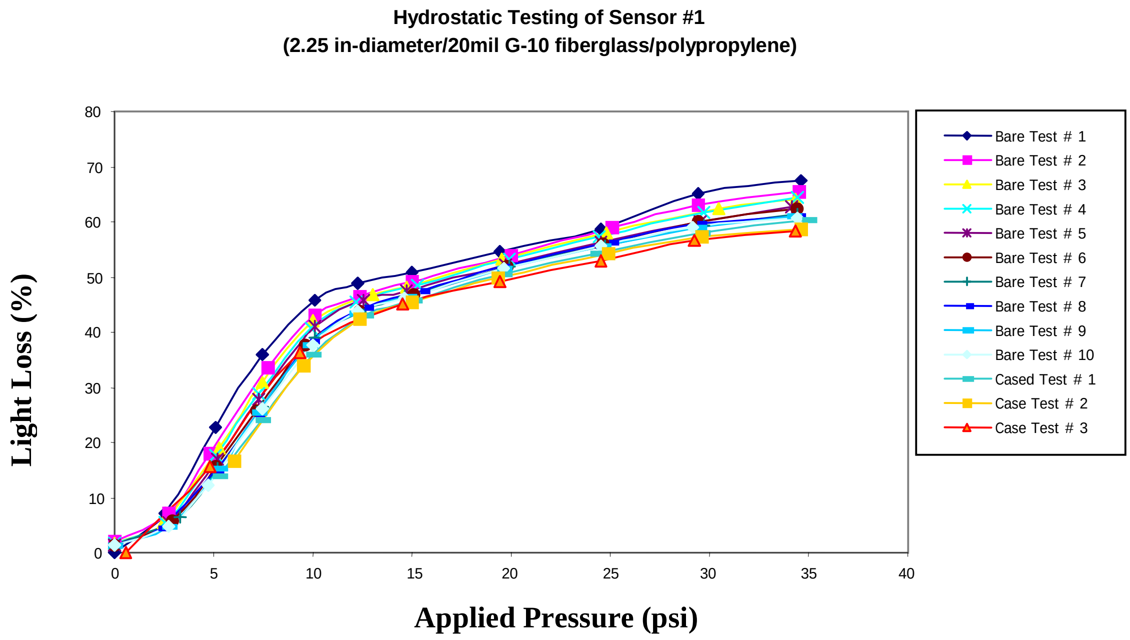

Figure 4.8. Output from hydrostatic testing with and without porous casing on Sensor 1.

Chapter 5

Conclusions and Recommendations

5.1 Conclusions

Four variations of circular fiber optic microbend sensors were successfully built and evaluated for use in geotechnical engineering. They demonstrated working ranges up to 70 psi (490 kPa). Calibration was accomplished using both axial compression and pneumatic pressurization of the specimens.

The testing program showed that pneumatic or hydrostatic testing yielded the best calibration curves. Based on the data obtained it is possible to identify poorly constructed sensors. If hydrostatic testing is not available axial compression with rubber pads on each side of the sensor yielded acceptable calibration curves however, poorly constructed sensors may be difficult to identify.

Axial testing with rubber cushions on one side of the sensor was used to simulate field response to possible stress concentrations. Calibration curves from this process showed more variability than the other two approaches, however, the data was still reliable.

The calibration curves were nonlinear with percent light loss on the y-axis and pressure on the x-axis. The curves have a hyperbolic shape; therefore, linear calibration curves can only be used to predict light losses to 40%. Subsequently, a data analysis procedure was developed that indicated that third order polynomials yielded promising calibration curves with regression coefficients nearing unity.

Of the four construction variables evaluated during the testing mesh stiffness caused the most variation in sensor response. Sensors constructed with the softer ETFE mesh yielded more consistent calibration curves than those constructed from polypropylene. The smaller sensors had a better working range than the larger sensors when evaluating the results at 40% light loss. This range was nearly double that of the larger sensors. The thickness of the sensor cover plates indicated that the 10 mil G-10 fiberglass produced more variability than the 20-mil thickness.

5.2 Recommendations

- If the time interval between tests cannot be controlled during an application of the FOPS, then one should ignore the initial five percent light loss.
- Further tests to investigate the effects of the adhesive on the response of the FOPS.
- These sensors should be evaluated under controlled field conditions to show how they compare to other geotechnical total pressure and pore pressure sensors. This comparison should include accuracy of the signal and ruggedness of the sensor.
- All future sensors should be constructed with the ETFE mesh and tested hydrostatically under pneumatic pressures up to 100 psi.
- Sensors should be constructed in batches of 3 to 5 and lab calibration data should be analyzed using 3rd degree polynomial fits to detect outlier or poorly performing sensors.
- Sensors should be subjected to rigorous durability testing to show how they could be used under severe loading conditions, such as those encountered during pile driving.
- A complete system should be developed for FDOT applications. It should include the sensors, their leads and computer readout.

Chapter 6

References

Ansari, F., editor. 1993. Applications of Fiber Optic Sensors in Engineering Mechanics. ASCE.

Berthod, J.W. 1995. "Historical Review of Microbend Fiber-Optic Sensors," *J. Lightwave Technol*., vol. 13, no. 7, pp. 1193-1199.

Bartholomew, C.L., Murray, B.C., Goins, D.L. (1987), Embankment Dam Instrumentation Manual US Department of the Interior, Bureau of reclamation.

Bishop, A.W., Kennard, M., Penman, A.D. (1960), "Pore Pressure Observations at Selset Dam", Proceedings of the Conference on Pore Pressure and Suction in Soils, Butterworths, London, pp. 91-102.

Brooker, E. W., Lindberg, D. A. (1965) Field Measurement of pore pressure inn high plasticity soils", Engineering effects of moisture changes in soils, proceedings of the international Research and engineering conference on expansive soils, Texas A& M University, college Station, pp57-68.

Bozozuk, M. (1960) "Description and installation of Piezometers for Measuring Pore Water Pressures in Clay Soils", Division of Building Research, National Research Council of Canada, Building Research, Note No. 37.

Casagrande, A., "Piezometers for pore water pressure measurements in clay" Division of Engineering and Applied Physics, Harvard University, Cambridge, MA, unpublished.

Castro, M., (1997) “Investigation of Stresses in a Fiber Optic Traffic Classifying Sensor”, M.S. Thesis, Florida Institute of Technology at Melbourne, Fl.

Choquet, P., Quirion M,. and Juneau, F., (2000) “Advances in Fabry-Perot Fiber Optic Sensors and Instrumentation for Geotechnical Monitoring”, Vol 18, No. 1: Geotechnical News.

Corning Glass Works Telecommunications Product Division. 1988. *At the Core*. Corning, NY.

Cosentino, P.J., Doi, S., Grossman, B.G., Kalajian, E. H., Kumar, G., Lai, P., and Verghese, J. (1994). “Fiber Optic Pore Water Pressure Sensor Development.” *Transportation Research Record Number 1432 Soils, Geology and Foundations, Innovations in Instrumentation and Data Acquisition Systems,* 76 - 85.

Cosentino, P.J., and Grossman, B.G. (1996). “Development and Implementation for a Fiber Optic Vehicle Detection and Counter System.” FDOT Report Agency Contract No. B-9213, School of Civ. Engrg., Florida Institute of Technology, Melbourne, Fl.

Cosentino, P.J., and Grossman, B.G. (1997). “Development of Fiber Optic Dynamic Weigh-in-Motion Systems.” FDOT Final Report Agency Contract No. BA-021, School of Civ. Engrg., Florida Institute of Technology, Melbourne, Fl.

Cosentino, P.J., and Grossman, B.G. (2000). “Optimization and Implementation of Fiber Optic Sensors for Traffic Classification and Weigh-in-Motion Systems, Phase 3 Final Report.” Contract Number BB-038, FDOT Transportation Statistics Office, Tallahassee, Fl.

Dunnicliff, J. (1988), “Geotechnical Instrumentation for monitoring Field Performance”, Wiley – Interscience Publication, New York, pp. 79-177.

Eckroth, W. V. (1999). “Development and Modeling of Embedded Fiber-optic Traffic Sensors.” PhD Thesis, Florida Institute of Technology at Melbourne, Fl.

Holtz R. D., and Kovacs W. D., (1981) “An Introduction to Geotechnical Engineering”, Prentice Hall Publishing.

Kim, B. Y., Shaw, H. J. (1989) “Multiplexing of fiber optic sensors”, optic news, pp. 35-42.

Kersey, A.D. and Dandridge, A., Distributed and Multiplexed Fiber Optic Sensors”, Optical Fiber Sensors, 1988 Technical Digest Series, vol. 2, Part 1, pp. 60-71.

Kumar, G., (1993) “Microbending Properties of Optical Fiber Sensors for Load, Pressure or Pore Water Pressure Measurements” M.Sc. Thesis, Florida Institute of Technology.

Lagakos, N., Cole, J.H., Bucaro, J.A. (1987), “Microbend Fiber Optic Sensor”, Applied Optics, Vol. 26, No 11, pp. 2171-2180.

Lindsay, K.E., Paton, B.E. (1986), “Wide Range Optical Fiber Microbending Sensor”, SPIE, Vol. 661, Optical Testing and Metrology, pp. 211-217.

Mital, S.K., and Bauer, E.G. (1989) “Screw Plate Test for Drained and Undrained Soil Parameters”, Conference on Foundation Engineering: Current Principles and Practices, ASCE, New York, Vol. I, pp. 67-79.

Ott, L., (1984) “An Introduction to Statistical Methods and Data Analysis”, 2nd Edit. PWS Publishers.

Penman, A.D., (1960) “A Study of the Response Time of Various Types of Piezometers”, Proceedings of the Conference on Pore Pressure and Suction in Soils, Butterworths, London, pp. 53-58.

Penman, A.D., (1978), “Pore Pressure and Movement in Embankment Dams”, Water Pore and Dam Construction, London, Vol. 30, No. 4, pp.32-39.

Powers, J.P. (1997),. *An Introduction to Fiber Optic Systems*. Richard D. Irwin, Inc. and Askin Associates Inc. Illinois.

Taylor, C.L. (1995), *Investigation of Fiber Optic Microbend Sensors for use in Traffic Applications*. Masters Thesis, Florida Institute of Technology, Melbourne, Florida.

Torstensson, B.A. (1984), Pore Pressure Sounding Instrument", Proceedings of the ASCE, Specialty Conference on *In Situ* Measurement of Soil Properties, North Carolina State University, Raleigh, NC, ASCE, New York, Vol. II, pp. 48-54.

Udd, E. (1995). "Fiber Optic Sensor Overview:" *Fiber Optic Smart Structures,* E. Udd, eds., John Wiley & Sons, Inc., ISBN 0-471-55488-0. 155-171.

USBR (1974), Earth Manual, 2nd Edition, US Department of the Interior, Bureau of Reclamation.

Wolfbeis, O. S. (1989), "novel techniques and materials for fiber optic chemical sensing", optic Fiber Sensors, Springer –Verlag, Berlin, pp. 416-424.

Appendix A

Sensor Construction Process

Construction Procedure for FOS

A. Drill two circular pieces, having some known diameter out of a sheet of G-10 fiberglass.

B. Cut a strip of mesh with the desired weave count along its weft highlight the tracks on which the optical fiber is to be placed with a marker (this is dependent upon which mesh is used)

C. Align the mesh on the center of the G-10 and mark a line down from the highlighted tracks to the edge of the G-10.

D. Remove about a 1/8-inch width of G-10 along the line that was marked on the plate in the previous step. Repeat this step for the other circular plate.

E. Mark a distance down from the top of one of the plates for the loop of the fiber to be placed and then affix the mesh to that plate using spray adhesive.

F. Cut a length of fiber optic cable approximately 80-inches and determine the halfway point of that length.

G. Lightly spray the setup again and run the fiber along the first highlighted track, position the top of the loop at the marked spot and return the rest of the fiber along the other highlighted track.

H. Place the other plate on top of the previous setup making sure that the notched areas are aligned and put small pieces of tape at the four quadrants.

I. Pass the bare fiber leads through 36-inch lengths of furcation tubing remembering to remove the pull string before or after doing so. (Ensure that the tubes are abutted against the G-10 within notched areas)

J. Using a wooden toothpick place 3M™5200 between the opening along the edges of the two plates and over the furcation tubes within the notched areas.

K. After the 3M™5200 becomes tack-free (one hour) strip off approximately 1½-inch of the orange PVC jacket and cut the exposed Kevlar® fibers down to about ¼-inch length. Carefully cut the inner tight buffer with a single edge razor blade, to be somewhat flush with the orange jacket.

L. Strip the acrylate coating off the bare fiber and wipe the remaining glass with isopropyl alcohol wipes.

M. Put epoxy on the exposed Kevlar® and also the uncoated fiber. Be careful not to put too much epoxy on the fiber or it will not pass through the ceramic connector.

N. Slowly pass the fiber through the ST connector so that the epoxy coated Kevlar® fibers are folded back over the orange tubing.

O. With the connector in place crimp the back body of the connector to the orange tubing and Kevlar®, then place a bead of epoxy where the fiber is protruding from the connector.

P. After the epoxy fully hardens (24 hours at room temperature) cut the fiber down to the top of the epoxy bead and wet polish the end until the blue color disappears.

Appendix B

Axial Testing with 1 Rubber Cushion

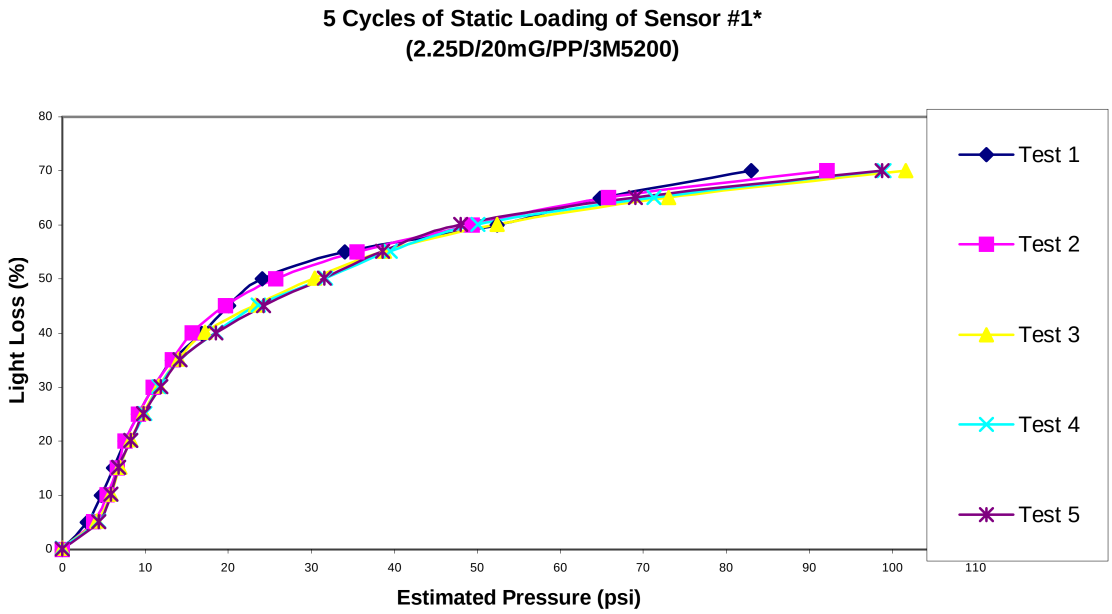

Figure B.1. Sensor 1, mesh type: polypropylene, diameter: 2.25" thickness:20 mils, 26 microbends

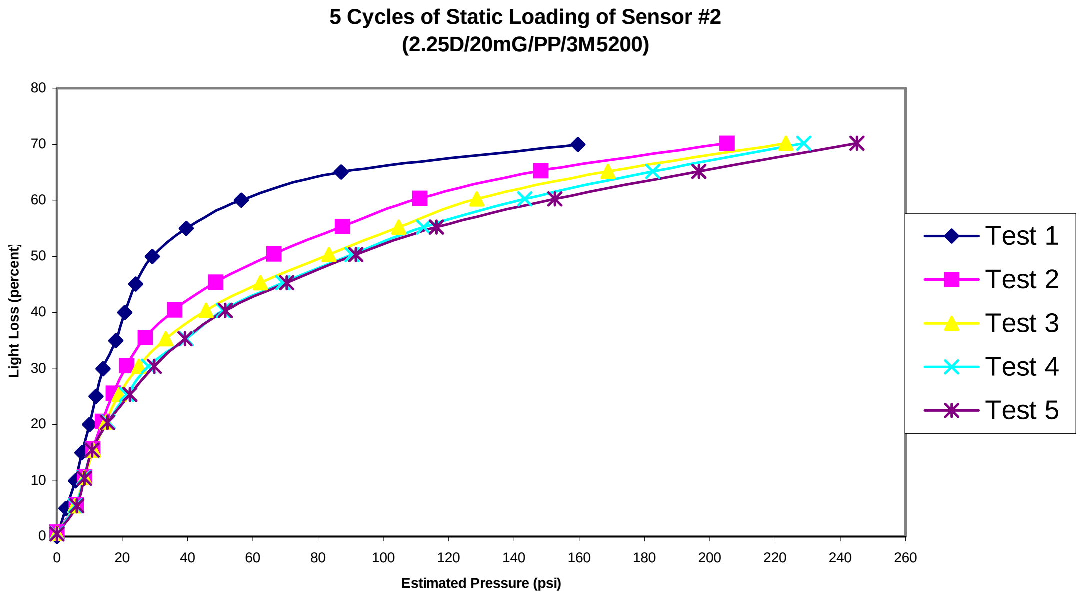

Figure B.2. Sensor 2, mesh type: polypropylene, diameter:2.25" thickness:20 mils, 26 microbends.

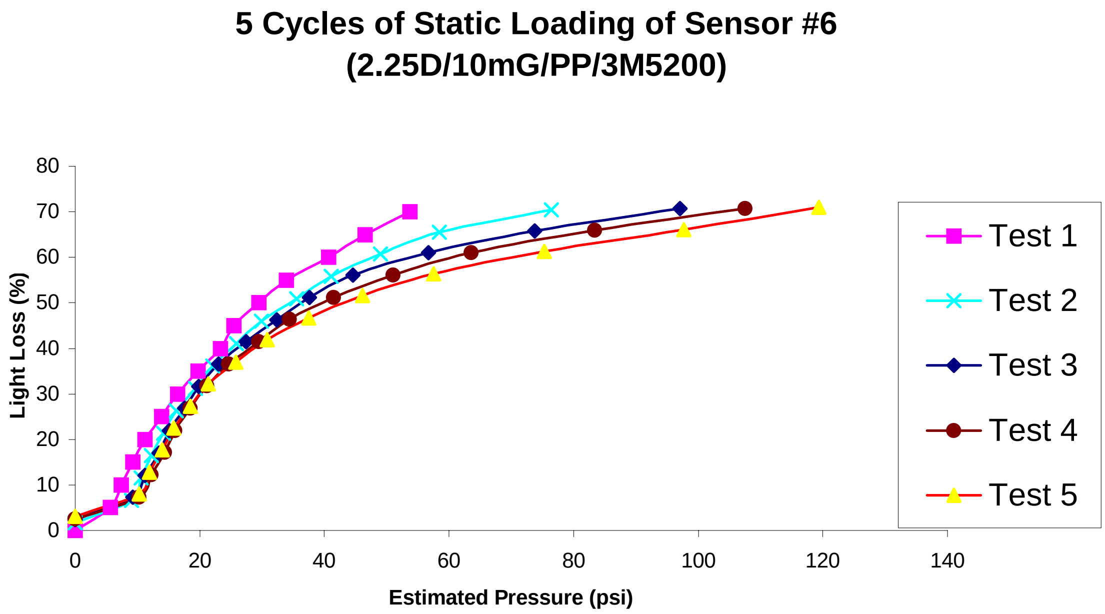

Figure B.3. Sensor 6, mesh type: polypropylene, diameter:2.25" thickness:20 mils, 26 microbends.

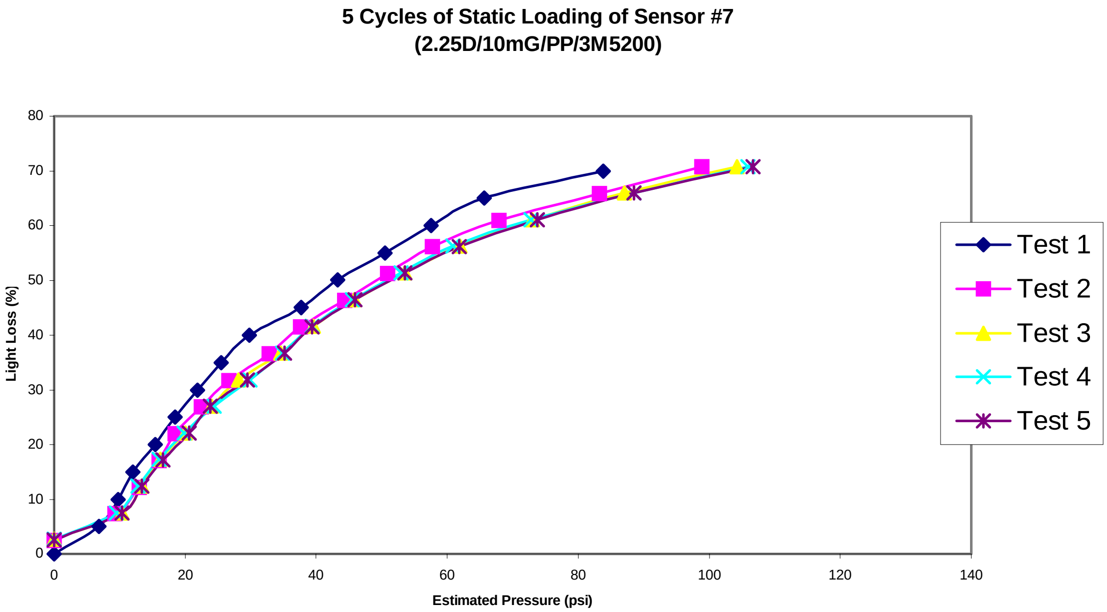

Figure B.4. Sensor 7, mesh type: polypropylene, diameter:2.25" thickness:20 mils, 26 microbends.

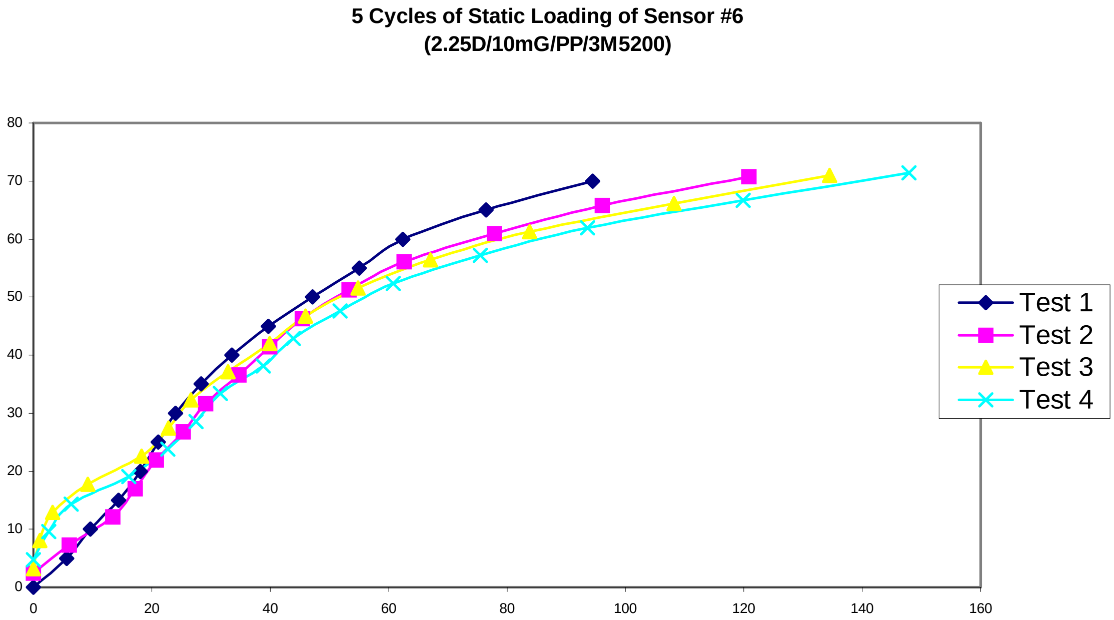

Figure B.5. Sensor 7, mesh type: polypropylene, diameter:2.25” thickness:20 mils, 26 microbends.

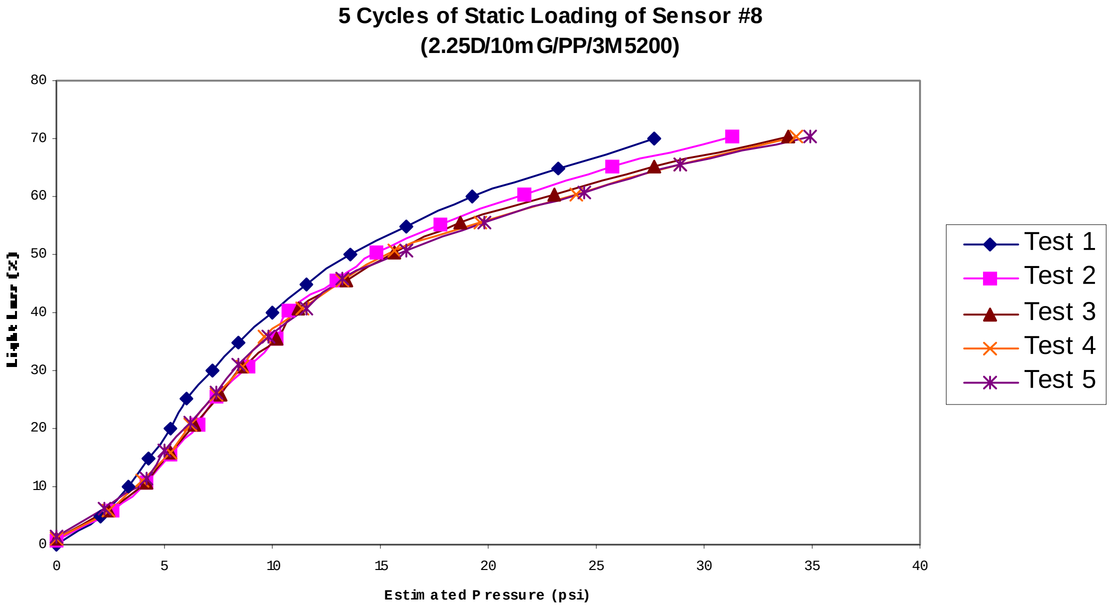

Figure B.6. Sensor 8, mesh type: polypropylene, diameter:2.25” thickness:20 mils, 26 microbends.

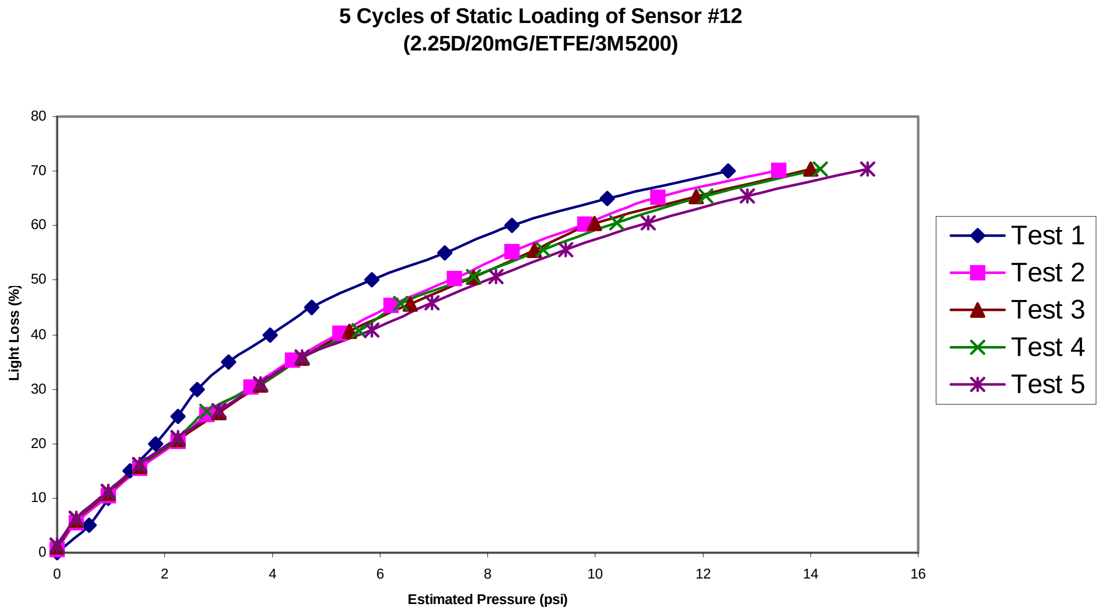

Figure B.7. Sensor 12, mesh type: Fluortex ETFE, diameter:2.25” thickness:20 mils, 26 microbends.

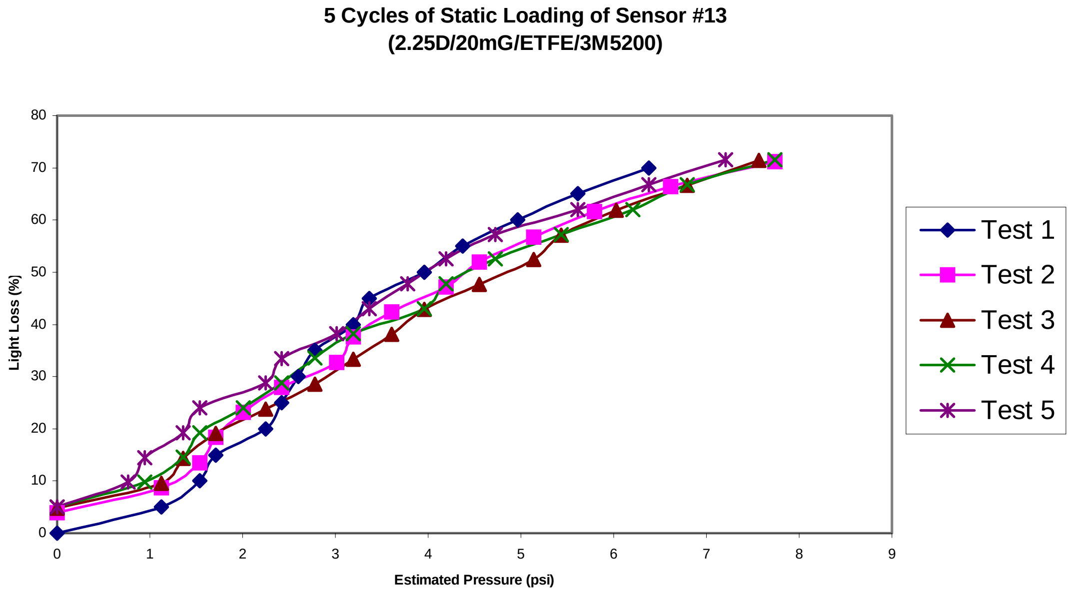

Figure B.8. Sensor 13, mesh type: Fluortex ETFE, diameter:2.25” thickness:20 mils, 26 microbends.

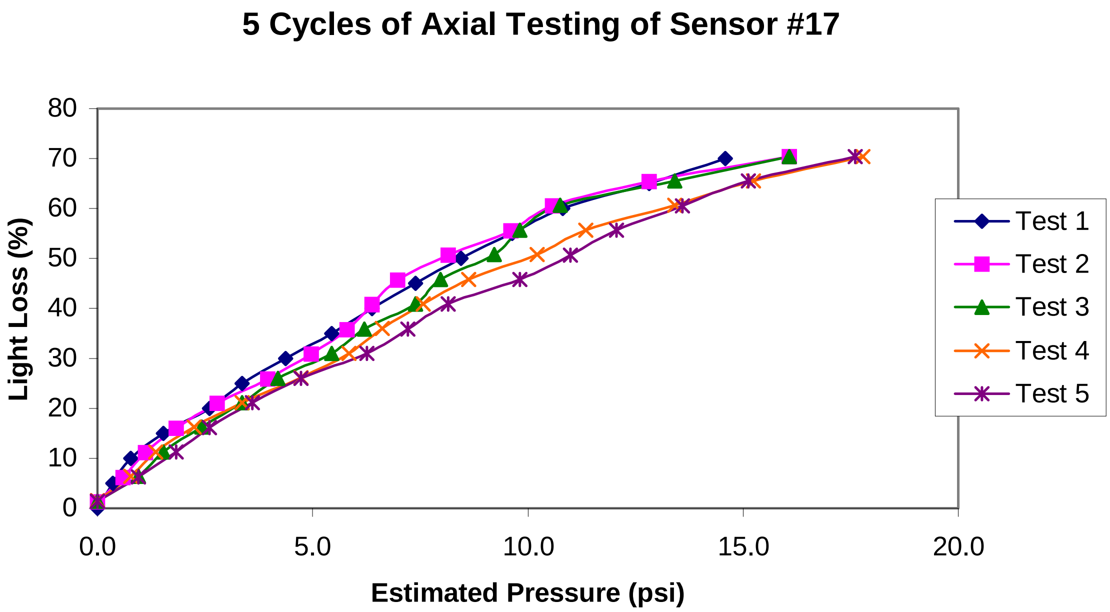

Figure B.9. Sensor 17, mesh type: Fluortex ETFE, diameter:2.25” thickness:20 mils, 24 microbends.

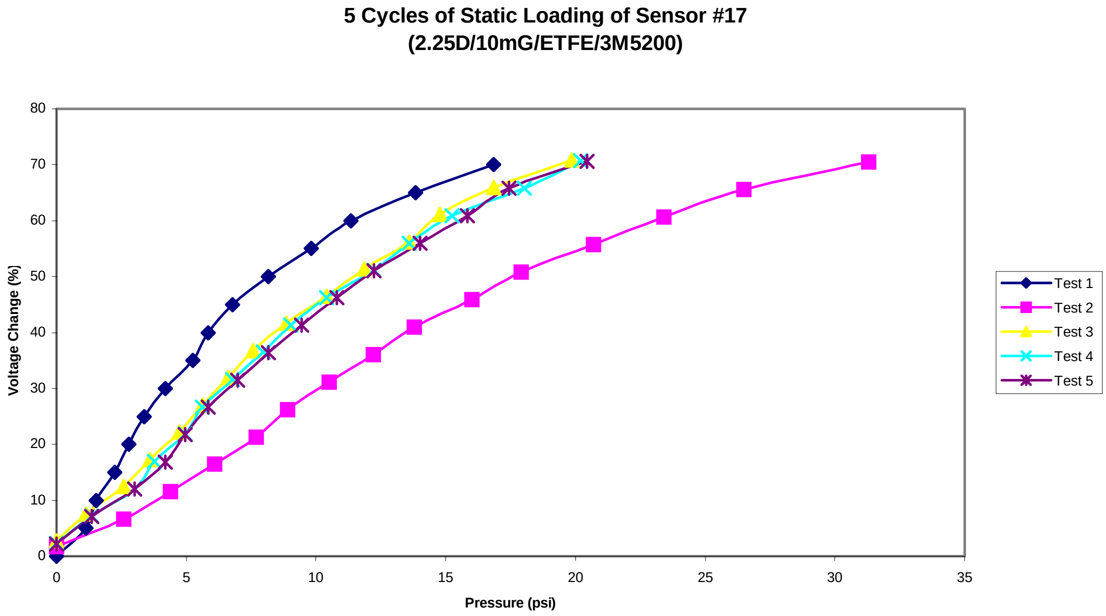

Figure B.10. Sensor 17, mesh type: Fluortex ETFE, diameter: 2.25” thickness:20 mils, 24 microbends.

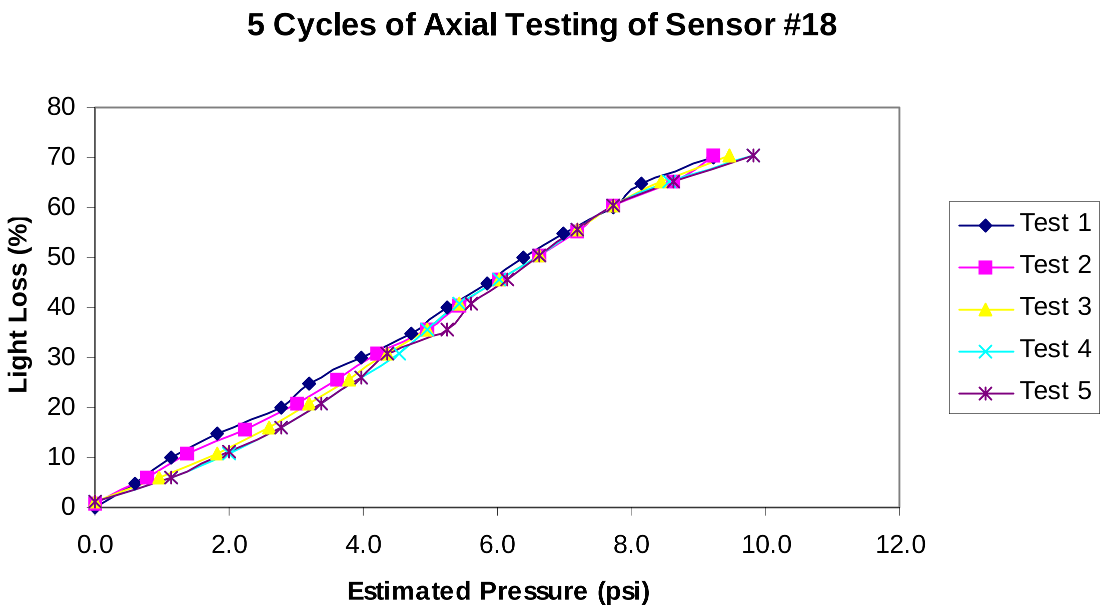

Figure B.11. Sensor 18, mesh type: Fluortex ETFE, diameter: 2.25” thickness:20 mils, 24 microbends.

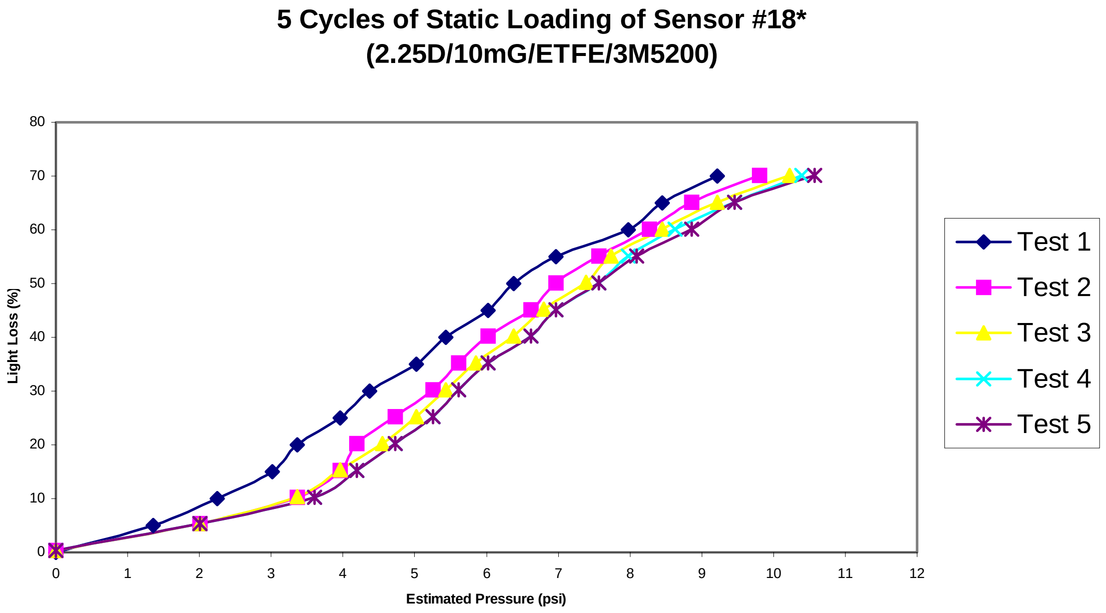

Figure B.12. Sensor 18, mesh type: Fluortex ETFE, diameter: 2.25” thickness:20 mils, 24 microbends.

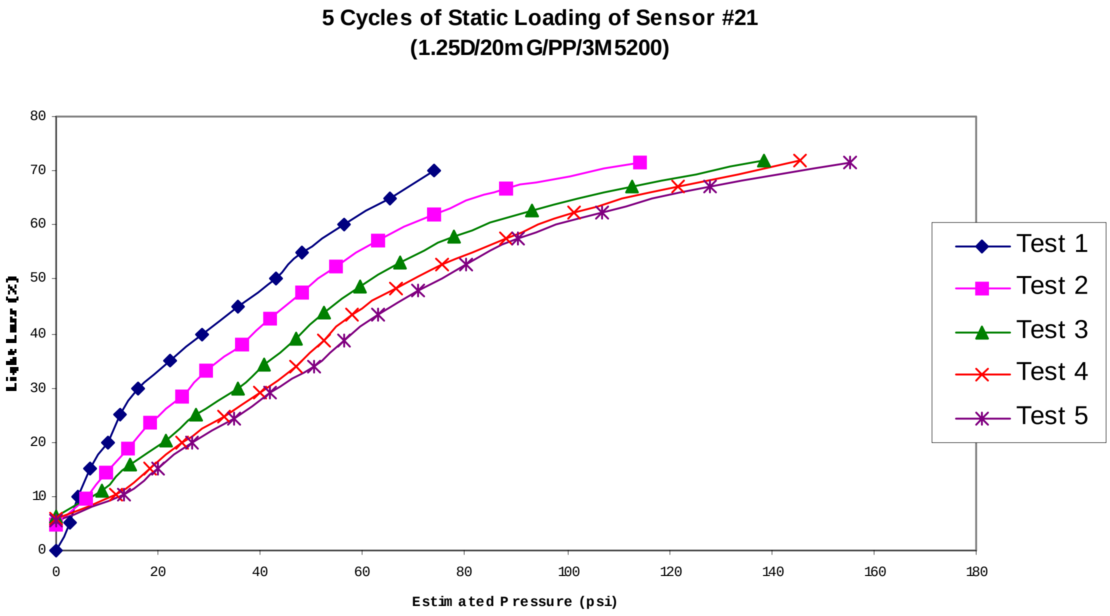

Figure B.13. Sensor 21, mesh type: polypropylene, diameter: 2.25” thickness:15 mils

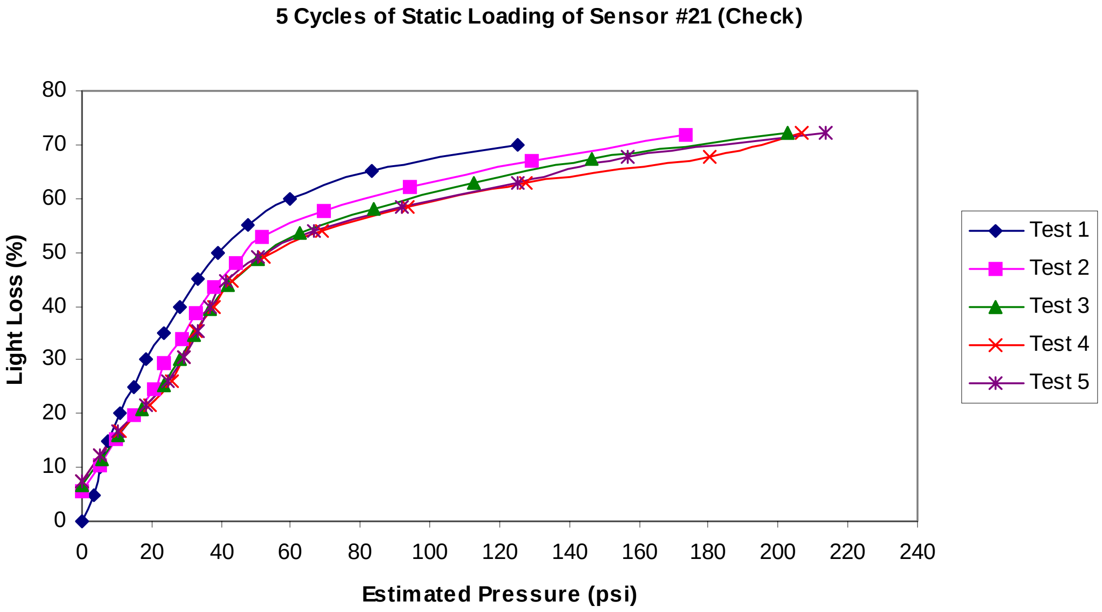

Figure B.14. Sensor 21, mesh type: Fluortex ETFE, diameter: 2.25” thickness:15 mils

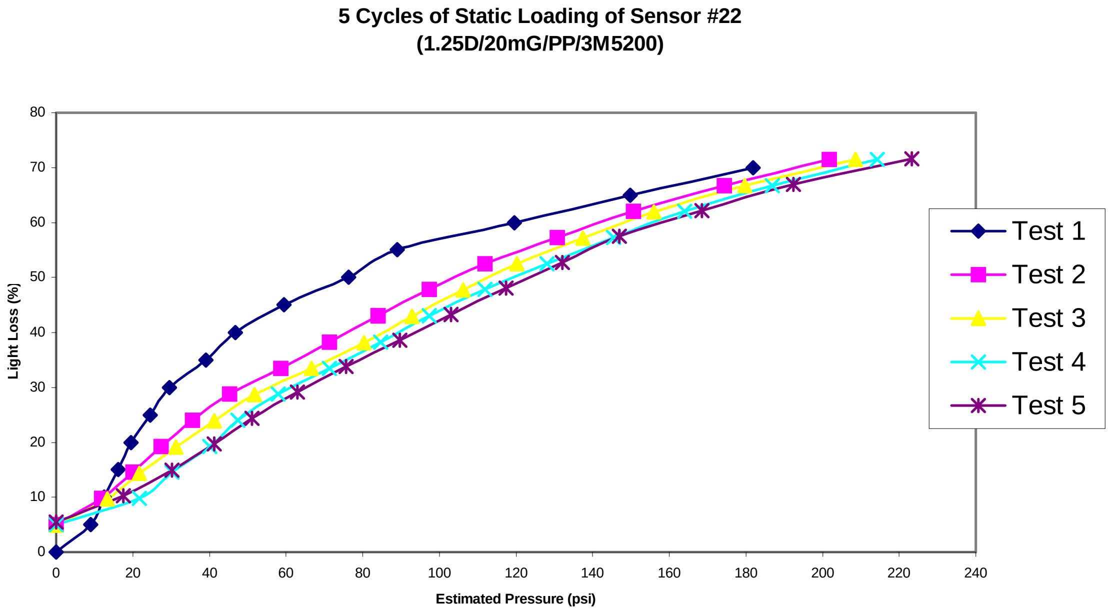

Figure B.15. Sensor 21, mesh type: polypropylene, diameter: 2.25” thickness:15 mils

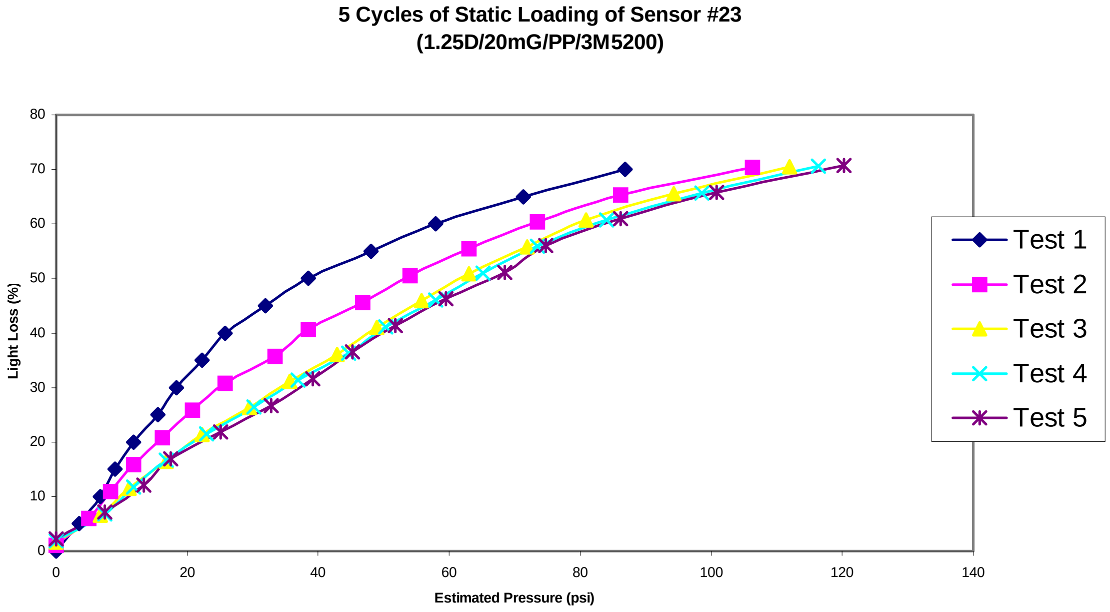

Figure B.16. Sensor 23, mesh type: polypropylene, diameter: 1.25” thickness:20 mils

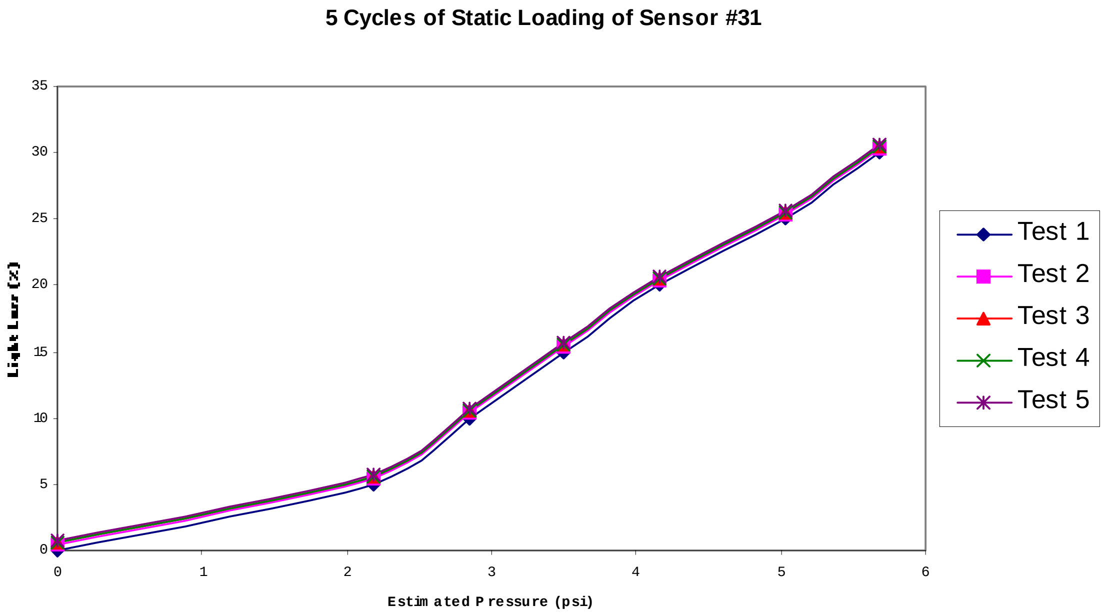

Figure B.17. Sensor 31, mesh type: polypropylene, diameter: 1.25” thickness:15 mils, 13 microbends.

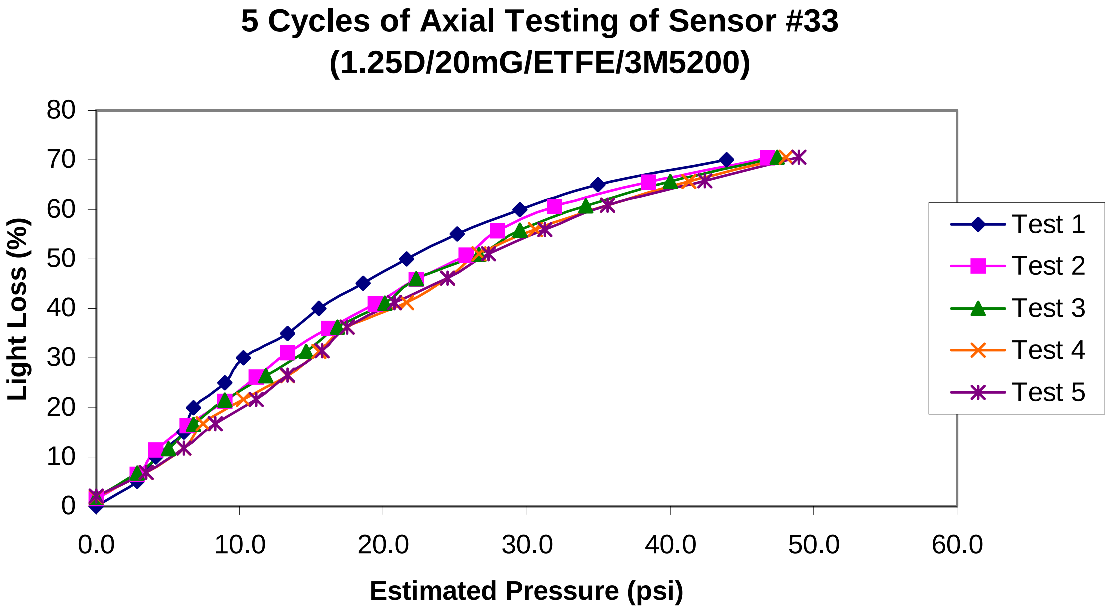

Figure B.18. Sensor 33, mesh type: ETFE, diameter: 1.25” thickness:15 mils, 13 microbends.

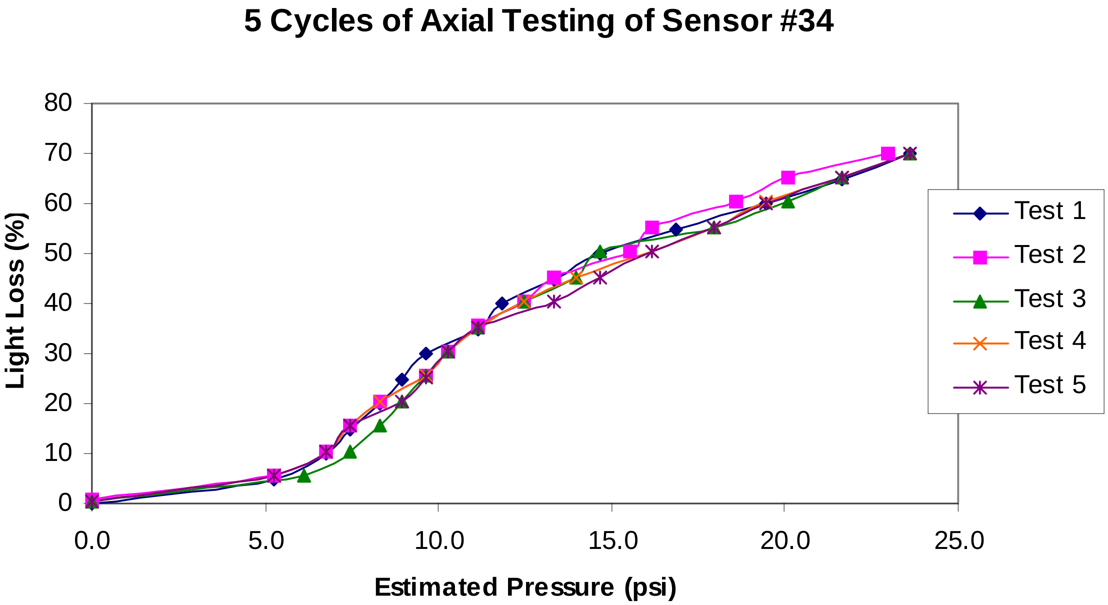

Figure B.19. Sensor 34, mesh type: polypropylene, diameter: 1.25" thickness:15 mils, 13 microbends.

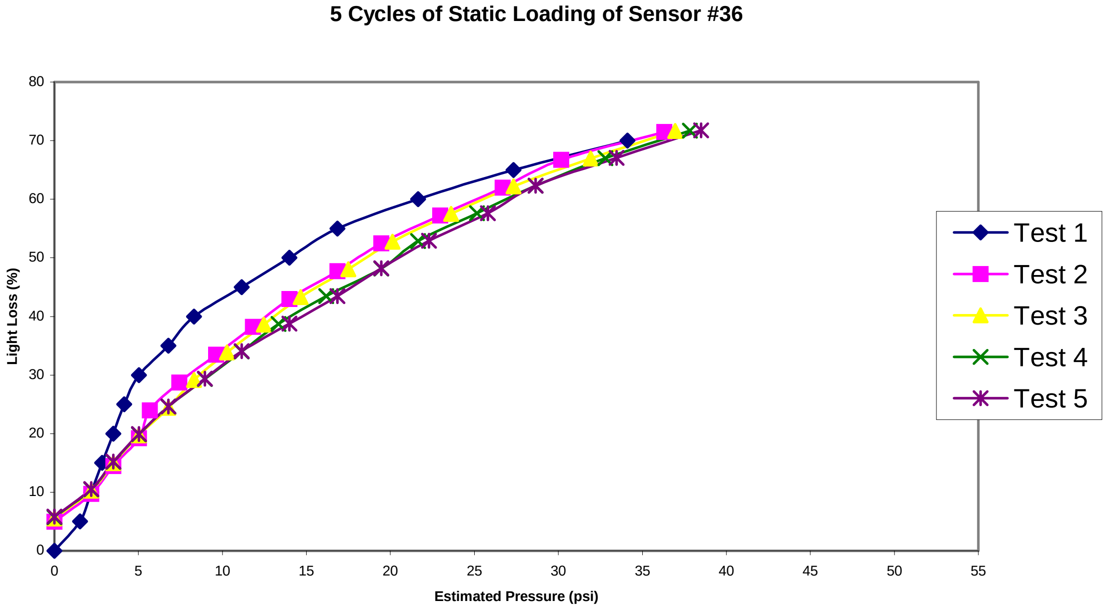

Figure B.20. Sensor 36, mesh type: polypropylene, diameter:1.25" thickness:15 mils, 13 microbends.

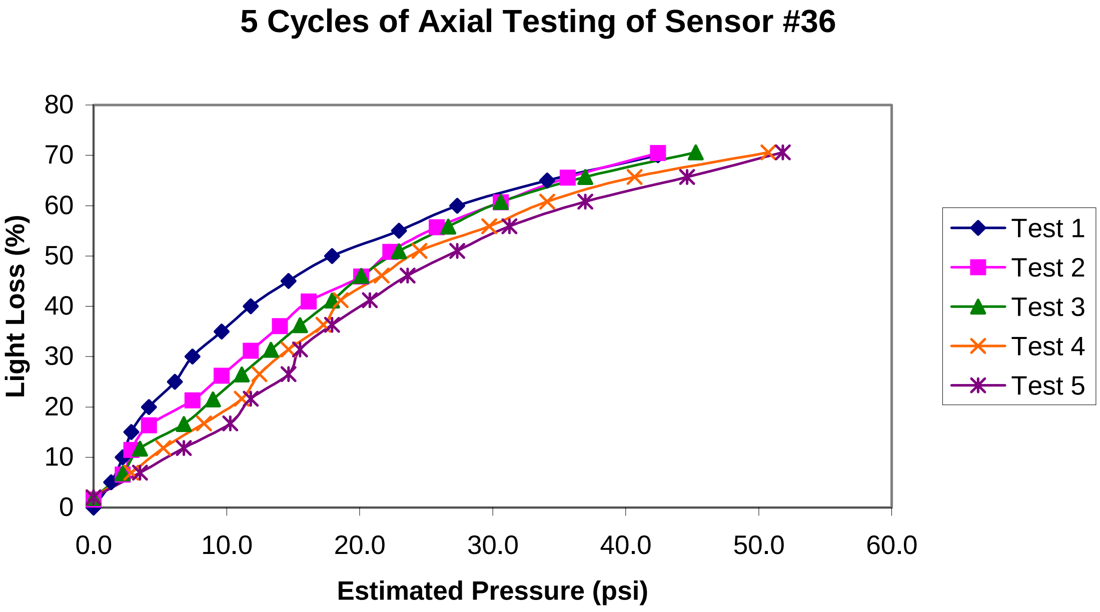

Figure B.21. Sensor 36, mesh type: polypropylene, diameter:1.25” thickness:15 mils, 13 microbends.

Appendix C

Axial Testing with 2 Rubber Cushions

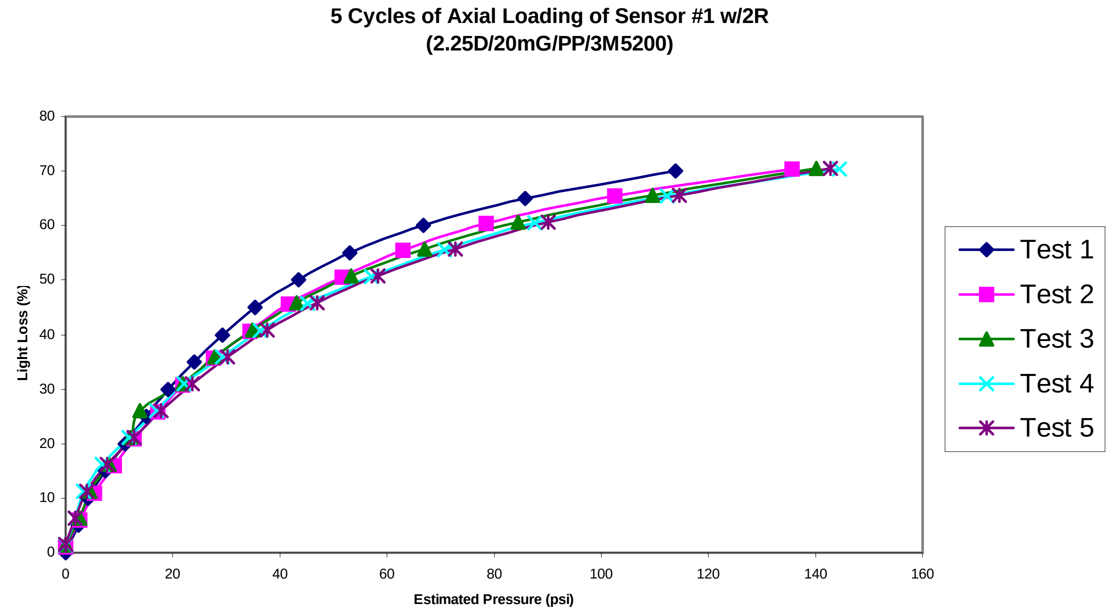

Figure C.1. Sensor 1, polypropylene, diameter:2.25” thickness:20 mils, 26 microbends

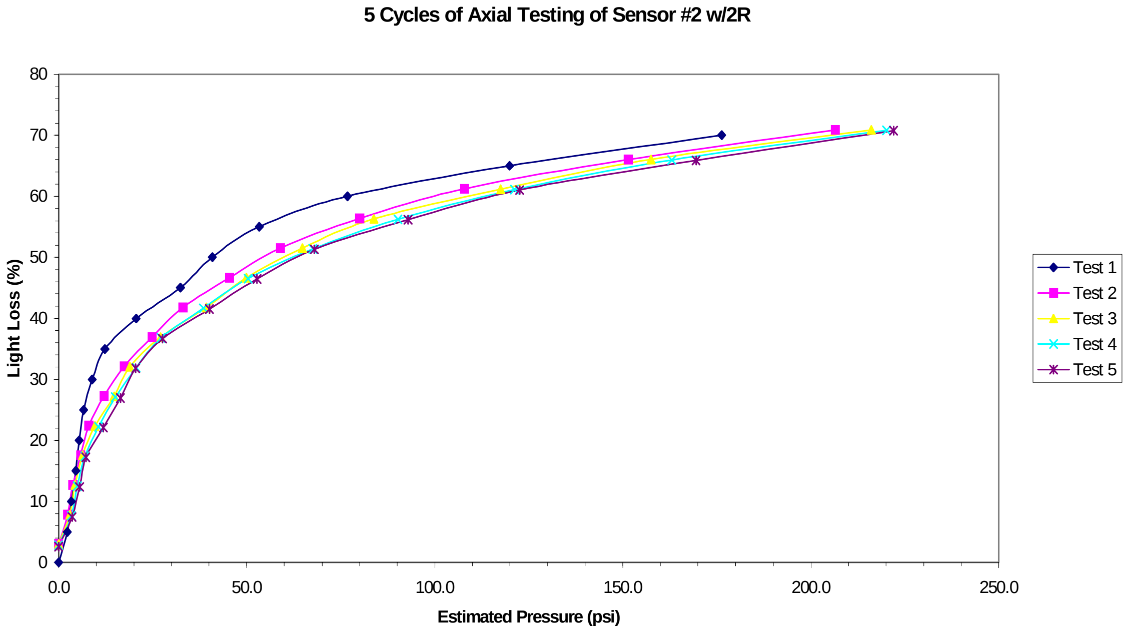

Figure C.2. Sensor 2, polypropylene, diameter:2.25” thickness:20 mils, 26 microbends.

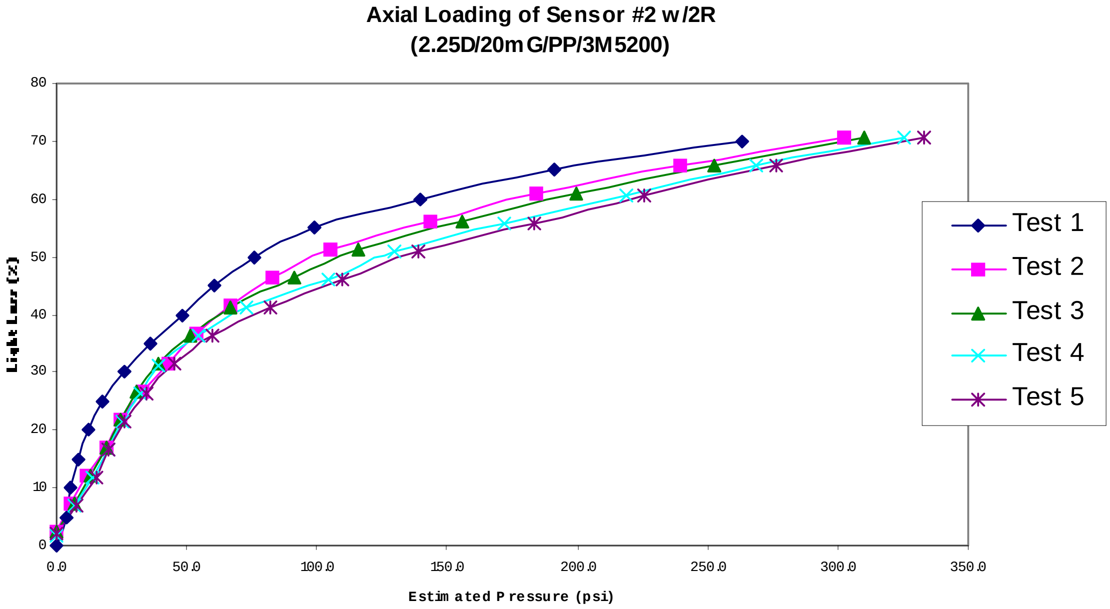

Figure C.3. Sensor 2, polypropylene, diameter:2.25" thickness:20 mils, 26 microbends.

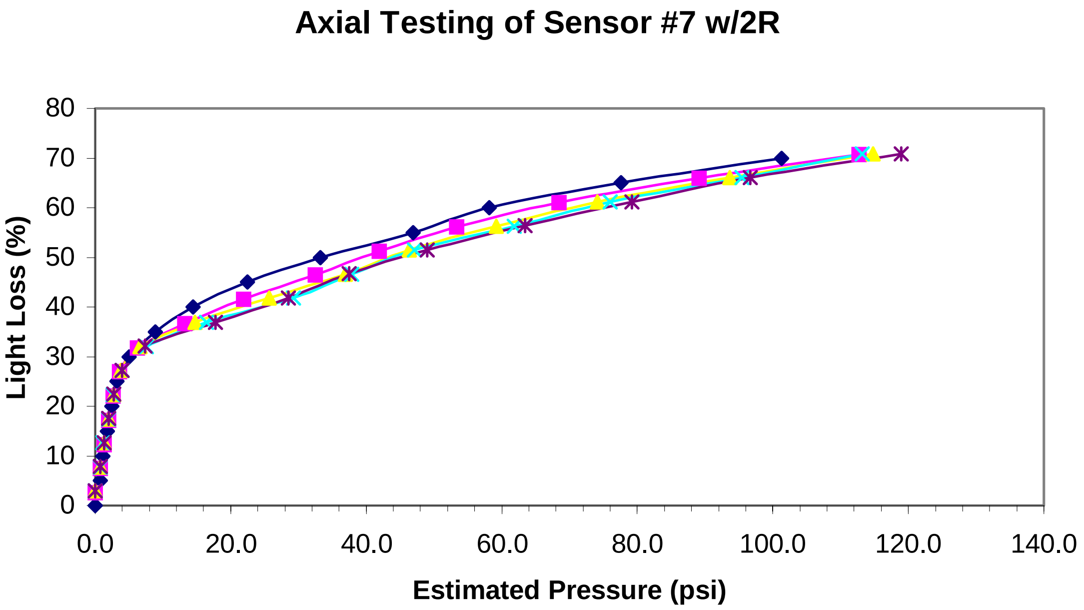

Figure C.4. Sensor 7, polypropylene, diameter:2.25" thickness:20 mils, 26 microbends.

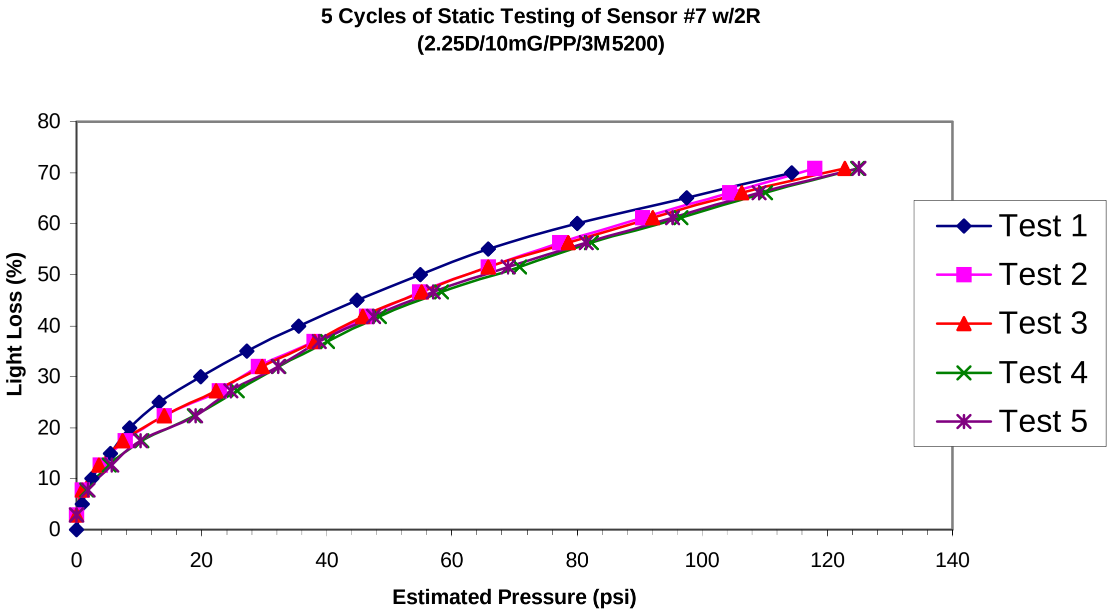

5 Cycles of Static Testing of Sensor #7 w/2R
(2.25D/10mG/PP/3M5200)

Figure C.5. Sensor 7, polypropylene, diameter:2.25” thickness:20 mils, 26 microbends.

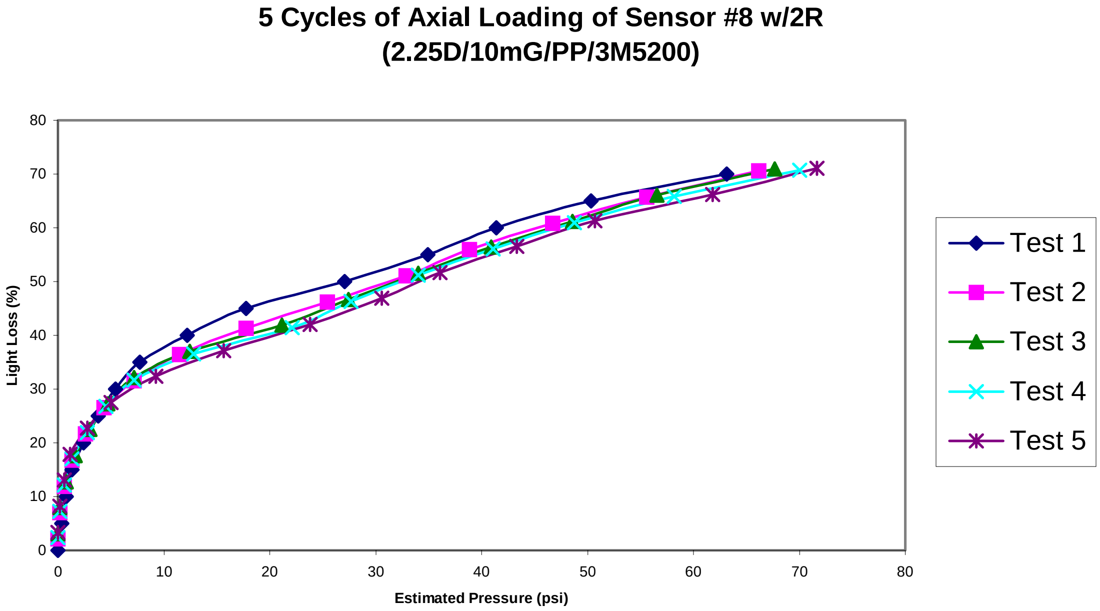

5 Cycles of Axial Loading of Sensor #8 w/2R
(2.25D/10mG/PP/3M5200)

Figure C.6. Sensor 8, polypropylene, diameter:2.25” thickness:20 mils, 26 microbends.

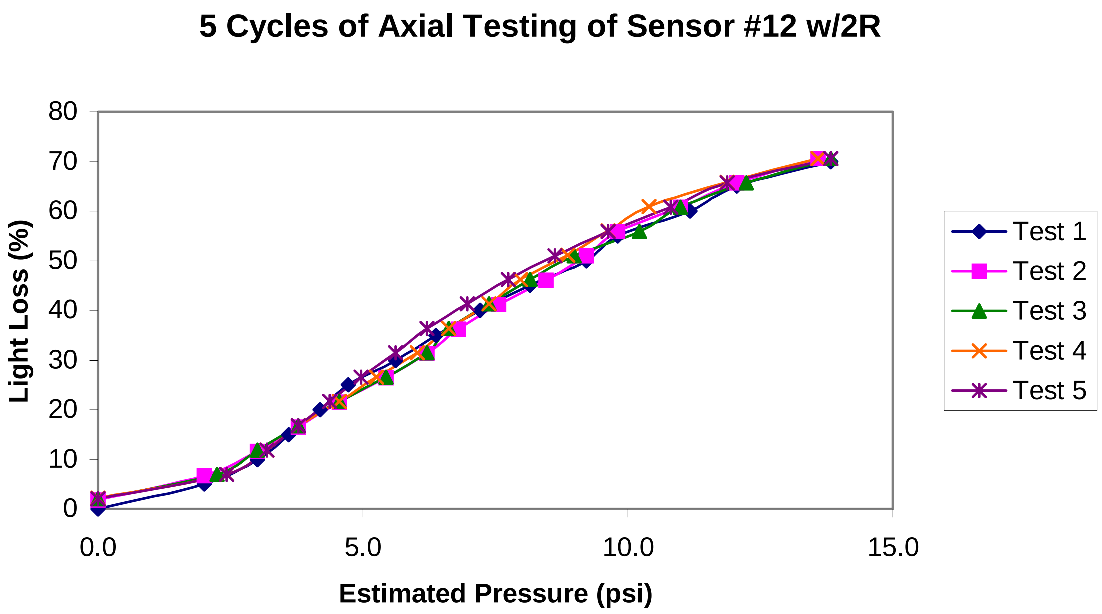

Figure C.7. Sensor 12, polypropylene, diameter:2.25” thickness:20 mils, 26 microbends.

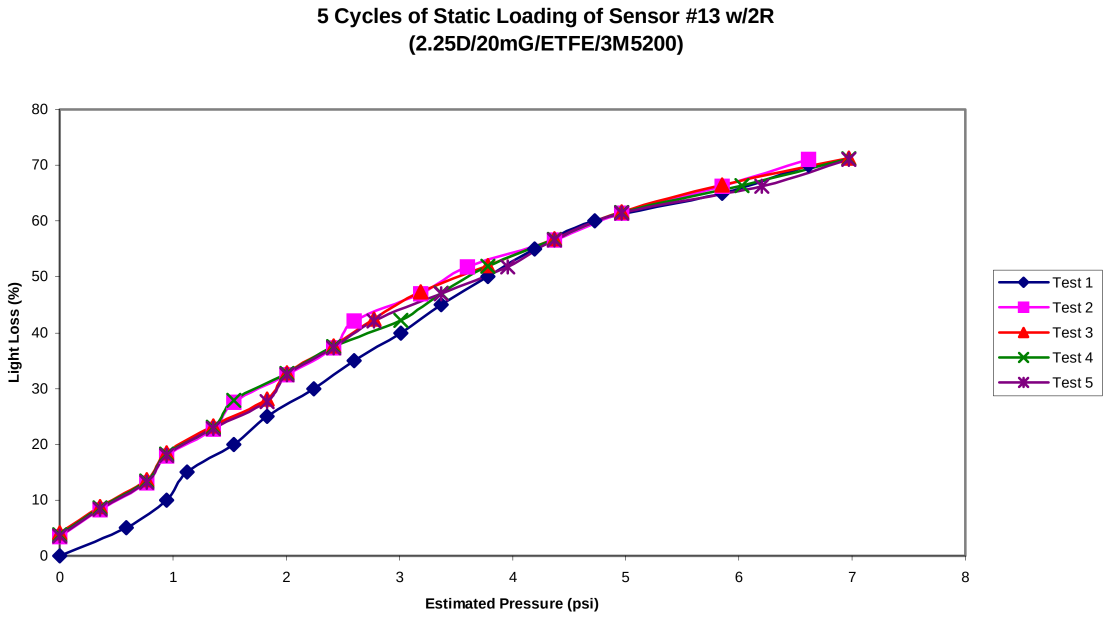

Figure C.8. Sensor 13, polypropylene, diameter:2.25” thickness:20 mils, 26 microbends.

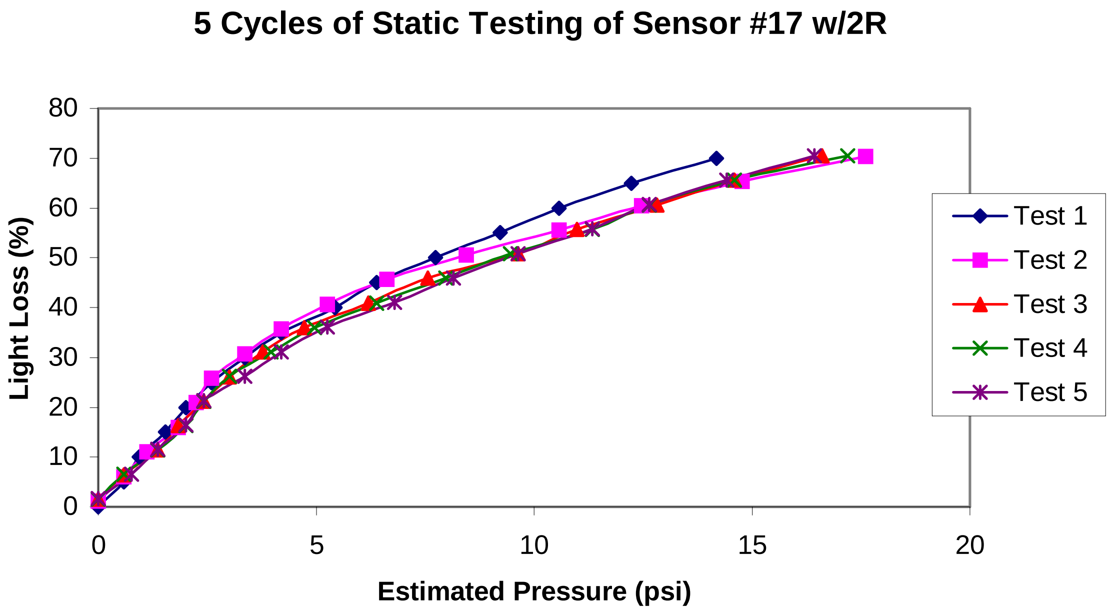

Figure C.9. Sensor 17, Fluortex ETFE, diameter:2.25” thickness:20 mils, 24 microbends.

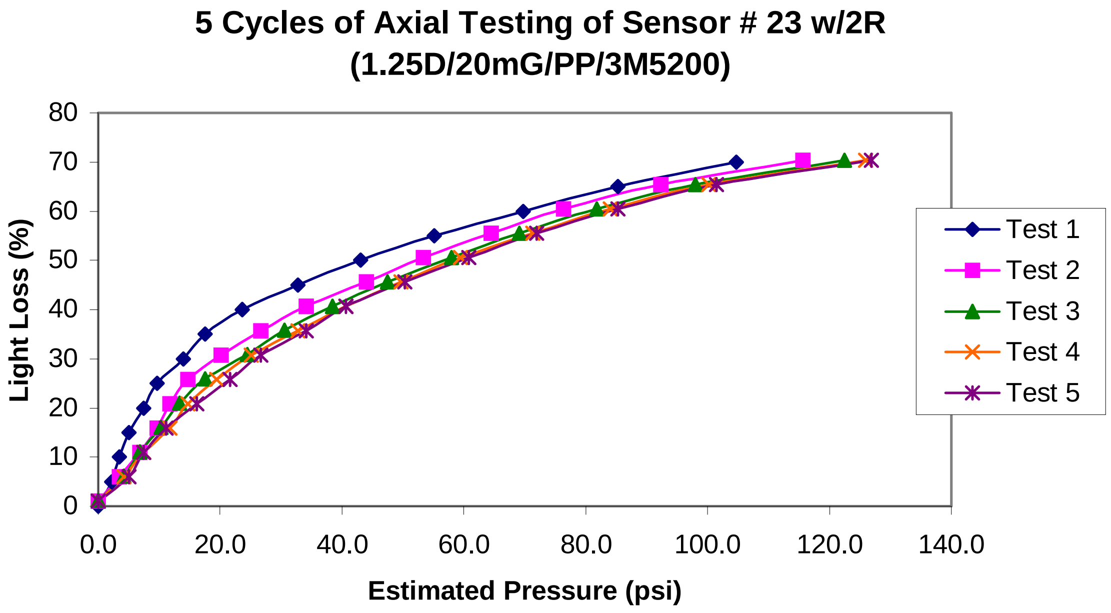

Figure C.10. Sensor 23, Fluortex ETFE, diameter:1.25” thickness:?? 20, 11 microbends.

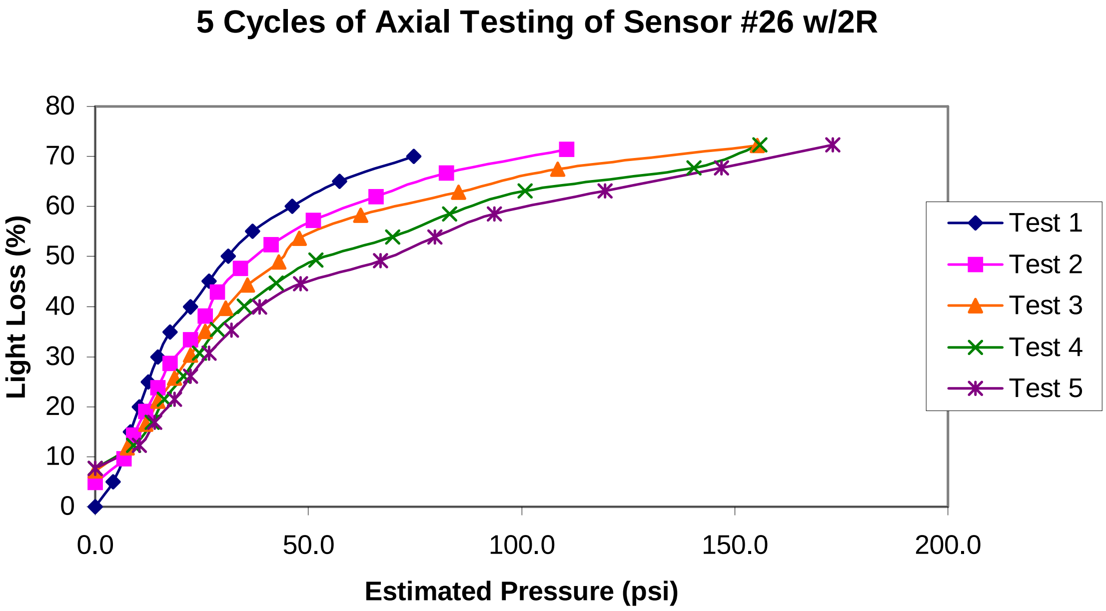

Figure C.11. Sensor 26, Fluortex ETFE, diameter:1.25" thickness:15 mils, 11 microbends.

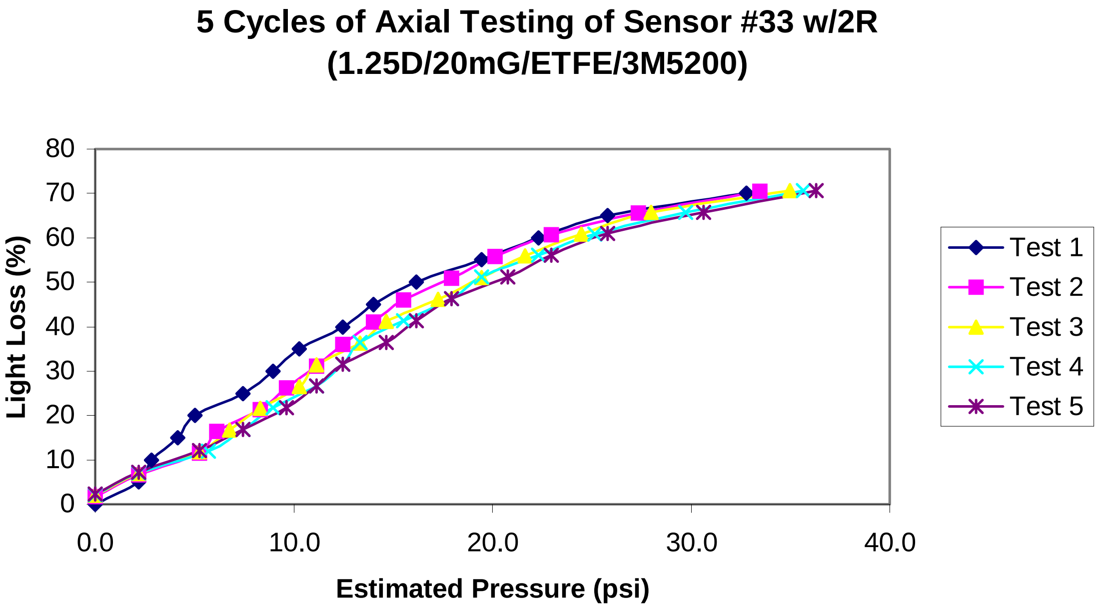

Figure C.12. Sensor 33, Fluortex ETFE, diameter:1.25" thickness:15 mils, 11 microbends,.

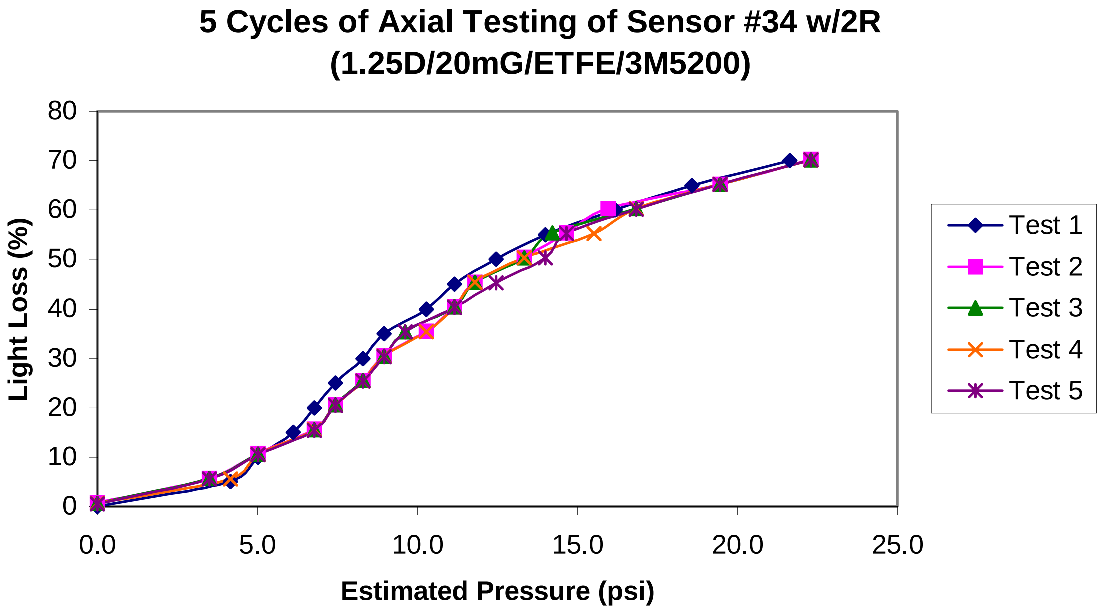

Figure C.13. Sensor 34, Fluortex ETFE, diameter:1.25" thickness:15 mils, 11 microbends.

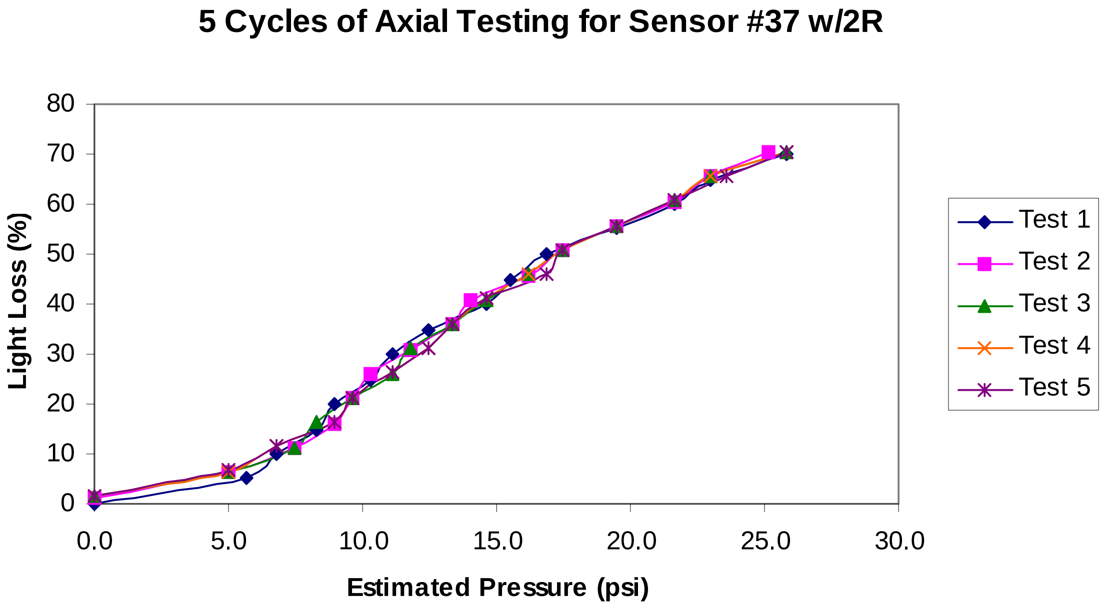

Figure C.14. Sensor 37, polypropylene, diameter:1.25" thickness:15 mils, 13 microbends.

Appendix D

Hydrostatic Testing

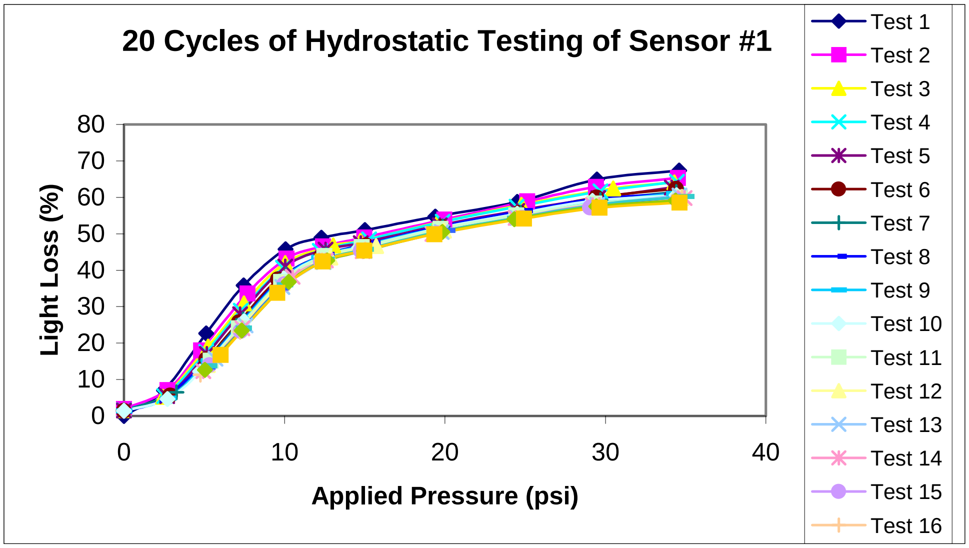

Fig. D.1. Sensor 1, polypropylene, diameter:2.25” thickness:20 mils, 26 microbends.

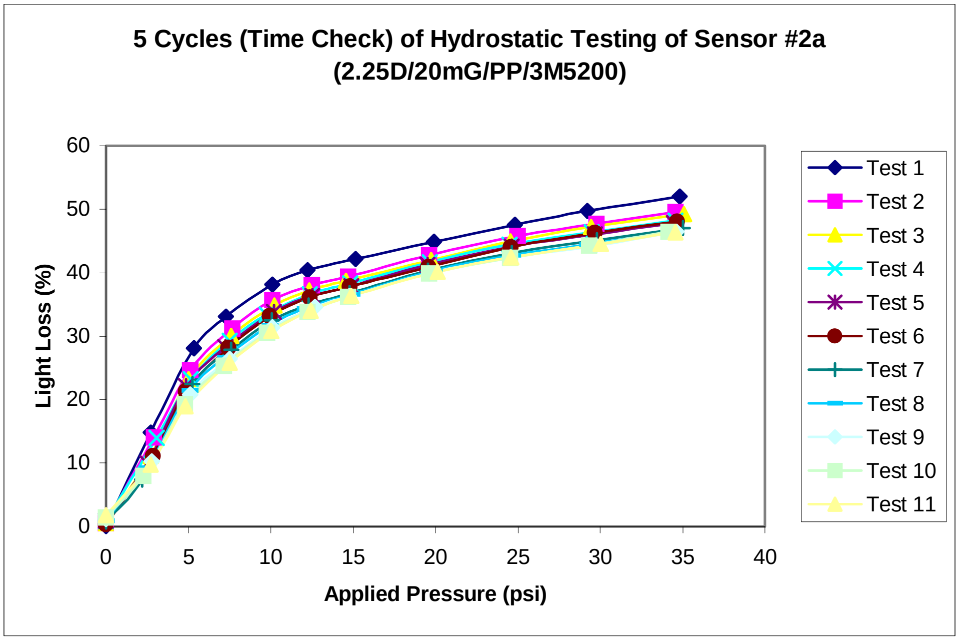

Fig. D.2. Sensor 2a, polypropylene, diameter:2.25" thickness:20 mils, 26 microbends.

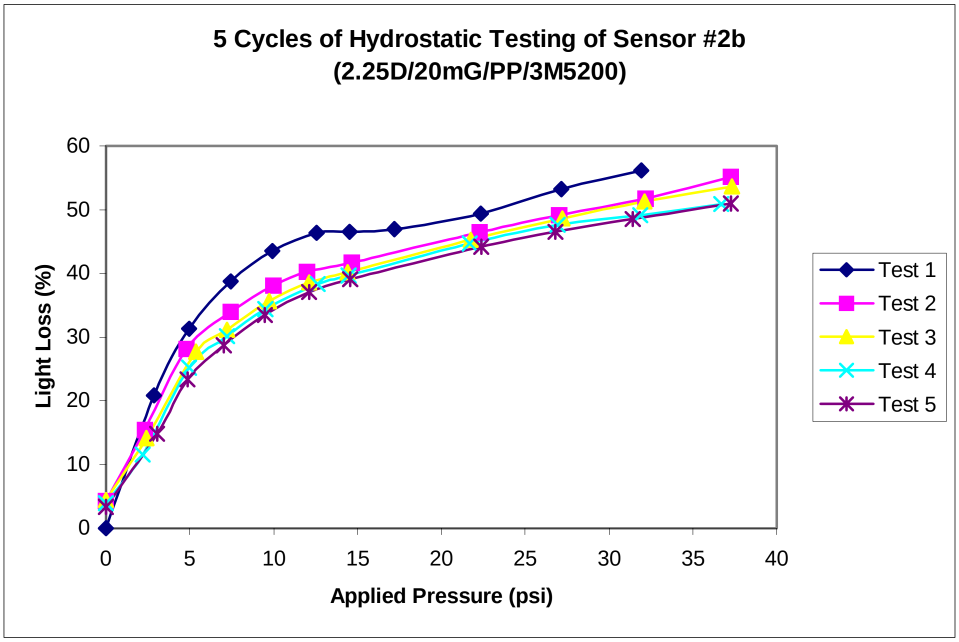

Fig. D.3. Sensor 2b, polypropylene, diameter:2.25" thickness:20 mils, 26 microbends.

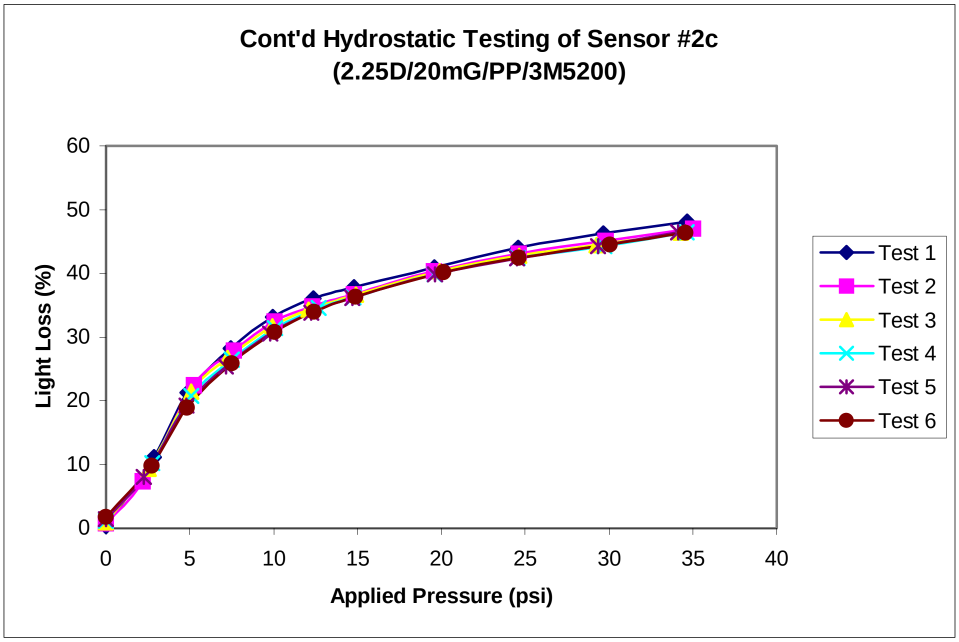

Fig. D.4. Sensor 2c, polypropylene, diameter:2.25” thickness:20 mils, 26 microbends.

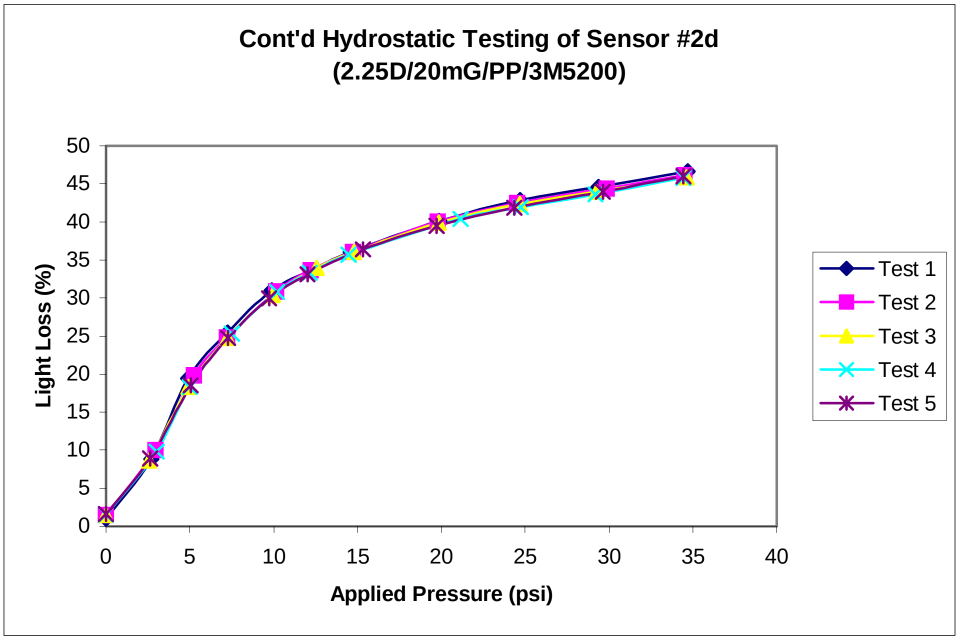

Fig. D.5. Sensor 2d, polypropylene, diameter:2.25” thickness:20 mils, 26 microbends.

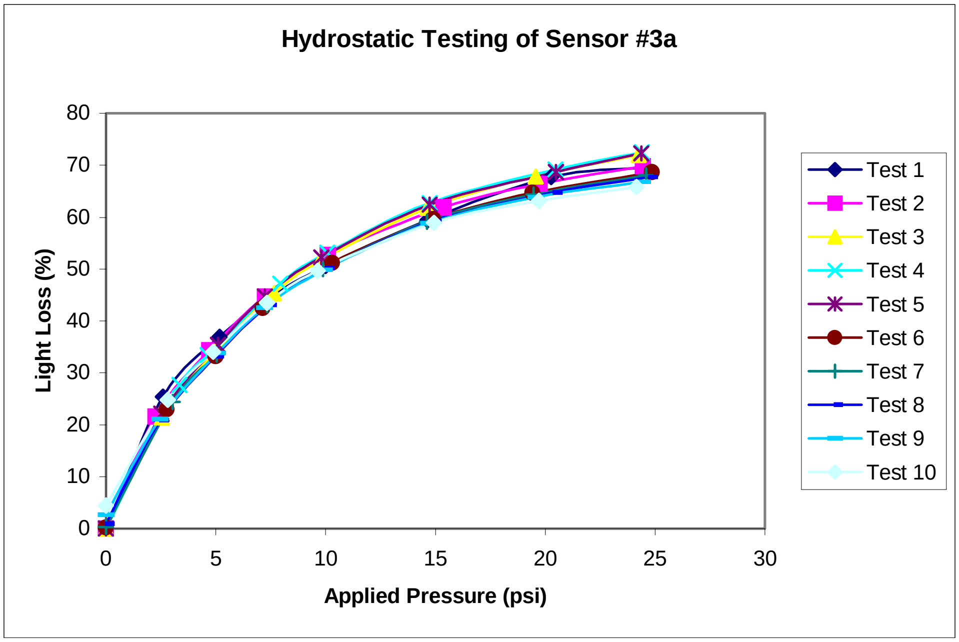

Fig. D.6. Sensor 3a, polypropylene, diameter:2.25” thickness:20 mils, 26 microbends.

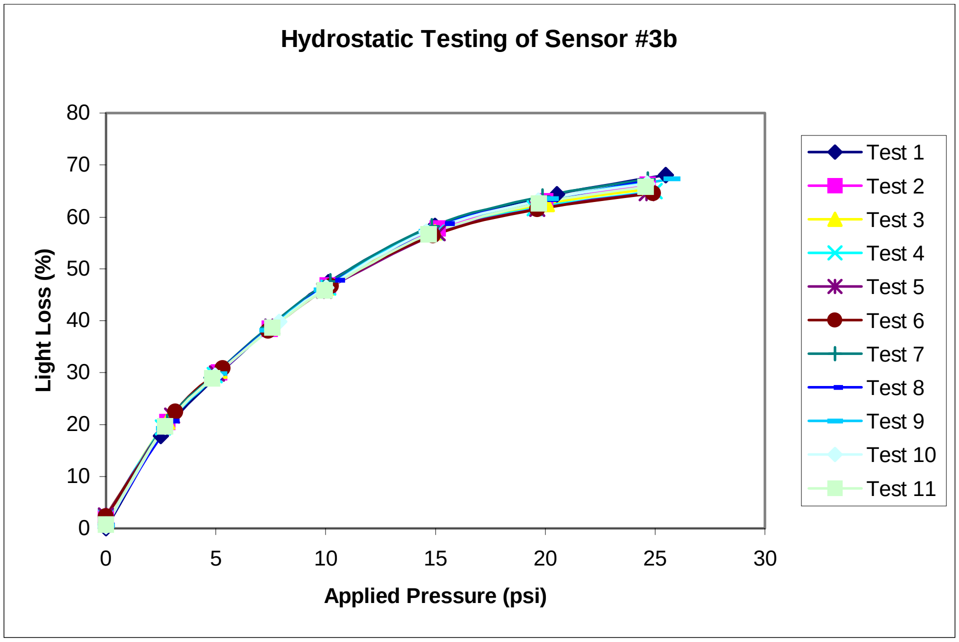

Fig. D.7. Sensor 3b, polypropylene, diameter:2.25” thickness:20 mils, 26 microbends.

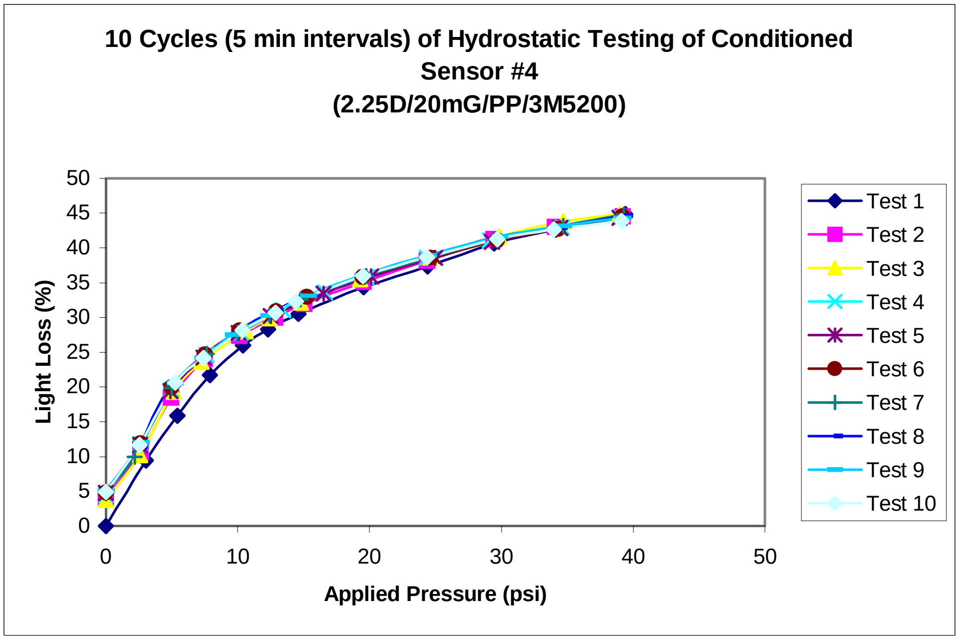

Fig. D.8. Sensor 4, polypropylene, diameter:2.25” thickness:20 mils, 26 microbends.

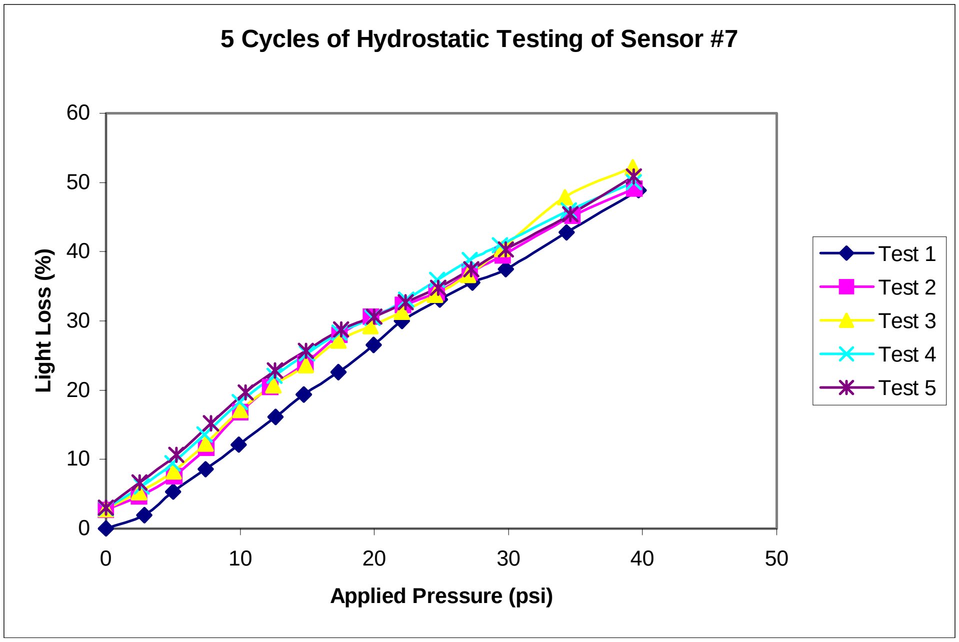

Fig. D.9. Sensor 7, polypropylene, diameter:2.25” thickness:20 mils, 26 microbends.

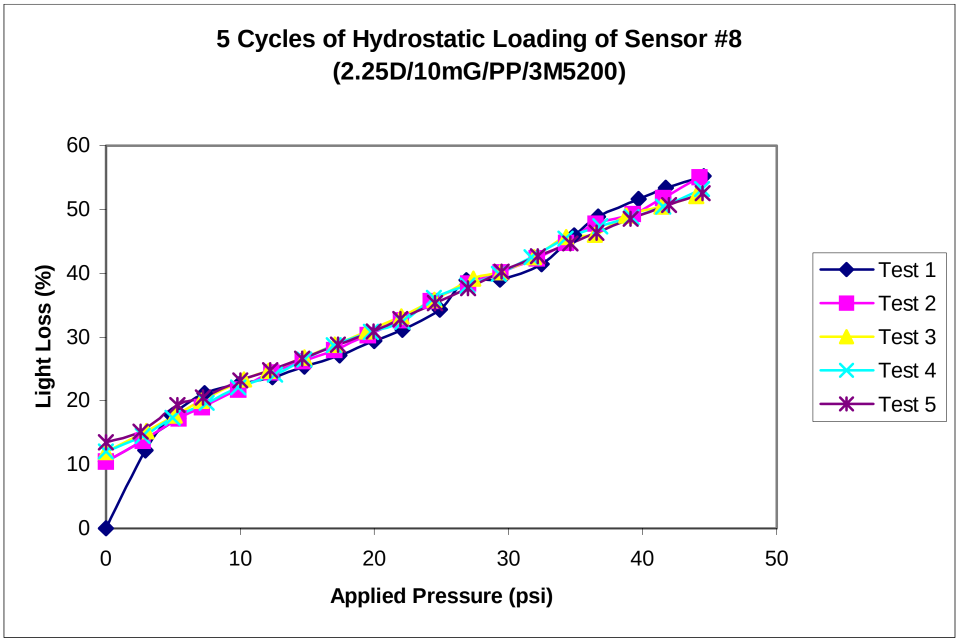

Fig. D.10. Sensor 8, polypropylene, diameter:2.25” thickness:20 mils, 26 microbends.

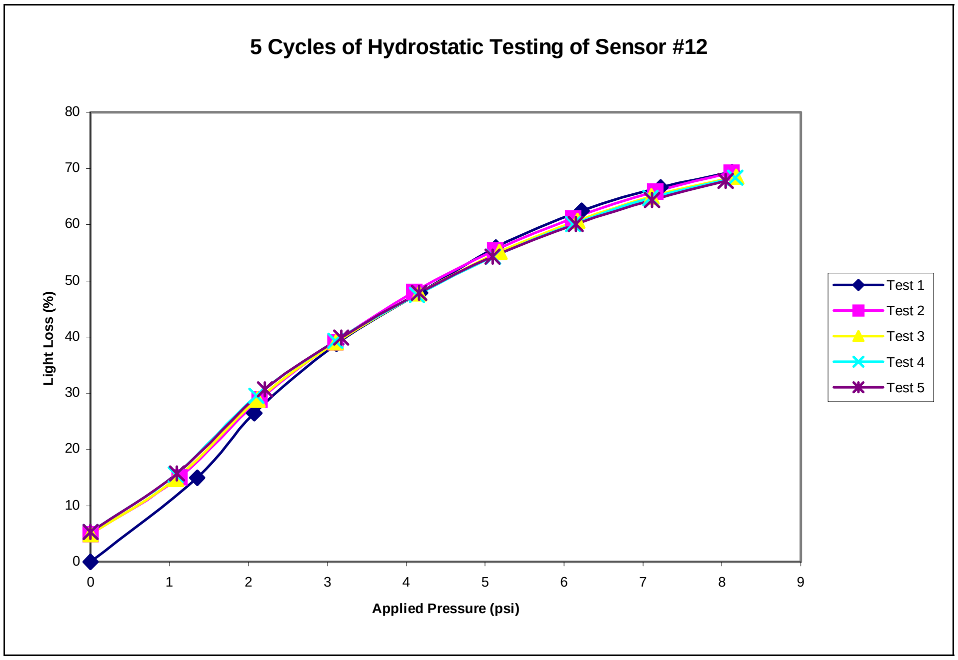

Fig. D.11. Sensor 12, polypropylene, diameter:2.25” thickness:20 mils, 26 microbends.

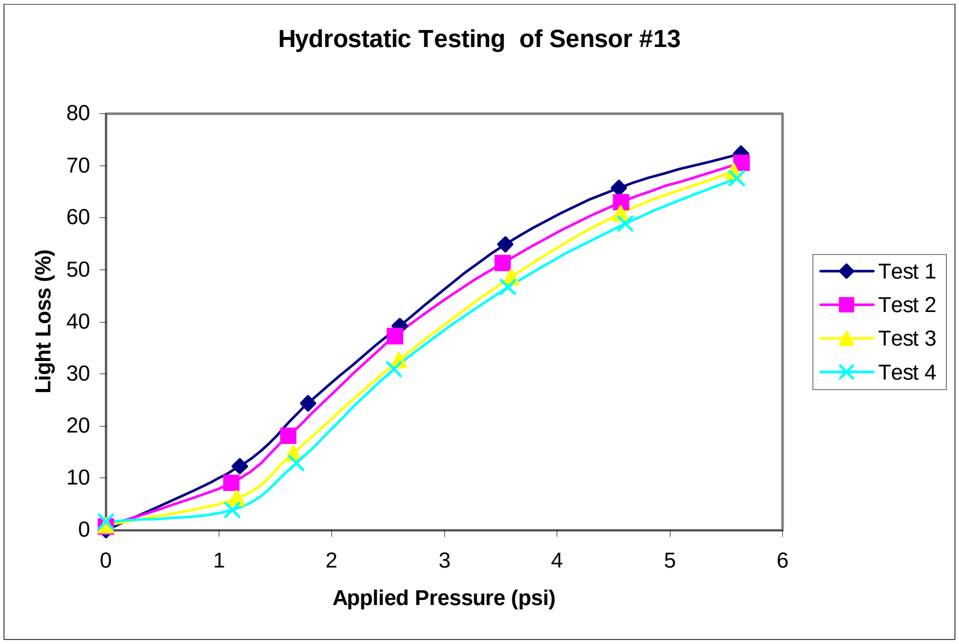

Fig. D.12. Sensor 13, polypropylene, diameter:2.25” thickness:20 mils, 26 microbends.

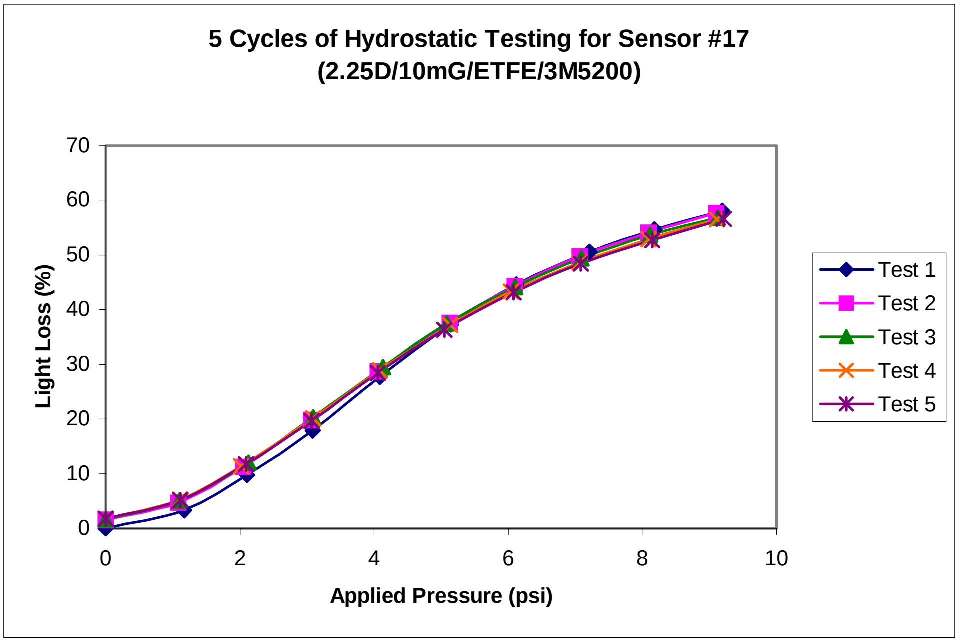

Fig. D.13. Sensor 17, Fluortex ETFE, diameter:2.25” thickness:20 mils, 24 microbends.

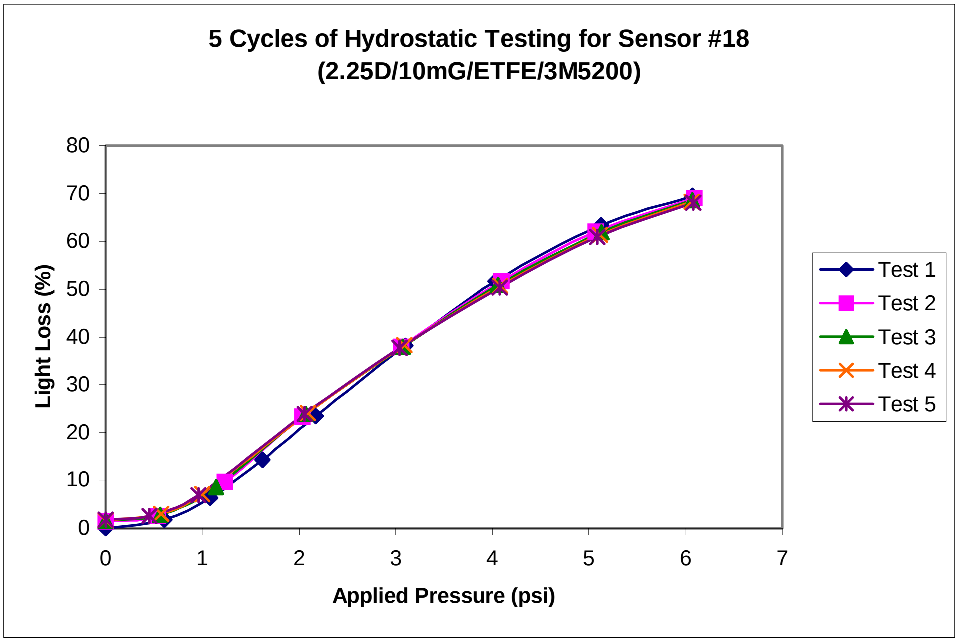

Fig. D.14. Sensor 18, Fluortex ETFE, diameter:2.25” thickness:20 mils, 24 microbends.

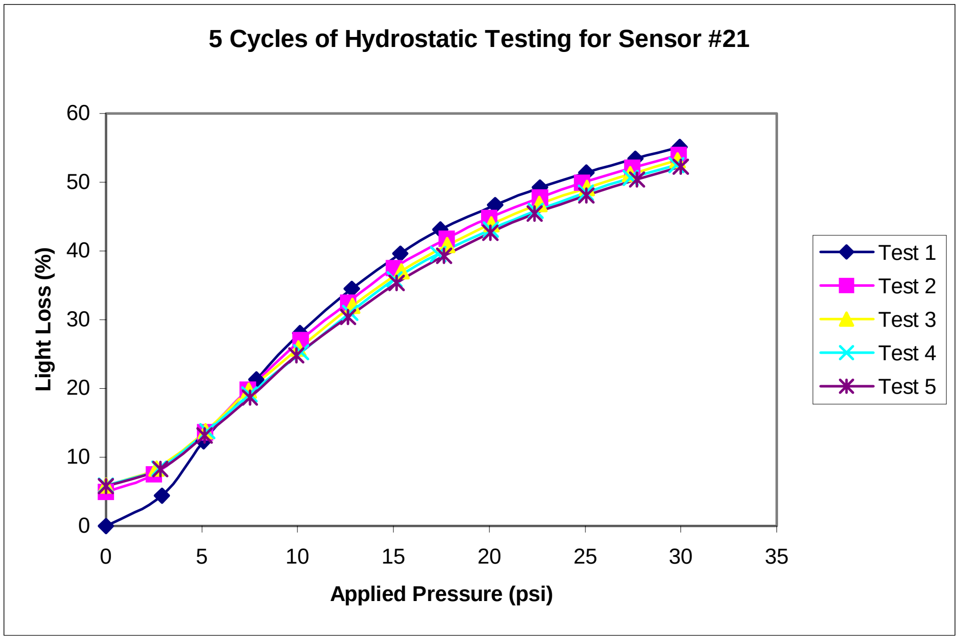

Fig. D.15. Sensor 21, Fluortex ETFE, diameter:2.25” thickness:15 mils, 24 microbends.

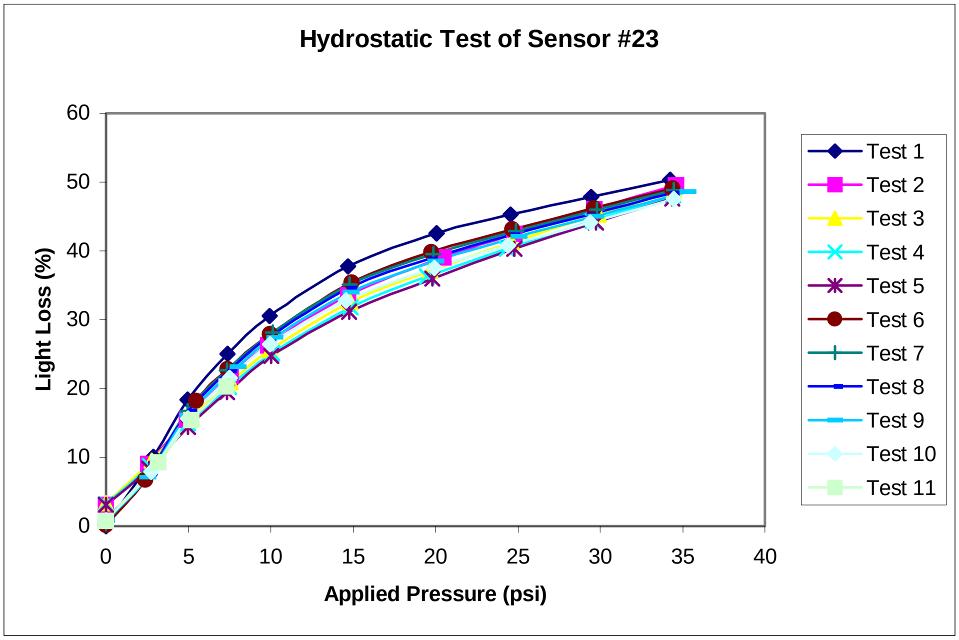

Fig. D.16. Sensor 23, Fluortex ETFE, diameter:1.25” thickness:20 mils, 11 microbends.

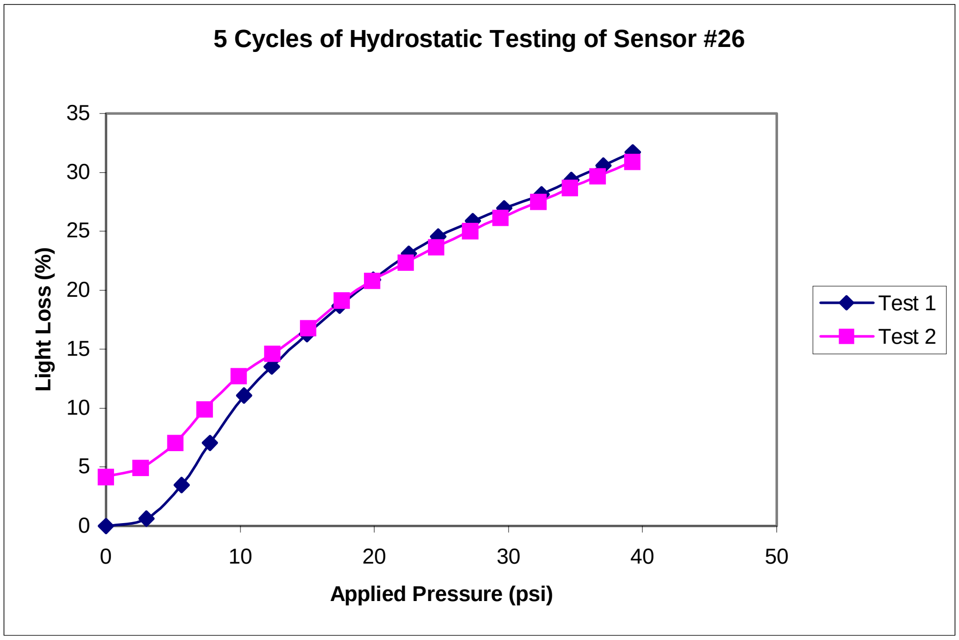

Fig. D.17. Sensor 26, Fluortex ETFE, diameter:1.25” thickness:15 mils, 11 microbends.

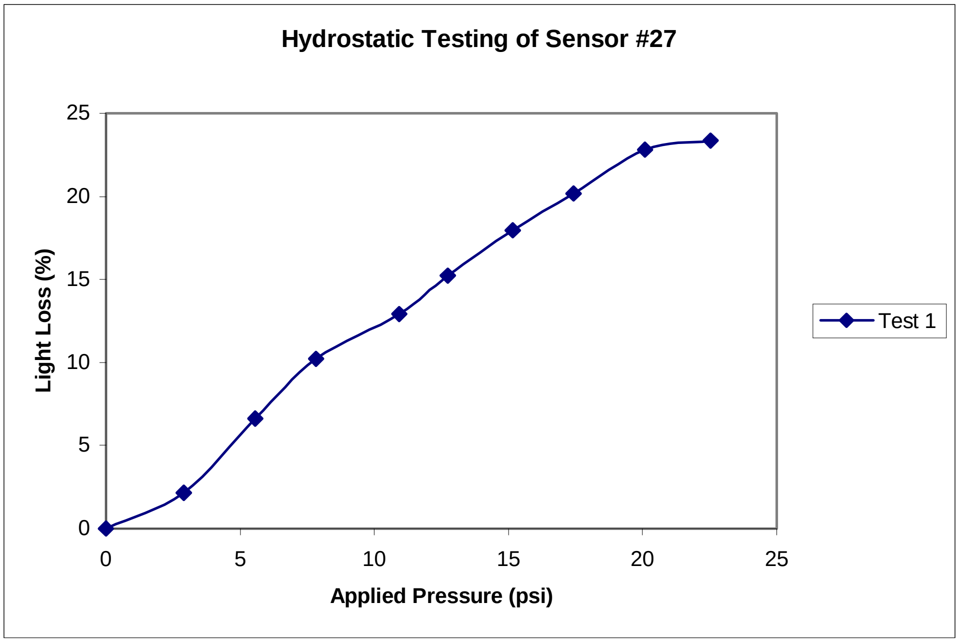

Fig. D.18. Sensor 27, Fluortex ETFE, diameter:1.25” thickness:15 mils, 11 microbends.

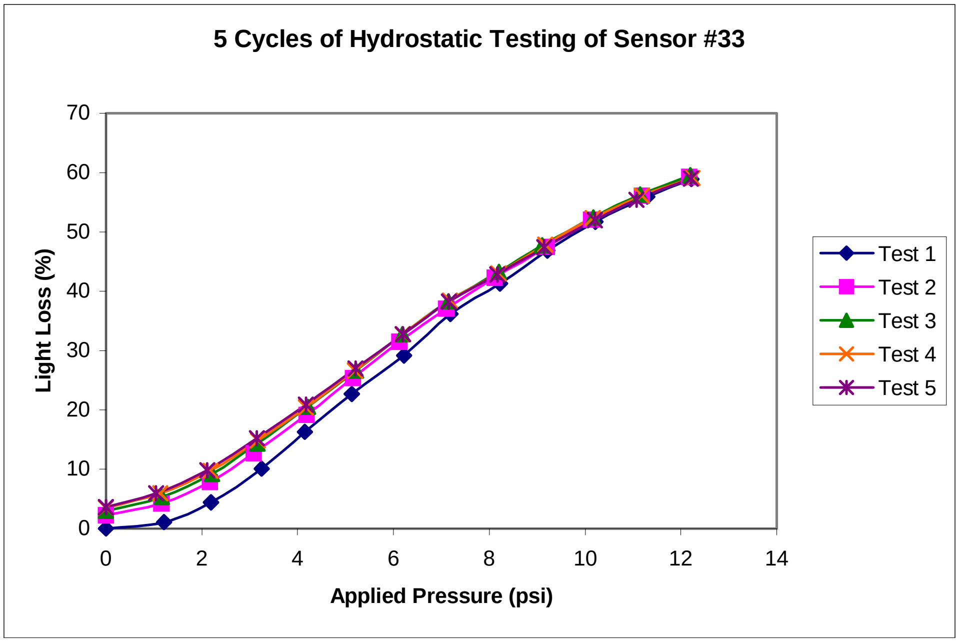

Fig. D.19. Sensor 33, polypropylene, diameter:1.25” thickness:15 mils, 13 microbends.

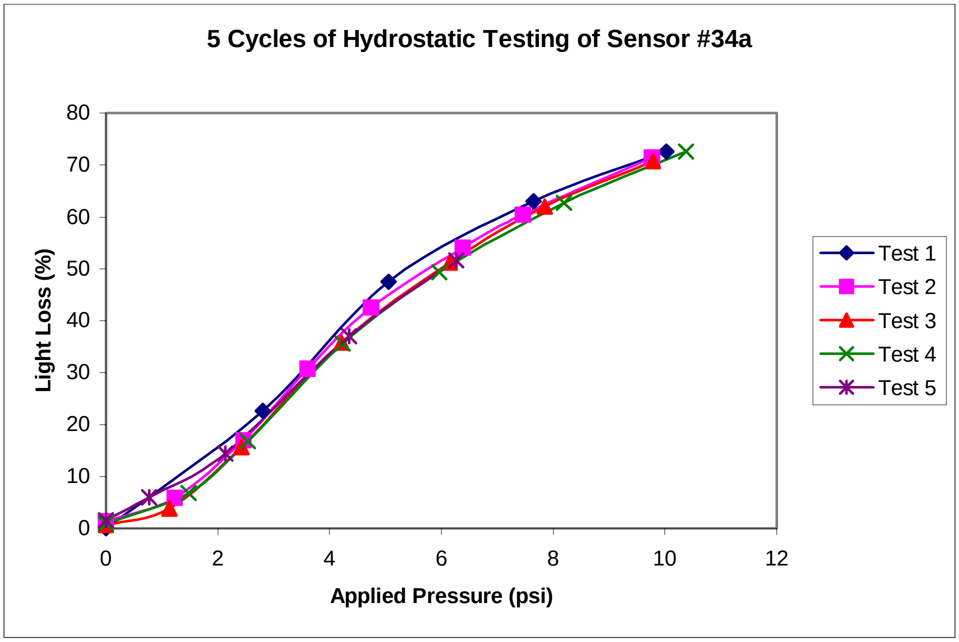

Fig. D.20. Sensor 34a, polypropylene, diameter:1.25” thickness:15 mils, 13 microbends.

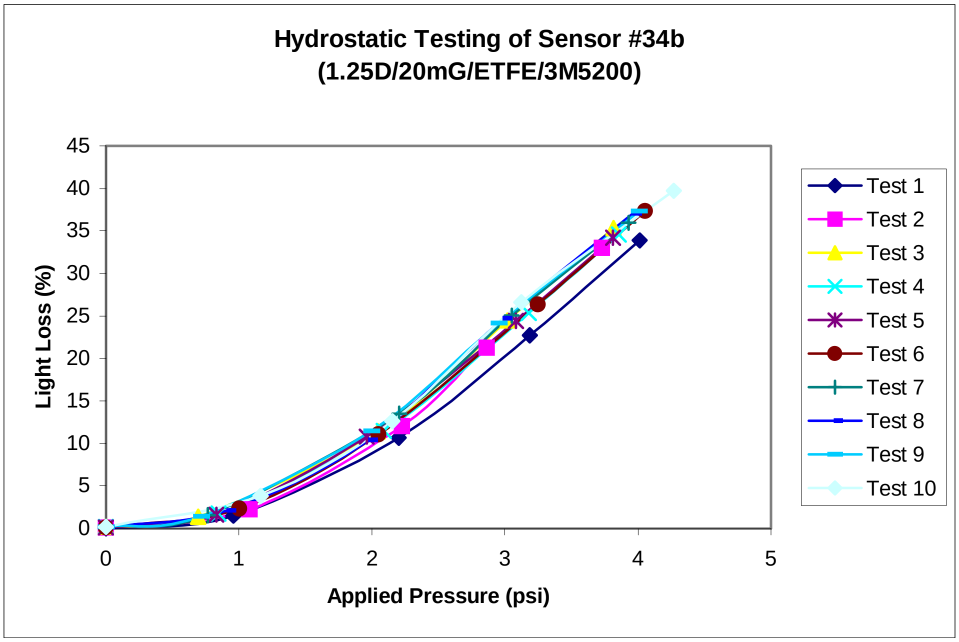

Fig. D.21. Sensor 34b, polypropylene, diameter:1.25” thickness:15 mils, 13 microbends.

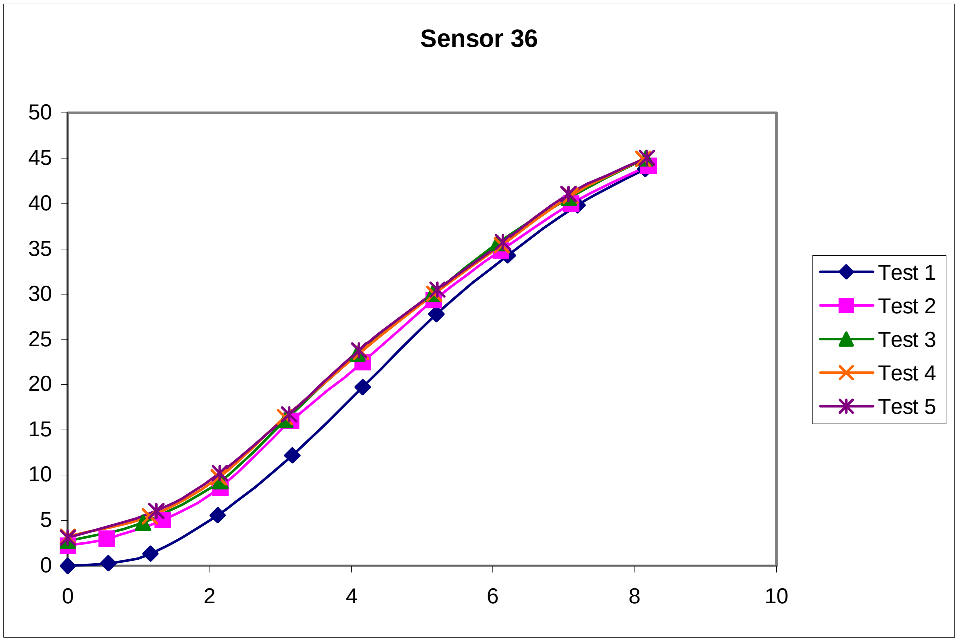

Fig. D.22. Sensor 36, polypropylene, diameter:1.25” thickness:15 mils, 13 microbends.

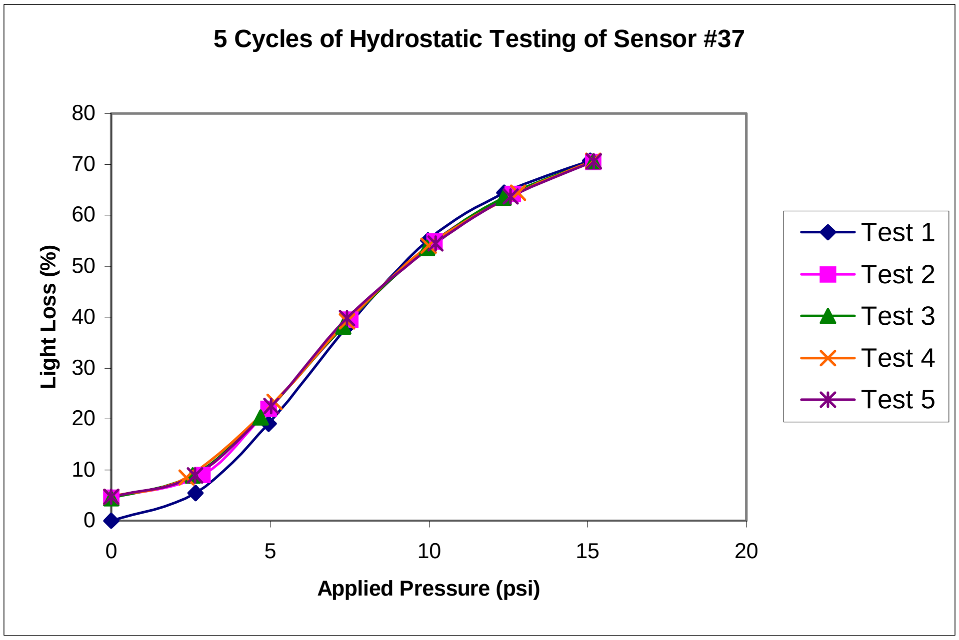

Fig. D.23. Sensor 37, polypropylene, diameter:1.25” thickness:15 mils, 13 microbends.